Uncertainty-Aware Distribution System State Estimation

A State Estimation Method for Medium Voltage Grids Using Heterogenous Measurement Input
Zur Erlangung des akademischen Grades Doktor-Ingenieur (Dr.-Ing.)
Genehmigte Dissertation von M. Sc. Eva Buchta aus Erlangen
Tag der Einreichung: 01.12.2023, Tag der Prüfung: 02.05.2024

1. Gutachten: Prof. Dr.-Ing. Stefan Niessen
2. Gutachten: Prof. Dr.-Ing. Jutta Hanson
Darmstadt – D17, Technische Universität Darmstadt

TECHNISCHE UNIVERSITÄT DARMSTADT

Electrical Engineering and Information Technology Department

Technik und Ökonomie Multimodaler Energiesysteme

Uncertainty-Aware Distribution System State Estimation
A State Estimation Method for Medium Voltage Grids Using Heterogenous Measurement Input

Accepted doctoral thesis by M. Sc. Eva Buchta

Date of submission: 01.12.2023
Date of thesis defense: 02.05.2024

Darmstadt – D17, Technische Universität Darmstadt

Bitte zitieren Sie dieses Dokument als:
URN: urn:nbn:de:tuda-tuprints-274675
URL: https://tuprints.ulb.tu-darmstadt.de/274675
Jahr der Veröffentlichung auf TUprints: 2024

Dieses Dokument wird bereitgestellt von tuprints,
E-Publishing-Service der TU Darmstadt
https://tuprints.ulb.tu-darmstadt.de
tuprints@ulb.tu-darmstadt.de

Erklärungen laut Promotionsordnung

§ 8 Abs. 1 lit. c PromO

Ich versichere hiermit, dass die elektronische Version meiner Dissertation mit der schriftlichen Version übereinstimmt.

§ 8 Abs. 1 lit. d PromO

Ich versichere hiermit, dass zu einem vorherigen Zeitpunkt noch keine Promotion versucht wurde. In diesem Fall sind nähere Angaben über Zeitpunkt, Hochschule, Dissertationsthema und Ergebnis dieses Versuchs mitzuteilen.

§ 9 Abs. 1 PromO

Ich versichere hiermit, dass die vorliegende Dissertation selbstständig und nur unter Verwendung der angegebenen Quellen verfasst wurde.

§ 9 Abs. 2 PromO

Die Arbeit hat bisher noch nicht zu Prüfungszwecken gedient.

Darmstadt, 01.12.2023

E. Buchta

Abstract

In Germany, as in many other countries, the “Energiewende” is a central political and social goal to counteract climate change. To achieve this goal, dependence on fossil fuels must be reduced and a transition to a sustainable energy economy promoted. However, this paradigm shift towards renewable energies, decentralized energy sources, and electrification of different sectors significantly impacts the distribution grids’ structure and strains. Integrating decentralized, primarily volatile energy sources, such as solar and wind power plants, leads to a locally and temporally fluctuating electricity feed in. In addition, new consumers, such as electric vehicles and heat pumps, place heavy strains on the lower voltage levels.

The distribution grid operators are now faced with the task of keeping the power supply stable despite highly variable feed-in and load. In order to continue to ensure the reliability and efficiency of the power supply, the integration of technologies for real-time monitoring and analysis of the status is crucial. By using innovative monitoring that provides early warning of critical system conditions and automated control applications, existing grids can usually continue to operate safely for a longer period without needing immediate grid expansion.

In this thesis, a state estimation method for medium-voltage grids is developed. The aim is to estimate the current state of the power system as accurately as possible. The focus here is on detecting limit violations, such as voltage bands or thermal limit currents, and on the modeling of uncertainties. Since medium-voltage grids are usually only equipped with a scarce measurement infrastructure, additional input, usually only available historically, is used as background information for the state estimation. This input has significantly higher uncertainties than the precise real-time measurements. Therefore, it is particularly important in medium-voltage grids to apply state estimation methods that consider these uncertainties in the output assessment.

Based on this requirement, a probabilistic state estimation method is developed that is suitable for practice-relevant measurement availability scenarios. The basic algorithm of the developed state estimation method is based on the Bayes’ rule. This algorithm was extended in the present work by corresponding modules in order to fulfill the analyzed requirements for state estimation methods for medium-voltage grids. These extensions include evaluating the probability distribution regarding critical system states and parameterizing the statistical properties of loads using the available measurement information. Annual simulations of a representative German medium-voltage grid are used for the evaluation. With the developed method, it is possible to estimate the probability of critical system states. The estimation takes less than one second, and the critical system states can be reliably identified with a detection rate of over $90\,\%$. The method also includes classification and output of warning and alarm stages, which provides an early warning of bottlenecks in the grid. In order to be practicable for field usage, the method places particular emphasis on a realistic assumption of the temporally available input data in medium-voltage grids.

Zusammenfassung

In Deutschland, wie auch in vielen anderen Ländern, ist die Energiewende ein zentrales politisches und gesellschaftliches Ziel, um dem Klimawandel entgegenzuwirken. Um dieses Ziel zu erreichen, muss die Abhängigkeit von fossilen Brennstoffen reduziert und ein Übergang zu einer nachhaltigen Energiewirtschaft gefördert werden. Dieser Paradigmenwechsel hin zu erneuerbaren Energien, dezentraler Stromversorgung und Elektrifizierung verschiedener Sektoren hat jedoch erhebliche Auswirkungen auf die Struktur und Belastung der Verteilnetze. Die Integration von dezentralen, volatilen Energiequellen wie Solar- und Windkraftanlagen, führt zu einem örtlich und zeitlich schwankenden Stromangebot. Hinzu kommen neue Verbraucher wie Elektroautos und Wärmepumpen, welche die unteren Spannungsebenen zusätzlich stark belasten.

Die Verteilnetzbettreiber stehen nun vor der Aufgabe die Stromversorgung, trotz stark variabler Einspeisung und Last, stabil zu halten. Um die Zuverlässigkeit und die Effizienz der Stromversorgung weiterhin sicherzustellen, ist der Einsatz von Technologien zur Echtzeitüberwachung und -analyse des Netzzustands von entscheidender Bedeutung. Durch den Einsatz von innovativen Monitoringapplikationen, welche frühzeitig vor kritischen Systemzuständen warnen, und automatisierten Regelungsapplikationen können die bestehenden Netze meist für einen längeren Zeitraum ohne einen sofortigen Netzausbau sicher weiter betrieben werden.

In dieser Arbeit wird eine Zustandsschätzungsmethode für Mittelspannungsnetze entwickelt. Ziel ist es, den aktuellen Zustand des Stromsystems damit möglichst genau einzuschätzen. Hierbei liegt der Fokus auf der Erkennung von Grenzwertverletzungen, so wie von Spannungsbändern oder thermischen Grenzsströmen, und auf der Modellierung von Unsicherheiten. Da Mittelspannungsnetze meist nur geringfügig mit Messinfrastruktur ausgestattet sind, werden zusätzliche, meist nur historisch verfügbare Daten als Hintergrundinformation für die Zustandsschätzung verwendet. Dieser Input weist im Vergleich zu den präzisen Echtzeitmessungen deutlich höhere Unsicherheiten auf. Daher ist es in der Mittelspannung besonders wichtig, Zustandsschätzungsmethoden einzusetzen, die diese Unsicherheiten auch in der Output-Bewertung berücksichtigen.

Basierend auf dieser Anforderung wird ein probabilistisches Zustandsschätzungsverfahren entwickelt, das für praxisrelevante Messverfügbarkeitsszenarien geeignet ist. Der Basisalgorithmus der entwickelten Zustandsschätzungsmethode beruht auf dem Konzept von Bayes. Dieser Algorithmus wurde in der vorliegenden Arbeit durch entsprechende Module erweitert, um die analysierten Anforderungen an Zustandsschätzungsmethoden für Mittelspannungsnetze zu erfüllen. Diese Erweiterungen beinhalten eine Auswertung der Wahrscheinlichkeitsverteilung hinsichtlich kritischen Systemzuständen sowie eine Parametrierung der statistischen Eigenschaften von Lasten mittels der zur Verfügung stehenden Messinformationen. Für die Auswertung werden Jahressimulationen eines repräsentativen deutschen Mittelspannungsnetzes herangezogen. Mit der entwickelten Methode ist es möglich, die Wahrscheinlichkeit für kritische Systemzustände abzuschätzen. Die Abschätzung

erfolgt in weniger als einer Sekunde und die kritischen Systemzustände lassen sich mit einer Erkennungsrate von über $90\,\%$ zuverlässig identifizieren. Die Methode beinhaltet zudem eine Klassifizierung und Ausgabe von Warn- und Alarmstufen, welche frühzeitig vor Engpässen im Netz warnen. Um praktikabel für den Feldeinsatz zu sein, wird besonderer Wert auf eine realistische Annahme der in Mittelspannungsnetzen zeitlich verfügbaren Inputdaten gelegt.

Contents

List of Figures

List of Tables

Acronyms

AC Alternating Current

BLSE Bayesian Linear State Estimation

CSS Critical System State

CT Current Transformer

DS Distribution System

DSO Distribution System Operator

EEG Renewable Energy Sources Act (german: Erneuerbare-Energien-Gesetz)

EKF Extended Kalman Filter

EnWG German Energy Industry Act (german: Energiewirtschaftsgesetz)

EV Electric Vehicle

GEG Building Energy Law (german: Gebäudeenergiegesetz)

GML Generalized Maximum-Likelihood

GPS Global Positioning System

HP Heat Pump

HV High Voltage

LAV Least Absolute Value

LMS Least-Median of Squared

LS Least Squares

LTS Least Trimmed Squares

LV Low Voltage

MAP Maximum-A-Posterior

MIS Measurement Instrumentation Scenario

ML Maximum-Likelihood

MMSE Minimized Mean Square Error

MV Medium Voltage

NDP Network Development Plan

P2H Power-to-Heat

PMU Phasor Measurement Units

PV Photovoltaic

RES Renewable Energy Sources

RLM Recorded Power Measurements (german: Registrierende Leistungsmessung)

RMS Root-Mean-Square

RTU Remote Terminal Units

SCADA Supervisory Control and Data Acquisition

SE State Estimation

SLP Standard Load Profiles

SM Smart Meter

TS Transmission System

UHV Ultra-High Voltage

VT Voltage transformers

WLS Weighted Least Square

1 Motivation - Increasing Need for State Estimation in Medium-Voltage Grids

1.1 Expected Strong Increase of Operational Limit Violations in Medium-Voltage Grids

In the last three decades, the generation structure of the German electricity supply system has changed significantly [1]–[3]. In the design of conventional power grids, a few centralized large generation units directly connected to the Transmission System (TS) supplied electricity to the customers in the underlying Distribution System (DS). The German TS operates at the highest voltage level (ultra-high voltage, UHV). In the DS, the power is conventionally distributed from high voltage (HV) over medium voltage (MV) to low voltage (LV) grids[1].

The progressive change in the generation structure mainly originates from two trends: the strong increase in renewable energy sources (RES) [4] and the phase-out of large coal and nuclear power plants [5]. These trends are increasingly leading to decentralized power generation by small-to-medium power plants that are closer to energy consumption [6].

The major types of RES for power generation are solar, wind, biomass, and hydropower [7], [8]. Figure 1.1 shows the installed capacity of RES in 2012 and 2019. During these seven years, the installed capacity increased strongly. In particular, for the volatile generation sources photovoltaic (PV) and wind power, the capacity increased by a factor of 1.5 and 2, respectively. According to the German Network Development Plan (NDP) [9], the installed RES capacity is expected to double between 2019 and 2035. As can be seen in Figure 1.1, RES are primarily ($> 98\,\%$) installed in the DS (LV-, MV- and HV-level). Consequently, the function of the DS is no longer consumption-determined only.

The phase-out of large coal and nuclear power plants in Germany are driven by governmental actions of coal exit [10], to meet the targets of the Paris climate agreement [11], and by the Federal Parliament resolution to gradually shut down all nuclear power plants [12]. Figure 1.2 shows the forecasted decrease in the installed capacity of hard coal, lignite, and nuclear power plants. All nuclear power plants were shut down on 15th of April, 2023. The numbers for installed coal plants for 2025 result from legally binding decommissioning, i.e., § 50d German Energy Industry Act (Energiewirtschaftsgesetz, EnWG). The values for 2035 are taken from the NDP. In two scenarios (B and C) from NDP, all coal plants should be shut down until 2035. In scenario A, there is a remaining $7\,\mathrm{MW}$ for lignite.

[1] For Germany: UHV: $380/220\,\mathrm{kV}$, HV: $110\,\mathrm{kV}$, MV: 6-$35\,\mathrm{kV}$, LV: $0.4\,\mathrm{kV}$. In other countries different voltage levels are defined, e.g., the US levels reform to the ANSI C84.1-2020 standard.

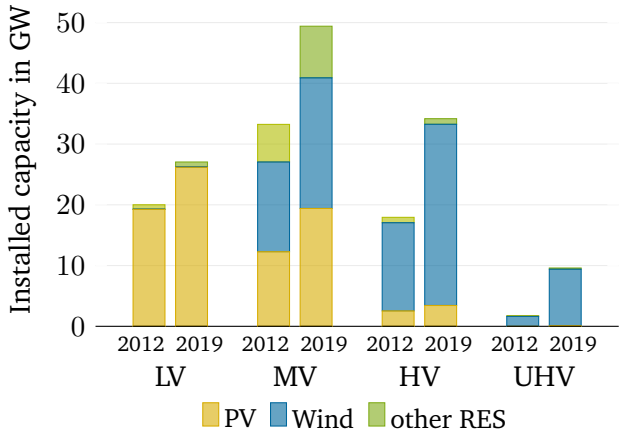

Figure 1.1: Installed capacity of RES in Germany in 2012 and 2019 for varying voltage levels in GW [13]. It is clear to see that the overall RES capacity has increased and that the major part is installed in DS (LV-, MV- and HV-level)

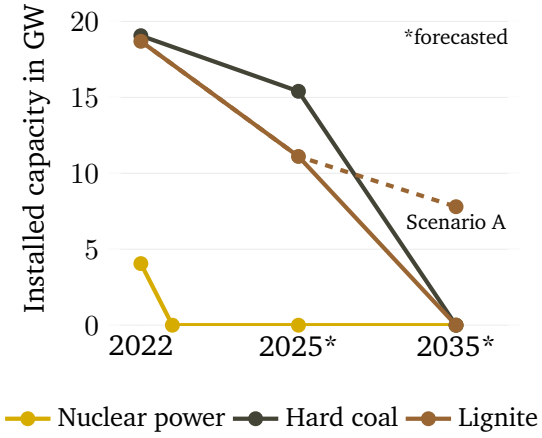

Figure 1.2: Forecasted phase-out of coal and nuclear power plants in Germany [5], [9]

Additional challenges for power grids arise from the increasing integration of new load types, such as electric vehicles (EV) [14] and heat pumps (HP) [15] or new storage systems [16]. According to the German Federal Ministry for the Environment, an EV increases the electricity demand of a 4-person household by about 50 % [17]. The most significant load from EVs on the power grids is expected from the “evening charging peak” resulting from the simultaneous charging by commuters. In January 2023, the total number of electric vehicles was over 1 million EVs [18], and the number of public charging stations reached over 80 thousand [19].

The current concerns about gas shortages and high gas prices increase the desire for heat pumps. The trade association for heat pumps expected a plus of 52 % for newly installed devices in 2023 [20]. When the new Building Energy Law (Gebäudeenergiegesetz, GEG) [21] comes into force, the demand for heat pumps is expected to increase continuously. The long-term goal of the law is to eliminate fossil fuel heating until 2045. Further, new heating equipment should be operated with 65 % RES, for which heat pumps are suitable. Since charging stations and heat pumps are mainly installed in low- and medium-voltage grids, a strong, temporally fluctuating increase in load is to be expected in these lower voltage levels.

Due to the changing generation structure and the additional consumers, the German power grids are increasingly driven to their limits, in particular, the LV- and MV levels. However, actions like grid extensions to increase the transmission capability are delayed or cannot be implemented fast enough [22]. As a result, operational limits are more and more often violated [1], [23]. Stationary operational limits of a power system are given by upper and lower voltage limits (voltage band) and by thermal current limitation of lines and transformers [24]. Overloading equipment leads to high temperatures, possibly damaging or prematurely aging grid components. In addition to grid extension, a promising solution to avoid limit violations is to use flexibility options such as storage systems or Power-to-Heat (P2H) applications [25] and delaying EV charging [26].

Monitoring, control, and protection applications are necessary to prevent the grid from limit violations. The basis for these applications is the quasi-stationary state of the system [27]. If an operational limit is violated, the system state is claimed to be critical. The information whether the grid is in a normal, nearly critical or critical state is necessary for distribution system operators (DSOs) to know if recovering or preventive operational actions are required. Based on the system state, operators can execute mitigation measures to bring the system back within operational limits.

The system state is estimated by an application called State Estimation (SE). For the TS and HV grids, there is a widely used state estimation method [28], but not for the MV- and LV grids. In the historical centralized power system, the consumption by customers in the lower voltage levels was sufficiently predictable and volatile generation sources were not yet installed. Hence, there was no need for state estimation applications in LV and MV levels, which would have justified the associated costs and efforts. Until now, there are no widely used state estimation methods for these voltage levels. However, the need for LV and MV grid state estimation methods strongly increases with the transformation of the power system.

Since several LV grids are connected to one MV grid, the number of customers affected by disruptions in the corresponding grid is larger on MV than on LV level. Hence, the development for monitoring applications in MV grid should be a priority. Further, the output of state estimation methods is usually used as decision support for appropriate mitigation measures. Since system operators in MV grids have higher degrees of freedom than in LV grids, e.g., in controlling generation plants, the mitigation measures can be realized faster and easier here. Hence, this thesis focuses on state estimation for MV grids.

In the German DS, the MV level has the largest share of installed RES capacity at $49.4\,\%$ ($51.71\,\mathrm{GW}$, 2021). Until 2031 the DSOs expect an increase to $69.5\,\mathrm{GW}$ in the MV grids. According to a study from German Energy Agency (Deutsche Energie-Agentur, dena)[1], this increase is leading to more and more frequent back feeds from the MV level. This leads to voltage band and overload problems that require grid expansion and operational management measures. On the demand side, an increasing number of bottlenecks and limit violations due to e-mobility, heat pumps and partly new storage systems is expected, especially in the MV and LV levels. Figure 1.3 shows the consumption-related limit violations of line sections in German MV grids according to a poll among 58 (2021) respectively 82 (2022) DSOs by the German Federal Network Agency (Deutsche Bundesnetzagentur, BNetzA). In 2021, there were only nine limit violations [29]. In 2022, there are already 59. They are expected to rise by a factor of 50 to nearly 3000 limit violations in 2027 [23].

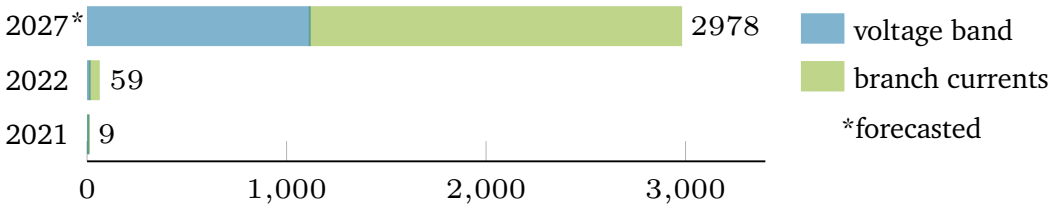

Figure 1.3: Consumption-related limit violations of line sections in German MV grids in 2021 [29], 2022 and forecast for 2027 [23]

Given the strong expected increase of operational limit violations in MV grids, it becomes increasingly important to monitor and control MV grids, as it has been done for the higher voltage levels for years. However, in MV grids, there is only little development of real-time measurement instrumentation and it is not expected to increase much in the medium term due to the high retrofitting costs. Therefore, the widely used state estimation approach from TS, which depends on a high amount of real-time measurements, can not be used directly in MV grids. In addition, other state estimation approaches may be more suitable for MV grid state estimation.

Hence, there is an increasing need to develop state estimation methods for MV grids to monitor the feasibility of the system state under changing system conditions.

This is considered a precondition to mitigate the grid impact due to the increased share of RES and the electrification of other energy sectors. Figure 1.4 summarizes the motivation in an overview of changing system conditions and the status quo for MV grid state estimation methods.

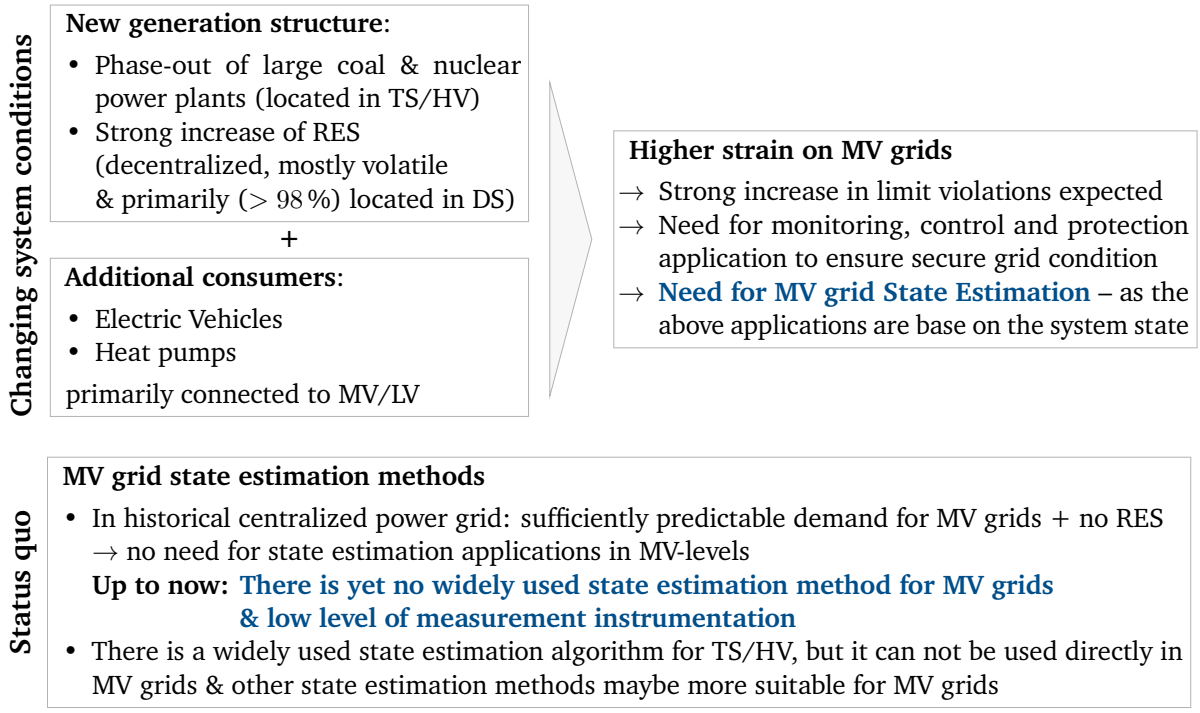

Figure 1.4: Overview of changing grid conditions and the status quo for MV grid state estimation methods

1.2 Objective, Structure and Contributions of this Thesis

As shown in Section 1.1, there is an increasing need for state estimation methods for MV grids to ensure secure grid conditions further.

To meet the upcoming challenges of MV grids, it becomes increasingly important to deploy state estimation methods adapted to the characteristics of MV grids

In order to reach this objective, the thesis is structured as follows:

To define the research question of this thesis, Chapter 2 discusses the requirements and challenges for MV-state estimation. At first, the requirements for state estimation methods of MV grids are defined. There are several challenges in meeting these requirements, mainly resulting from the characteristics of the MV grids. For this, an overview of the characteristic of MV grids is given. It focuses on the differences compared to TS and HV grids, where state estimation has been in operation for years. It is followed by a discussion of the challenges for MV grid state estimation to fulfill the previously defined requirements. It results in a derivation of necessary properties for MV grid state estimation methods. The research questions arising from the preceding analysis are given in Section 2.3.

The aim of Chapter 3 is to find a suitable approach for MV grid state estimation. Therefore different state estimation algorithms are compared. The chapter starts with a definition of the power system. After this, a literature review of MV grid state estimation approaches is given. In the subsequent section, different state estimation algorithms are compared to determine which approach fits best to the required properties defined in Section 2.2. Based on this, an analytic probabilistic approach using Bayes' theorem is chosen. After this, the basic principle of the selected Bayesian state estimation algorithm is given. Own contributions have adapted the algorithm from the literature to incorporate branch capacities, consider load correlations and use all measurable variables from Remote Terminal Units (RTU) and Phasor Measurement Units (PMU).

To identify the research gaps for Bayesian state estimation approaches, Chapter 4 compares previously published Bayesian state estimation methods. First, the uncertainties and availability of the inputs for Bayesian state estimation methods are analyzed. This section contains an end-to-end real-time measurement uncertainty analysis for RTUs and PMUs and an overview of Smart Meter (SM) coverage in European countries and US states. Second, Bayesian state estimation methods from literature are compared to fulfill the requirements defined in Section 2.2. This clearly shows the research gaps addressed in this thesis (Section 2.3). To face the research gaps two new modules are developed which are added to the selected state estimation algorithm from 3.3: The post-processing module calculates the probability of critical system states due to limit violations. The pre-processing module is a statistics module for varying data sources with different levels of temporal resolution. It focuses on considering correlations between customer behaviors, which significantly benefits to the state estimation results.

Chapter 5 contains several case studies. It starts by describing the simulation environment including the test grid, the synthesized data and all defined test assumptions. The central part of this chapter is the evaluation of accurately recognizing critical system states due to voltage band and thermal current limit violations. Another essential part is the evaluation of the benefits of the correlation-aware synthesis method for the state estimation results. The chapter concludes with a summary of the strengths and limitations of the proposed MV grid state estimation method.

The main results of this thesis are summarized in Chapter 6. Also, an outlook on future research topics is provided.

2 Analysis – Requirements and Challenges for State Estimation of MV Grids

This chapter analyzes the requirements for state estimation methods for MV grids and their associated challenges. From this derive appropriate properties for MV grid state estimation methods and the research questions of this thesis.

2.1 Requirements for State Estimation of MV Grids

Monitoring, control, and protection applications are required to protect the grid from limit violations [27]. These applications are based on the current system state of the power grid. Monitoring applications use the system state as a basis for decision support. In control applications, the system state can be used for switching connections or congestion management, such as load control or generation curtailment. Further, the system state can also be used to adapt the protection parameters in protection applications. Hence, the system state and, consequently, state estimation methods are essential to react in case of critical system states with correct mitigation measures.

State estimation generally describes an approach to processing raw measurement data and topology information to an estimate of the current state of a power system. The process can consist of several steps linked with each other, including grid topology processing, observability analysis, a state estimation algorithm, and bad data detection [24], [30]. The topology processor usually captures the status of lines, tap changers, and switching devices and configures the current grid topology. The observability analysis checks the measurement data availability[1]. Then, the processed grid topology and available measurement data are used by the state estimation algorithm to estimate the current state of the system. The function of bad data detection is to identify and remove data affected by gross measurement errors.

The general objective of state estimation methods is to estimate the quasi-stationary system state as accurately as possible [24], [31], [32]. For MV grids, the requirements for state estimation are defined here by

- sufficient **accuracy** with a focus on the detection of limit violations and
- **near real-time** for timely interventions by system operators.

[1] If not enough real-time measurements are available, additional non-real-time input is used, or a grid reduction is executed.

The first requirement concerns the accuracy of the results. For a DSO, it is primarily important to know whether any operational limit is violated that could disrupt the operation or whether the system is in normal condition. Hence, the aim is not to find the best deterministic estimate but to detect operational limit violations as accurately as possible. The considered operational limits are voltage band and thermal current limit violations. If critical system states can be detected prematurely, measures can be taken before the equipment gets harmed or the protection devices are triggered. This thesis aims to achieve possibly high detection rates with the scarce measurement instrumentation in MV grids. The target threshold value for detection rates is exemplary set at 90 %[2].

The near real-time condition must also be defined more precisely: Only static, non-dynamical effects are considered. The state estimation results should be available timely after the measurements are received. A millisecond interval would be unnecessary as the results are given to human-in-the-loop actions for switching or congestion management and also because of the thermal inertia of the components. This thesis aims for a computational time limit of up to 60 seconds for the state estimation process. This requirement is in line with the definition for the real-time condition of the German BNA [33][3]. Internal exchanges with system operators have confirmed that time limits in the range of 30 to 60 seconds are appropriate. The faster the results are available and, thus, the quicker it is possible to react, the better the aging of the electrical equipment and triggering of the protection devices can be prevented.

The fulfilment of these requirements for state estimation of MV grids faces some challenges, which are analyzed in the following.

2.2 Challenges to Fulfill the Defined Requirements for State Estimation of MV Grids

As the challenges for MV grid state estimation result mainly from the characteristics of the MV grids, these are considered first. Table 2.1 compares MV grid characteristics to TS and HV grids, where state estimation methods have been used for years.

One challenge to meet the **near real-time** requirement is the possible high number of buses in MV grids. Large grid sizes can cause high calculation times and computational complexity, especially for iterative calculation processes, e.g., required to handle non-linear models. Furthermore, power flow model simplification (e.g., DC power flow) that can be used in TS to decrease calculation time is not applicable for MV grids. The typical simplifications in UHV/HV levels take advantage of neglectable small line resistances for the overhead lines (high X/R-value). MV grids typically have a high wiring rate of 70 % to 90 %. Since the X/R-value is mostly below 1 for cables [38], the line resistances must be addressed in power grid equations in MV grids.

[2] The target value for detection rates is a freely chosen parameter that can be adapted.
[3] The German BNA defines the term “real-time” as the period of time in which the information to be transmitted has to be updated.
[4] In rural areas also, 40 % possible
[5] Line inductance to resistance values
[6] Mostly only at HV/MV substations and central MV nodes [45]

Table 2.1: Comparison of MV grid and TS/HV grids characteristics

Characteristic	MV grid	TS and HV grid
Grid structure	Ring structure mostly operated openly [34], [35]	Meshed
Wiring rate	Typical 70 % to 90 %[4] [36]	UHV $< 1\%$ & HV $< 10\%$ [37]
X/R-value[5]	Mostly below 1 [38]	Mostly between 4 and 6 [38]
Number of buses	Possibly high number of buses [39]	Limited to one connected TS grid
Phase imbalances	Possible but rare [40], [41]	Symmetrical, three-phase operation [3]
Uncertainty in grid topology	Possible but mostly assumed to be known	Grid parameters and switching states are fully known [1]
Measurement coverage	Low [42]–[44], often less than 10 % busbar coverage[6]	Mostly every busbar is equipped with real-time measurements [34]

In case of phase imbalances, a three-phase calculation for the correctness of the results is needed, which leads to higher complexity and calculation times. Phase imbalances can result from unsymmetrical phase loading or structural asymmetry of operating equipment. In Germany, the power grid is three-phase, so only unsymmetrical phase loading is relevant here[7]. The imbalance ratio in German MV and LV grids is limited by DIN EN 50160 norm to 2 %[8]. For MV grids, the loads are ordinarily three-phase and balanced. Large single-phase or two-phase loads can be connected, such as AC overhead lines for trains or induction and resistance furnaces, but they can be mitigated by using special transformers[9] [40]. Imbalances between the three phases are more relevant for the LV grids. Low voltage loads, e.g. PCs or lighting systems, are usually single-phase. So, the load circuits are often distributed among the three outer conductors, for example, one per floor of a building. The LV grid imbalances could be transformed to MV level, but this happens only rarely for two reasons: Due to the usually large number of customers connected at one secondary substation, the imbalances stochastically balance each other. Further, the star-delta switching[10] of the transformer compensates most effects of the LV side imbalance [41]. Consequently, imbalances for MV grids are not considered further in this thesis and symmetrical grid operation is assumed.

[7] Structural asymmetry is present in US grids with single- and two-phase laterals MV feeders.
[8] measured as 10-minute values with an instantaneous maximum of 4 %.
[9] e.g., transformer includes additional load for balancing
[10] Dyn5: Delta connection on primary side, star connection on the secondary side, star point led out on the secondary side and 150 ° phase shift between primary and secondary side. For unbalanced loading on LV side the currents flow in the star point of the transformer, so the secondary system receives a zero component. Because of the delta configuration of the MV side, the primary system can not have a zero component. So, the current in the star point causes uniformly distributed magnetizing flows on the transformer legs on the primary side.

The **accuracy** of the state estimation results can be affected by the uncertainty of the grid model. Any faulty assumption of switch configuration or uncertainty in line parameters can cause uncertainty in grid topology[11]. Hence, there is a large research field for topology identification in distribution grids [47]–[49]. Nevertheless, the grid topology is assumed here to be known to maintain the focus on state estimation. The main challenge for MV grid state estimation results from low real-time measurement coverage. The lack of real-time information affects the accuracy of the results. Due to cost aspects, a full real-time meter coverage of MV grids with real-time PMU or RTU sensors is not expected in the medium term. However, selectively placed micro-PMU can be a cost-efficient option in the future [50]. Further, the small number of real-time measurements in predominantly radially operated grids (open ring structure) could lead to single feeders with no available measurement information. This affects the accuracy of the results in this feeder tremendously.

One option to compensate for the scarce measurement infrastructure in MV grids is using non-real-time input from additional data sources. This input is typically a batch of data available historically or as forecast. A probability distribution can model the uncertainty of this input, and an empirical probability distribution can fit the data batches. Hence, the state estimation method should be able to take a probability distribution as input to consider the uncertainties of the input. Since iterative approaches may have difficulty converging when processing inputs with high uncertainties, this is also an argument for using non-iterative approaches or MV grid state estimation. As the input has uncertainties, so does the output. Hence, to be aware of the output uncertainties, a probability distribution is a valuable representation of the results. In addition, it should be noted that the available non-real-time input for MV grid state estimation may have different temporal resolution (time-resolved vs. only annual data). Therefore, the method should further be able to process non-real-time data with varying levels of detail.

The following required properties for MV grid state estimation methods are derived from the above challenge analysis and the defined state estimation requirements from Section 2.1:

1. The ability to process **probability distributions as input**: For accuracy aspects, the uncertainties of the input have to be taken into account. So, the state estimation algorithm should be able to process probability distributions as input.

2. Assume realistic **availability** for **non-real-time inputs**: The method should accommodate inputs with varying levels of detail.

3. Being **time-efficient**: Time-saving non-iterative approaches help to achieve near real-time conditions and also to avoid struggling with convergence issues.

4. **Output** the state estimation results as a **probability distribution**: The output of the algorithm should be modeled as a probability distribution to reach uncertainty awareness for the results.

[11] For LV grid, where often no detailed and reliable grid model is given [46], the grid uncertainty is highly challenging for state estimation.

Figure 2.1 summarizes the results of this chapter. It compares the defined state estimation requirements with MV grid characteristics and summarizes the resulting properties for MV grid state estimation methods in an overview chart.

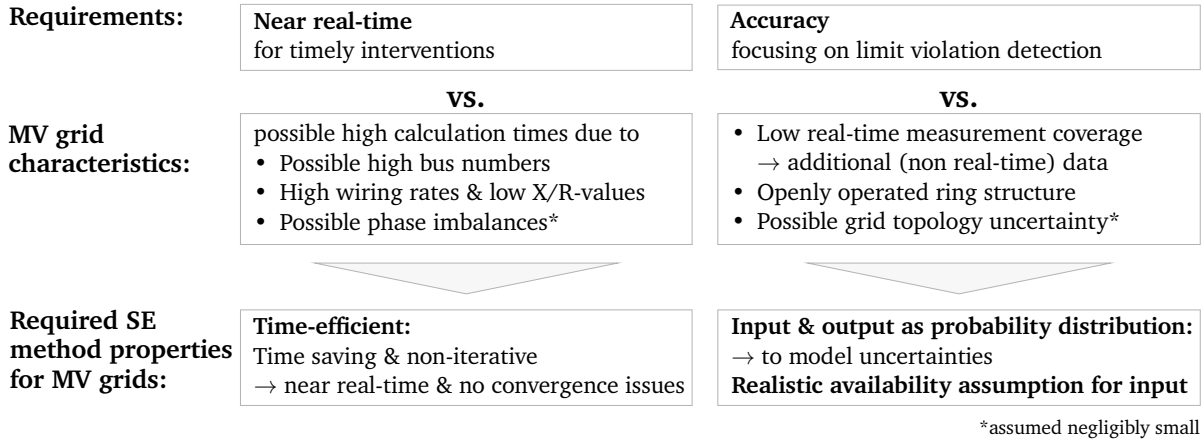

Figure 2.1: Comparing defined state estimation requirements with MV grid characteristics and summarizing the resulting properties for state estimation methods in MV grids

2.3 Research Questions of this Thesis

From the above-defined properties for MV grid state estimation method and the requirements from Section 2.1, the main Research Question of this thesis results:

Research Question 1

Which method is efficient & practical for uncertainty-aware state estimation for MV grids?

The adjectives used to describe the properties required for the state estimation method are defined as follows:

- **Efficient**: The method should be **accurate** with a focus on detecting limit violations. The considered operating limits are voltage band and thermal current limits. High identification rates ($> 90\,\%$) of limit violations are required. Further, the results should be available in **near real-time** for timely interventions of DSOs. Delay times of up to 60 seconds are tolerated.

- **Practical**: The method should be feasible under the scarce measurement infrastructure in MV grids. This includes the ability to process the resulting uncertainties of the input, e.g., in the form of a probability distribution, and to handle input data with varying levels of detail.

- **Uncertainty-aware**: The estimates should be a probability distribution to be aware of the uncertainty of the result.

The relevant information for MV grid operators is the current, possibly critical, state of their system. As described in Section 2.1, the system state is used as a basis for monitoring applications. The system state can be compared to operational limits to declare warning or alert messages. The operational use case of this thesis is the decision support for monitoring applications. Future research topics, not considered in this thesis, are use cases for control and protection applications.

As the state estimation output should be a probability distribution resulting from the requirement of uncertainty awareness, the probabilistic information must be utilized for relevant operation use cases. Hence, the probabilistic output should be processed so that the monitoring application can output warning or alert messages. This results in a second Research Question:

Research Question 2

How can the probabilistic state information be utilized for practical decision support in grid operation?

3 Modeling - State Estimation Approaches

This chapter aims to find a suitable basis algorithm for MV grid state estimation methods. For this, it compares different state estimation approaches from literature according to the defined requirements from the previous Chapter 2. The first section contains the modeling of the power system. The second section continues with a literature overview for state estimation algorithms. In the following section, the selected Bayesian linear state estimation algorithm is given. In the last section, the widely used state estimation approach for higher voltage levels is set as benchmark for the case study analysis and is therefore described and compared to the selected approach.

3.1 Definition of the Power System

In this section, the power system is described. Firstly, it concentrates on the basic grid variables for power system modeling. Secondly, the system state variables and the measurements, which are the main elements for state estimation applications, are described. Thirdly, the operational limits are defined.

3.1.1 Basic Power Grid Variables

Description of power grid basics can be found in many publications [3], [35], [51]–[53]. In this thesis, the power grid is operated with alternating current (AC) for a given grid frequency, e.g. $50\,\text{Hz}$. The electrical grid variables in a power system are voltages V (kV), currents I (kA), apparent power S (MVA) and admittances Y (Ω^{-1}). They are assumed quasi-stationary and the calculations are performed with RMS values[1] [54]. The grid variables are complex-valued and can be represented by the real and imaginary parts of the variable (rectangular form) a_{re} respectively a_{im} or alternatively by magnitude and phase (polar form) a_{mag} respectively a_{ang}.

- rectangular form: $a = a_{\text{re}} + j \cdot a_{\text{im}}$
- polar form: $a = a_{\text{mag}} \cdot e^{j a_{\text{ang}}} = a_{\text{mag}} \cdot (\cos(a_{\text{ang}}) + j \sin(a_{\text{ang}}))$

The transformation steps from polar to rectangular (see Equations 3.1 and 3.2) and from rectangular to polar form (see Equations 3.3 and 3.4) are below.

$$a_{\text{re}} = a_{\text{mag}} \cdot \cos(a_{\text{ang}}) \tag{3.1}$$

$$a_{\text{im}} = a_{\text{mag}} \cdot \sin(a_{\text{ang}}) \tag{3.2}$$

$$a_{\text{mag}} = |a| = \sqrt{(a_{\text{re}}^2 + a_{\text{im}}^2)} \tag{3.3}$$

[1] In electronics, the RMS value is the Root-Mean-Square error of a time-varying physical quantity. For a sinusoidal waveform, it is equal the peak value divided by $\sqrt{2}$.

$$a_{\text{ang}} = arg(a) = \begin{cases} \arctan(\frac{a_{\text{im}}}{a_{\text{re}}}) & \text{if } a_{\text{re}} > 0 \\ \arctan(\frac{a_{\text{im}}}{a_{\text{re}}}) + \pi & \text{if } a_{\text{re}} < 0, a_{\text{im}} \geq 0 \\ \arctan(\frac{a_{\text{im}}}{a_{\text{re}}}) - \pi & \text{if } a_{\text{re}} < 0, a_{\text{im}} < 0 \\ \frac{\pi}{2} & \text{if } a_{\text{re}} = 0, a_{\text{im}} > 0 \\ -\frac{\pi}{2} & \text{if } a_{\text{re}} = 0, a_{\text{im}} < 0 \end{cases} \tag{3.4}$$

An asterisk * next to a complex variable denotes a complex conjugation:

$$a^* = a_{\text{re}} - j \cdot a_{\text{im}} = a_{\text{mag}} \cdot e^{-j a_{\text{ang}}} \tag{3.5}$$

Multiple variables can be written as a matrix $\boldsymbol{A}$. They are printed in bold to distinguish them from the scalar variables. A one-dimensional matrix is a vector. A Transpose operation of matrix A is denoted by $\boldsymbol{A}^{\text{T}}$, and a Hermitian conjugation by $\boldsymbol{A}^{\text{H}} = \boldsymbol{A}^{*\text{T}}$. A diagonal matrix is a square matrix with zero elements outside the main diagonal. The diagonal operation (diag) of a vector returns a diagonal matrix with the elements of the vector on the main diagonal.

Based on the assumption of symmetrical grid operation, the modeling is done single-phase and is adapted to a three-phase model at the end of this subsection. The grid is modeled with $N+1$ nodes, also called buses. There are N non-slack buses and one slack bus marked with index “ns” and “0”, respectively. The slack bus sets the reference voltage angle (mostly 0 °). Further, it balances the apparent node power $S_{\text{bus},n}$ of the grid nodes $n \in \{1, ..., N+1\}$. The real part of the apparent power is called active power P and the imaginary part reactive power Q. Q is set to be positive for inductive components. This thesis uses the passive sign convention (see Figure 3.1). This convention defines a power flow from the grid into the connected component as positive and power flowing from the component to the grid as negative [55]. So, the generation power is counted as negative $S_{\text{gen},n} < 0$ and the consumption power as positive $S_{\text{load},n} > 0$. The whole grid is balanced when the sum of the generation and consumption units minus the resulting grid losses $S_{\text{loss}} > 0$ over all grid nodes results in zero.

$$\sum_{n=1}^{N+1} S_{\text{bus},n} - S_{\text{loss}} = \sum_{n=1}^{N+1} \left(S_{\text{load},n} + S_{\text{gen},n} \right) - S_{\text{loss}} \stackrel{!}{=} 0 \tag{3.6}$$

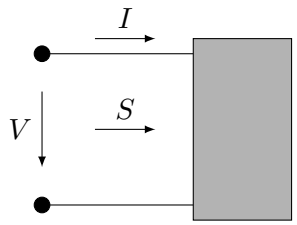

Figure 3.1: Passive Sign Convention [55]

The nodes are connected by B branches, including lines and transformers. The power is transported via the branches. This power flow's driving source is the voltage potential differences between the nodes [56]. The line losses can be divided into ohmic losses caused by the real-valued branch resistances R and into inductive and capacitive losses, which sources can be summarized in a real-valued branch reactance X. The resulting complex valued branch impedance Z is given by:

$$Z = R + j \cdot X \tag{3.7}$$

Its inverse is the branch admittance denoted by $Y = Z^{-1}$.

The branches are modeled as π-equivalent circuits [57], which is given in Figure 3.2. Each branch $b \in \{1, ..., B\}$ has a "from" $a_{\mathrm{f},b}$ and a "to" $a_{\mathrm{t},b}$ side.

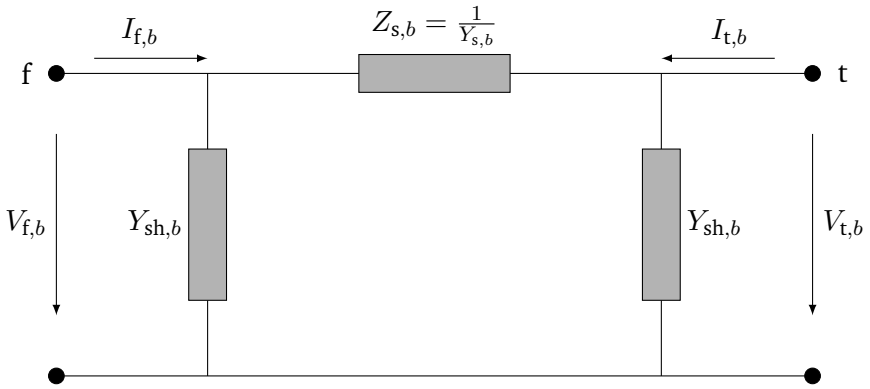

Figure 3.2: π-equivalent branch model

The currents at both ends of the branch $I_{\mathrm{f},b}$ and $I_{\mathrm{t},b}$ can be calculated by the series branch admittance $Y_{\mathrm{s},b}$ (resp. series branch impedance $Z_{\mathrm{s},b}$), the shunt branch admittance $Y_{\mathrm{sh},b}$, and the node voltages at each end of the branch $V_{\mathrm{f},b}$ and $V_{\mathrm{t},b}$ respectively. The shunt branch admittance results mainly from the line charging and is primarily capacitive.

$$\begin{bmatrix} I_{\mathrm{f},b} \\ I_{\mathrm{t},b} \end{bmatrix} = \begin{bmatrix} Y_{\mathrm{ff},b} & Y_{\mathrm{ft},b} \\ Y_{\mathrm{tf},b} & Y_{\mathrm{tt},b} \end{bmatrix} \begin{bmatrix} V_{\mathrm{f},b} \\ V_{\mathrm{t},b} \end{bmatrix} \tag{3.8}$$

$$\begin{bmatrix} Y_{\mathrm{ff},b} & Y_{\mathrm{ft},b} \\ Y_{\mathrm{tf},b} & Y_{\mathrm{tt},b} \end{bmatrix} = \begin{bmatrix} (Y_{\mathrm{s},b} + Y_{\mathrm{sh},b}) \cdot \frac{1}{|\tau_b|^2} & -Y_{\mathrm{s},b} \cdot \frac{1}{\tau_b^*} \\ -Y_{\mathrm{s},b} \cdot \frac{1}{\tau_b} & (Y_{\mathrm{s},b} + Y_{\mathrm{sh},b}) \end{bmatrix} \tag{3.9}$$

If the branch element is a transformer, the transformer ratio τ_b is given by Equation 3.10, otherwise, it is equal 1 (for lines). τ_b is defined by the ratio of primary to secondary windings w at the "from" node and by a possible phase shift θ_b in °.

$$\tau_b = w_b \cdot e^{j\theta_b \cdot \frac{\pi}{180^\circ}} \tag{3.10}$$

To generalize Equation 3.8 for all branch currents in the power grid, information about the node connection is necessary. The connectivity matrices $\boldsymbol{C}_{\mathrm{f}} \in \mathbb{R}^{B \times N+1}$ and $\boldsymbol{C}_{\mathrm{t}} \in \mathbb{R}^{B \times N+1}$ denote which bus is connected to which branch:

$$C_{\mathrm{f},b,n} = \begin{cases} 1 & \text{if node } n \in \{1, ..., N+1\} \text{ at “from” side of branch } b \in \{1, ..., B\} \\ 0 & \text{else} \end{cases} \tag{3.11}$$

$$C_{\mathrm{t},b,n} = \begin{cases} 1 & \text{if node } n \in \{1, ..., N+1\} \text{ at “to” side of branch } b \in \{1, ..., B\} \\ 0 & \text{else} \end{cases} \tag{3.12}$$

The “from” and “to” side branch admittance matrices $\boldsymbol{Y}_{\mathrm{f}} \in \mathbb{C}^{B \times N+1}$ and $\boldsymbol{Y}_{\mathrm{t}} \in \mathbb{C}^{B \times N+1}$ respectively, can be calculated with the connectivity matrices as follows:

$$\begin{bmatrix} \boldsymbol{Y}_{\mathrm{f}} \\ \boldsymbol{Y}_{\mathrm{t}} \end{bmatrix} = \begin{bmatrix} \mathrm{diag}(Y_{\mathrm{ff}}) & \mathrm{diag}(Y_{\mathrm{ft}}) \\ \mathrm{diag}(Y_{\mathrm{tf}}) & \mathrm{diag}(Y_{\mathrm{tt}}) \end{bmatrix} \begin{bmatrix} \boldsymbol{C}_{\mathrm{f}} \\ \boldsymbol{C}_{\mathrm{t}} \end{bmatrix} \tag{3.13}$$

$$Y_{\mathrm{ff}} = \begin{bmatrix} Y_{\mathrm{ff},1} \\ \vdots \\ Y_{\mathrm{ff},B} \end{bmatrix} \qquad Y_{\mathrm{ft}} = \begin{bmatrix} Y_{\mathrm{ft},1} \\ \vdots \\ Y_{\mathrm{ft},B} \end{bmatrix} \qquad Y_{\mathrm{tf}} = \begin{bmatrix} Y_{\mathrm{tf},1} \\ \vdots \\ Y_{\mathrm{tf},B} \end{bmatrix} \qquad Y_{\mathrm{tt}} = \begin{bmatrix} Y_{\mathrm{tt},1} \\ \vdots \\ Y_{\mathrm{tt},B} \end{bmatrix} \tag{3.14}$$

So, the generalized branch current equations for $\boldsymbol{I}_{\mathrm{f}} \in \mathbb{C}^{B}$ and $\boldsymbol{I}_{\mathrm{t}} \in \mathbb{C}^{B}$ are given by the product of branch admittance matrices and the node voltage vector $\boldsymbol{V} \in \mathbb{C}^{N+1}$:

$$\boldsymbol{I}_{\mathrm{f}} = \boldsymbol{Y}_{\mathrm{f}} \boldsymbol{V} \tag{3.15}$$

$$\boldsymbol{I}_{\mathrm{t}} = \boldsymbol{Y}_{\mathrm{t}} \boldsymbol{V} \tag{3.16}$$

The apparent branch power flows $\boldsymbol{S}_{\mathrm{f}} \in \mathbb{C}^{B}$ and $\boldsymbol{S}_{\mathrm{t}} \in \mathbb{C}^{B}$ can also be calculated in dependence on $\boldsymbol{V}$ and branch admittance matrices $\boldsymbol{Y}_{\mathrm{f}}$ and $\boldsymbol{Y}_{\mathrm{t}}$.

$$\boldsymbol{S}_{\mathrm{f}} = diag\left(\boldsymbol{V}_{\mathrm{f}}\right) \boldsymbol{Y}_{\mathrm{f}}^{*} \boldsymbol{V}^{*} \qquad \text{with } \boldsymbol{V}_{\mathrm{f}} = \boldsymbol{C}_{\mathrm{f}} \boldsymbol{V} \tag{3.17}$$

$$\boldsymbol{S}_{\mathrm{t}} = diag\left(\boldsymbol{V}_{\mathrm{t}}\right) \boldsymbol{Y}_{\mathrm{t}}^{*} \boldsymbol{V}^{*} \qquad \text{with } \boldsymbol{V}_{\mathrm{t}} = \boldsymbol{C}_{\mathrm{t}} \boldsymbol{V} \tag{3.18}$$

$\boldsymbol{V}_{\mathrm{f}} \in \mathbb{C}^{B}$ and $\boldsymbol{V}_{\mathrm{t}} \in \mathbb{C}^{B}$ are the voltage phasor vector of the voltages at the „from“ and „to“ sides of the branches.

The relation between node voltages $\boldsymbol{V}$ and apparent power at the nodes $\boldsymbol{S}_{\mathrm{bus}}$ is given by the bus admittance matrix $\boldsymbol{Y}_{\mathrm{bus}} \in \mathbb{R}^{N+1 \times N+1}$.

$$\boldsymbol{S}_{\mathrm{bus}} = diag\left(\boldsymbol{V}\right) \boldsymbol{Y}_{\mathrm{bus}}^{*} \boldsymbol{V}^{*} \tag{3.19}$$

$$\boldsymbol{Y}_{\mathrm{bus}} = -\left(\boldsymbol{C}_{\mathrm{f}}^{\mathrm{T}} \boldsymbol{Y}_{\mathrm{f}} + \boldsymbol{C}_{\mathrm{t}}^{\mathrm{T}} \boldsymbol{Y}_{\mathrm{t}} + \mathrm{diag}(\boldsymbol{Y}_{\mathrm{bsh}})\right) \tag{3.20}$$

$Y_{\text{sh},n}$ is the shunt element at the n-th bus. The vector for shunts at buses is given by:

$$\boldsymbol{Y}_{\text{bsh}} = \begin{bmatrix} Y_{\text{bsh},1} \\ \vdots \\ Y_{\text{bsh},N} \end{bmatrix} \tag{3.21}$$

For the passive sign convention, the diagonal elements ($n = m$) of the bus admittance matrix $\boldsymbol{Y}_{\text{bus},nn}$ are equal to the negative sum of the series admittances of the branches (and all shunt elements) connected to the corresponding node n. The non-diagonal elements ($n \neq m$) of $\boldsymbol{Y}_{\text{bus},nm}$ consist of the series admittance of the branch between the two corresponding nodes n and m. The negative and positive signs would be changed for the active sign convention.

The currents at the nodes $\boldsymbol{I}_{\text{bus}} \in \mathbb{C}^{N+1}$, which flow into the connected components, are given by

$$\boldsymbol{I}_{\text{bus}} = \boldsymbol{Y}_{\text{bus}}\boldsymbol{V} \tag{3.22}$$

For a balanced three-phase power system, the three-phase apparent power is three times the single-phase power: $\boldsymbol{S}_{\text{3ph}} = 3\boldsymbol{S}_{\text{ph}} = \boldsymbol{V}_{\text{ph}}\boldsymbol{I}^{*}_{\text{ph}}$. Depending on the star or delta connection of the phases, the values must be differentiated between phase-to-phase and phase values.

3.1.2 State Variables and Measurements

As defined by Roland E. Kalman in 1960, the **state** of a dynamical system is described by a set of system variables that capture all relevant information needed to predict the system's behavior over time [58].

Definition 1: State Variables

A minimum set of variables that contain all relevant information to describe the state of a system uniquely are called state variables according to [59]. From these state variables, all other system variables can be calculated. The state variable vector is denoted by $\boldsymbol{x}$. A distinction is made between true and estimated state variables. An estimated state variable vector is denoted by $\hat{\boldsymbol{x}}$.

The most common state variables for power systems consist either of all node voltage phasors $\boldsymbol{V} \in \mathbb{C}^{N+1}$ or of all branch currents $\boldsymbol{I}_{\text{f}} \in \mathbb{C}^{B}$ (resp. $\boldsymbol{I}_{\text{t}}$) phasors. Further state variables are all branch power or power node phasors. To address the research question, where accuracy with a focus on voltage band and thermal current limit violations is required, the voltage and current magnitudes are the relevant variables. For this thesis, voltage phasors in polar form are chosen as state variables. They already include the voltage magnitudes. The branch current magnitudes are part of the branch currents phasor, which can be calculated from the voltage phasors according to Equations 3.15 and 3.16.

The actual system state is not directly known but is measured by various meters. The resulting real-time measurements contain measurement errors. There can be systematic or random measurement errors [60]. Systematic errors reveal the same deviations for applying the measurement in the same way. The primary source for systematic measurement errors results from human misconduct (e.g., incorrect calibration, reversed connections of measurement devices or overdue maintenance). Random errors may vary for the same measurement procedure. To focus on the algorithm part of state estimation methods and their usability for monitoring applications, gross measurement errors, which would need a separate bad data detection step, are not considered here. Since therefore the uncertainty of real-time measurements is assumed to arise solely from random measurement errors, the assumption of homoscedasticity[2] for measurement errors is justified within the scope of this thesis. In addition to measurement errors, there may be too few real-time measurements to obtain a reliable result. In this case, input from additional data sources is required, as mentioned in Section 2.2. This input is primarily historical or forecasted and thus has higher uncertainties than real-time measurements. In summary, real-time measurements can not be directly taken for the system state, but they can be processed (along with additional input) by state estimation applications to provide an accurate estimate of the system state.

The state estimator receives a number M of real-time measurements z. The measurement function $h(\boldsymbol{x})$ maps $\boldsymbol{x}$ to the measured variables. Measurable variables are real and imaginary parts of apparent power for node and branch measurements, and magnitude and angle parts of voltage and branch current measurements. A fully occupied measurement function $h_{\text{full}}(\boldsymbol{x})$ with all measurable variables is given below.

$$h_{\text{full}}(\boldsymbol{x}) = \begin{bmatrix} \boldsymbol{P}_{\text{bus}} & \boldsymbol{P}_{\text{f}} & \boldsymbol{P}_{\text{t}} & \boldsymbol{Q}_{\text{bus}} & \boldsymbol{Q}_{\text{f}} & \boldsymbol{Q}_{\text{t}} & \boldsymbol{V}_{\text{mag}} & \boldsymbol{V}_{\text{ang}} & \boldsymbol{I}_{\text{f,mag}} & \boldsymbol{I}_{\text{t,mag}} & \boldsymbol{I}_{\text{f,ang}} & \boldsymbol{I}_{\text{t,ang}} \end{bmatrix}^T \tag{3.23}$$

3.1.3 Operational Limits

For safe grid operation, $\boldsymbol{V}_{\text{mag}} \in \mathbb{R}^N$ must be kept within a voltage band, which is determined by an upper V_{up} and a lower V_{low} voltage limit. The grid utilization is limited by the thermal branch current $I_{\text{th},b}$ of the respective operating equipment b. The three operational limits can be defined as follows:

$$V_{\text{low}} \leq V_{\text{mag},n} \leq V_{\text{up}} \qquad \forall\, n \in \{1, ..., N\} \tag{3.24}$$

$$I_{\text{f},b} \leq I_{\text{th},b} \qquad \forall\, b \in \{1, ..., B\} \tag{3.25}$$

$$I_{\text{t},b} \leq I_{\text{th},b} \qquad \forall\, b \in \{1, ..., B\} \tag{3.26}$$

According to the mandatory European norm, DIN EN 50160 [62], the voltage limits in MV and LV grids are set to $\pm 10\,\%$[3]. As though most of the secondary substations have a fixed transformation ratio, the voltage band must be divided for MV and LV level[4]. To ensure compliance with the

[2] Homoscedasticity means here the measurement errors are distributed in standard deviations [61].

[3] $95\,\%$ of 10-minute average of the measured value of each weekly interval must be within $\pm 10\,\%$ of nominal voltage.

[4] For this, voltage drops over the lines as well as over the secondary substation have to be considered. The voltage rises for connected generation units is limited to $3\,\%$ for LV and $2\,\%$ for MV grids [63]. Further, reserves for unbalances or manufacturing tolerances are also often taken into account.

combined limits for MV and LV grids, many distribution system operators set self-defined stricter voltage band limits for their MV grids. In Germany, the limits are often set to $\pm 4\,\%$ [64] or $\pm 6\,\%$ [65], [66]. In the USA, the limits are often $\pm 5\,\%$, as given in the ANSI norm C84.1. One option for higher grid utilization is a secondary transformer with controllable functionalities, often called a smart transformer (regelbarer Ortsnetztransformator, rONT) [67].

The thermal current limits for the branch elements are given in several standards[5] depending on cable type and the operation conditions [68]. The cable types can be found in the data sheets of the corresponding equipment.

Regarding the operational limits, normal and critical system states are defined as follows:

Definition 2: Normal vs. Critical System State

A **system state** is assumed **normal** if no operational limits, such as voltage band or thermal current limits, are violated. Otherwise, the state is claimed to be **critical** (Critical System State, CSS).

Only the quasi-stationary system state is considered here so that dynamical effects, which are relevant for, e.g., detecting frequency limit violations, are not considered.

3.2 Overview of State Estimation Algorithms from Literature

This section gives a literature overview of the different state estimation approaches for MV grids. For most state estimation approaches, firstly a measurement model is assumed. The conventional measurement model is given by

$$\boldsymbol{z} = h(\boldsymbol{x}) + \boldsymbol{e}\ . \tag{3.27}$$

$\boldsymbol{z}$ is an M-dimensional measurement vector, $\boldsymbol{x}$ denotes the state variable vector, h is the previously defined measurement function, and $\boldsymbol{e}$ is the measurement error vector. The measurement errors are assumed to be independent and normally distributed with mean vector $\boldsymbol{\mu}_\mathrm{e}$ equal to zero and standard deviation vector $\boldsymbol{\sigma}_\mathrm{e}$.

Concerning the state variables $\boldsymbol{x}$, the following state variables for MV grid state estimation approaches are used in literature:

- Voltage phasors in polar [28] and rectangular forms [69]
- Branch current phasors in polar [70] and rectangular forms [71],
- Branch power phasors [72]

The approaches use homogeneous types of state variables. So, for example, the authors do not mix voltage and current phasors in one subset or polar form with a rectangular form. This simplifies the subsequent calculation of other state variables to direct matrix calculations.

[5] Exemplary standards for thermal current limits are DIN VDE 0276, DIN VDE 0271 and DIN VDE 0298–4.

Concerning uncertainties, all state estimation approaches can be divided into two different approach types [73]:

Definition 3: Deterministic vs. Probabilistic Approaches

- Deterministic: The model produces a single, definite outcome for any given set of inputs.
- Probabilistic: The model considers a range of possible outcomes, and the results are expressed in probabilities.

Most **deterministic state estimation approaches** aim to estimate $\boldsymbol{x}$ by minimizing (or maximizing[6]) an objective function J. J can include the variables $\boldsymbol{x}$, $\boldsymbol{z}$ and $h(\boldsymbol{x})$. The results are received by the use of various solving algorithms.

$$\hat{\boldsymbol{x}} = \arg\min_{x} J(\boldsymbol{x}, \boldsymbol{z}, h(\boldsymbol{x})) \tag{3.28}$$

Most of the **probabilistic state estimation approaches** from the literature use the Bayes rule. It was first described by Thomas Bayes and was published posthumously in 1763 [75]. It describes the ability to determine the probability of an event when another event has already occurred. This is the basic idea of conditional probability. In the following, probabilistic state estimation methods are also called Bayesian state estimation methods. For state estimation applications, the Bayes rule is formulated as the conditional probability of the state variable vector $\boldsymbol{x}$ provided a measurement vector $\boldsymbol{z}$:

$$p\left(\boldsymbol{x} \mid \boldsymbol{z}\right) = \frac{p\left(\boldsymbol{z} \mid \boldsymbol{x}\right) p\left(\boldsymbol{x}\right)}{p\left(\boldsymbol{z}\right)}. \tag{3.29}$$

The left side of the Equation 3.29 is called **posterior** (po) probability. It is the probability for $\boldsymbol{x}$ after (= lat. post) consideration of real-time measurements. When considering continuous variables instead of discrete events, p are probability densities.

The **prior** (pr) probability $p\left(\boldsymbol{x}\right)$ is the probability of $\boldsymbol{x}$ before (= lat. prior) the availability of real-time measurements. The conditional probability for $\boldsymbol{z}$ given $\boldsymbol{x}$ is called the **likelihood** function $p\left(\boldsymbol{z} \mid \boldsymbol{x}\right)$. It expresses the probability of the observed measurements $\boldsymbol{z}$ for different settings of $\boldsymbol{x}$. $p\left(\boldsymbol{z}\right)$ is the normalizing constant to ensure that the sum for discrete events or the integral for continuous variables of the posterior probability over $\boldsymbol{z}$ equals one [76]. Hence, the posterior probability is proportional to the product of likelihood and prior probability.

$$p\left(\boldsymbol{x} \mid \boldsymbol{z}\right) \propto p\left(\boldsymbol{z} \mid \boldsymbol{x}\right) p\left(\boldsymbol{x}\right) \tag{3.30}$$

[6] Maximizing of an objective function is equal minimizing the negative objective function [74].

To decide between deterministic and probabilistic approaches, the following consideration is taken: The most widely used state estimation algorithm in TS and the other deterministic approaches have only single-value outputs instead of distributions. For this, they neglect the uncertainties of output. Concerning the research question 1, the following model decision is taken:

*As only probabilistic approaches can process probability distributions, which are necessarily needed for modeling the uncertainties of the input and output, a **Bayesian algorithm** is the most suitable option for state estimation of MV grids.*

However, many approaches in literature, especially the commonly used TS state estimation approach, are deterministic. To understand the idea and to be able to compare them to probabilistic approaches, some of the most common deterministic state estimation approaches are discussed in the following.

3.2.1 Overview of Deterministic Approaches

The conventional approach, which is widely used for TS and HV grids, uses voltage phasor in polar form for state variables, the Weighted-Least-Squares (WLS) as the objective function, and the Gauss-Newton optimization as an iterative solving algorithm. It was introduced by Schweppe in 1970 [28]. This approach desires full observability by measurements. Explicit the number of measurements M must be at least $2N-1$. In order to apply this approach to medium-voltage grids, where there is little coverage by real-time meters, the estimator was adapted to use additional non-real-time data as so-called pseudo-measurements [77]. These pseudo-measurements are given to the estimator in the same way as the real-time measurements but with high standard deviations for measurement accuracy.

Many approaches in literature have adapted the conventional approach in different ways. Some authors change the objective function to achieve more robustness against outliers or use different solving algorithms. Table 3.1 shows an overview of different objective functions used for state estimation approaches in literature.
The first five objective functions (WLS, LMS, LTS, LAV and GML) focus on minimizing the residuals r_m, which are defined as the difference between the measurement value z_m and its measurement function entry $h_m(x)$ for $m \in \{1, ..., M\}$.

$$r_m = z_m - h_m(x) \tag{3.31}$$

WLS, LMS, LTS, LAV and GML are all used for regression methods. The most common regression method is the method of Least Squares (LS), which goes back to Gauss or Legendre. It aims to minimize the sum of squared residuals:

$$\hat{\boldsymbol{x}}_{\text{LS}} = \arg\min_{x} \sum_{m=1}^{M} r_m^2 \tag{3.32}$$

Table 3.1: Objective functions for MV grid state estimation algorithms from literature

Abbreviation	Name	Objective function	Literature
WLS	Weighted Least Squares	$\arg\min_x(\boldsymbol{r}^T\boldsymbol{W}\boldsymbol{r})$	[28]
LMS	Least-Median of Squares	$\arg\min_x(\text{median}\{r_m^2\})$	[78]
LTS	Least Trimmed Squares	$\arg\min_x \sum_{m=1}^{M_{\text{trim}}}(r^2)_{(m)}$	[78]
LAV	Least Absolute Value	$\arg\min_x \sum_{m=1}^{M} \mid r_m \mid$	[79]
GML	Generalized Maximum-Likelihood	$\arg\min_x(\sum_{m=1}^{M}\sigma_{e,m}^{-2}\zeta(r_m))$	[80]
MMSE	Minimized Mean Square Error	$\arg\min_x(\mathbb{E}\left[(\boldsymbol{x}-\hat{\boldsymbol{x}})^T(\boldsymbol{x}-\hat{\boldsymbol{x}})\right])$	[81]
MAP	Maximum-A-Posterior	$\arg\max_x(p(\boldsymbol{x} \mid \boldsymbol{z}))$	[82], [83]

LS has computational simplicity but lacks robustness, as the squares heavily penalize large residuals. As LMS, LTS, LAV and GML are more robust against outliers, they are called robust regression methods [84]. They are more computationally demanding than LS.

- WLS: Minimizes the weighted sum of squared residuals. The weight matrix is denoted as $\boldsymbol{W} = (\text{diag}(\boldsymbol{\sigma}_e))^2 \in \mathbb{R}^{M\times M}$, where the weights on the diagonal elements are the inverse of the squared standard deviations. Measurements with higher variance are given lower weights and measurements with lower variance are given higher weights. This means that $\boldsymbol{z}$ with more reliable and less variable measurements has a stronger influence on the regression model, while $\boldsymbol{z}$ with more uncertainty has a reduced impact. Like the LS, it is pretty sensitive to outliers.

- LMS: Minimizes the median of the squared residuals. The median operation is denoted by median$\{\}$. The median is less sensitive to extreme values than the mean, which is used in the LS method.

- LTS: Minimizes the sum of the smallest ordered squared residuals. First, all residuals are squared and ordered by size from smallest to highest values. $r_{(m)}$ denotes the m-th ordered residual. Then only a subset of all measurements is taken into account, and the other part does not influence the fit. The trimming constant M_{trim} of the subset has to satisfy $\frac{M}{2} < M_{\text{trim}} \leq M$. As the residuals were ordered first, it considers only the smaller residuals.

- LAV: Minimizes the sum of absolute residuals. The idea is that absolute values treat large residuals more moderately than squared residuals.

- GML: Minimizes the weighted sum of a certain function ζ applied to the residuals. Commonly used functions include the absolute or normalized residuals, Huber's loss or Tukey's biweight [80].

MMSE and MAP have another focus than minimizing the residuals:

- MMSE aims to find $\hat{\boldsymbol{x}}$ that minimizes the average squared difference between $\hat{\boldsymbol{x}}$ and $\boldsymbol{x}$. $\mathbb{E}$ denotes the expectation value operation. MMSE focuses on minimizing the estimation error, not the measurement error.

- MAP intends to find $\hat{\boldsymbol{x}}$ that maximizes the conditional probability for $\boldsymbol{x}$ given measurements $\boldsymbol{z}$. With a normal distribution, this is the expectation value of the posterior probability.

The estimates of the above objective functions can be obtained by different solving algorithms. The overview in Table 3.2 of the mathematical modeling and exemplary solving algorithms for MV grid state estimation approaches covers most of the used models and algorithms from literature.

Table 3.2: Mathematical modeling and solving algorithms for optimization problems for MV grid state estimation approaches from literature

Mathematical modeling	Exemplary solving algorithm	Description	Literature
Unconstrained optimization	Gauss-Newton or Newton-Raphson	Iterative approximation algorithm for numerical solution of nonlinear systems of equations.	[28], [78]
Constrained optimization	Interior Point Optimization	Solve constrained optimization problems by finding points within the feasible region.	[85]
Neural Network	Back-propagation	Used in feed-forward neural networks to train the network by iteratively adjusting the weights of the connections.	[86], [87]
Swarm intelligence	Particle swarm, Ant colony, Artificial Bee Colony, Firefly	Inspired by the collective behavior of social insects, that communicate to solve optimization problems.	[88]–[91]
Fuzzy logic based	Fuzzy C-Means	Using fuzzy set theory to incorporate information affected by uncertainty.	[92], [93]

3.2.2 Overview of Bayesian Approaches

Bayesian state estimation approaches can be divided into analytic [94], iterative [83] and machine learning based [95] approaches. A short explanation for each of them in the context of state estimation is given below:

- **Iterative** approaches repeat an action multiple times to approach a numerical approximated solution of the non-linear analytically given state equations.
- In **Machine Learning** approaches for state estimation, an artificial neural network is trained by historical data to learn the behavior in order to predict current cases.
- An **Analytic** (or direct) approach obtains a solution through direct calculations.

The second defined property for MV grid state estimation methods from Section 2.2 requires methods to be non-iterative to achieve near real-time conditions and not to struggle with convergence issues. So, iterative Bayesian approaches are not considered for the method in this thesis.

The processes of neural networks take place in a black box and are, therefore, not easily comprehensible. Another disadvantage is the need for huge amounts of data to train the neural network usefully. As in MV grids, often only scarce measurements are available (see Section 2.2), this can cause difficulties for applying neural networks.

An analytic Bayesian approach is more transparent than a neural network and has better explainability. Further, it can deal with the scarce available meter data. Compared to iterative approaches, it is time-saving since it essentially consists of only a few matrix multiplications, and it has no convergence issues.

Consequently, in this thesis, an analytic Bayesian approach is chosen for the state estimation method for MV grids.

3.3 Basic Principle of Bayesian Linear State Estimation Algorithm

The basic principle of Bayesian linear state estimation for power distribution grids was established in 2014 by Schenato et al. [94]. The algorithm is further developed in this thesis by:

- Incorporating branch capacities (capacitive reactance) in linearized power flow equation.
- Considering load correlations by applying the multivariate complex normal distribution.
- Utilization of all measurable variables from (micro) Phasor Measurement Units (PMU) and Remote Terminal Unit (RTU) using Jacobi Matrix of $h(\boldsymbol{x})$.

3.3.1 Multivariate Normal Distribution

In the following, all distributions are assumed to be multivariate normal distributed with expectation value vector $\boldsymbol{\mu}$ and covariance matrix $\boldsymbol{\Sigma}$. The probability density function Φ_y for a multivariate normal distribution for D dimensional real-valued vector $\boldsymbol{y} \in \mathbb{R}^D$ is given by [76]

$$\Phi_y = \mathcal{N}\left(\boldsymbol{y} \mid \boldsymbol{\mu}_y, \boldsymbol{\Sigma}_y\right) = \frac{1}{(2\pi)^{\frac{D}{2}} \left|\boldsymbol{\Sigma}_y\right|^{\frac{1}{2}}} \exp\left\{-\frac{1}{2}\left(\boldsymbol{y}-\boldsymbol{\mu}_y\right)^{\mathrm{T}} \boldsymbol{\Sigma}_y{}^{-1}\left(\boldsymbol{y}-\boldsymbol{\mu}_y\right)\right\}. \tag{3.33}$$

The expectation value $\boldsymbol{\mu}_y \in \mathbb{R}^D$ and the covariance matrix elements $\Sigma_{y_i j}$ for $i, j \in \{1, ..., D\}$ are defined as

$$\boldsymbol{\mu}_y = \mathbb{E}[\boldsymbol{y}] = \int_{-\infty}^{\infty} \mathcal{N}\left(\boldsymbol{y} \mid \boldsymbol{\mu}_y, \boldsymbol{\Sigma}_y\right) y dy \tag{3.34}$$

$$\Sigma_{y_{ij}} = \mathbb{E}\left[(y_i - \mu_{y_i})(y_j - \mu_{y_j})\right]. \tag{3.35}$$

The diagonal elements ($i = j$) of the covariance matrix $\boldsymbol{\Sigma}_y \in \mathbb{R}^{D \times D}$ are the marginal variances, which are equal to the squares of the standard deviations σ_{y_i} .

$$\Sigma_{y_{ii}} = var(y_i) = \sigma_{y_i}^2 \tag{3.36}$$

The non-diagonal elements ($i \neq j$) can further be defined over the Pearson correlation coefficient $\rho_{y_{ij}}$ between element y_i and y_j and their standard deviations:

$$\rho_{y_{ij}} = \frac{\Sigma_{y_{ij}}}{\sigma_{y_i} \cdot \sigma_{y_j}} \tag{3.37}$$

If element y_i and y_j are uncorrelated ($\rho_{y_{ij}} = 0$), then the corresponding covariance matrix elements ($\Sigma_{y_{ij}}$ and $\Sigma_{y_{ji}}$) are zero. Hence, if all elements of the vector y are uncorrelated, $\boldsymbol{\Sigma}_y$ results in a diagonal matrix.

3.3.2 Calculation Steps of Bayesian Algorithm

In order to obtain the voltage posterior distribution $\Phi_{V_{\text{po}}}$, Bayes rule from 3.29 is applied. For this, it is necessary to build the product of the likelihood distribution $\Phi_{z|x}$ and the prior distribution of voltages $\Phi_{V_{\text{pr}}}$.

$$\Phi_{V_{\text{po}}} \propto \Phi_{z|x} \times \Phi_{V_{\text{pr}}} \tag{3.38}$$

When the prior distribution of voltages $\Phi_{V_{\text{pr}}}$ is not known or not available, it can be approximated from the distributions of loads using a linearized power flow calculation. A load probability distribution Φ_S can be used to capture the distribution of load cases in the system. The process is described in more detail below.

Background Distribution

Φ_S is given for the apparent power $\boldsymbol{S} \in \mathbb{C}^N$ of possible consumer and generation units connected to the non-slack nodes of the grid. In the context of Bayesian state estimation, this distribution for loads is often called Background distribution. The expectation values $\boldsymbol{\mu}_S$ and the covariance matrix $\boldsymbol{\Sigma}_S$ can be determined e.g., from historical power series. The algorithm is implemented in rectangular form. When using the multivariate normal distribution, the real and imaginary parts of vectors and matrices are stacked as shown in Equation 3.39 exemplary for $\boldsymbol{S}$, $\boldsymbol{\mu}_S$ and $\boldsymbol{\Sigma}_S$. The relation of real and imaginary parts in the stacked covariance matrix $\boldsymbol{\Sigma}_S \in \mathbb{C}^{2N \times 2N}$ are denoted with r and i for real and imaginary parts, respectively.

$$\Phi_S = \mathcal{N}\left(\boldsymbol{S} \mid \boldsymbol{\mu}_S, \boldsymbol{\Sigma}_S\right) = \mathcal{N}\left(\begin{pmatrix}\boldsymbol{S}_{\text{re}} \\ \boldsymbol{S}_{\text{im}}\end{pmatrix} \middle| \begin{pmatrix}\boldsymbol{\mu}_{S,\text{re}} \\ \boldsymbol{\mu}_{S,\text{im}}\end{pmatrix}, \begin{pmatrix}\boldsymbol{\Sigma}_{S,\text{rr}} & \boldsymbol{\Sigma}_{S,\text{ri}} \\ \boldsymbol{\Sigma}_{S,\text{ir}} & \boldsymbol{\Sigma}_{S,\text{ii}}\end{pmatrix}\right) \tag{3.39}$$

Linearized Power Flow

For the transformation of Φ_S to $\Phi_{V_{\text{pr}}}$, a linearized power flow is applied. The linearized power flow equation used here is equal to the first iteration step of the forward/backward sweep-based power flow algorithm [96]. For this, the bus admittance matrix is split into a slack row $\boldsymbol{L}_{0,\text{row}} \in \mathbb{C}^{1 \times N}$, a slack column $\boldsymbol{L}_{0,\text{col}} \in \mathbb{C}^{N \times 1}$, a slack variance $L_{0,0} \in \mathbb{C}$ and remaining non-slack parts $\boldsymbol{L} \in \mathbb{C}^{N \times N}$.

$$\boldsymbol{Y}_{\text{bus}} = \begin{bmatrix} L_{0,0} & \boldsymbol{L}_{0,\text{row}} \\ \boldsymbol{L}_{0,\text{col}} & \boldsymbol{L} \end{bmatrix} \tag{3.40}$$

With Equation 3.40, the bus current Equation 3.22 can be written as:

$$\begin{bmatrix} I_0 \\ \boldsymbol{I}_{\text{ns}} \end{bmatrix} = \begin{bmatrix} L_{0,0} & \boldsymbol{L}_{0,\text{row}} \\ \boldsymbol{L}_{0,\text{col}} & \boldsymbol{L} \end{bmatrix} \begin{bmatrix} V_0 \\ \boldsymbol{V}_{\text{ns}} \end{bmatrix} \tag{3.41}$$

The non-slack currents result in 3.42 and can be rewritten to Equation 3.43 for non-slack voltages V_{ns}. Substituting I_{ns} by the complex conjugated product of apparent power and voltage results in Equation 3.44.

$$\boldsymbol{I}_{\text{ns}} = \boldsymbol{L}_{0,\text{col}} V_0 + \boldsymbol{L}\boldsymbol{V}_{\text{ns}} \tag{3.42}$$

$$\boldsymbol{V}_{\text{ns}} = \boldsymbol{L}^{-1}(\boldsymbol{I}_{\text{ns}} - \boldsymbol{L}_{0,\text{col}} V_0) = -\boldsymbol{L}^{-1}\boldsymbol{L}_{0,\text{col}} V_0 + \boldsymbol{L}^{-1}\boldsymbol{I}_{\text{ns}} \tag{3.43}$$

$$= -\boldsymbol{L}^{-1}\boldsymbol{L}_{0,\text{col}} V_0 + \boldsymbol{L}^{-1}\boldsymbol{V}_{\text{ns}}^{-1*}\boldsymbol{S}^*. \tag{3.44}$$

For the first iteration step, all voltage phasors are assumed to equal the slack voltage phasor $V_{\text{ns},n} = V_0$. So, the linearized power flow equation is given by

$$\boldsymbol{V}_{\text{ns}} = -\boldsymbol{L}^{-1}\boldsymbol{L}_{0,\text{col}}V_0 + \frac{\boldsymbol{L}^{-1}}{V_0^*}\boldsymbol{S}^*. \tag{3.45}$$

The power flow equation contains the slack voltage phasor $V_0 \in \mathbb{C}$, the complex conjugated apparent power of consumers and generation units at all non-slack buses $\boldsymbol{S}^* \in \mathbb{C}^N$, as well as "non-slack" $\boldsymbol{L} \in \mathbb{C}^{N\times N}$ and slack column $\boldsymbol{L}_{0,\text{col}} \in \mathbb{C}^N$ of the bus admittance matrix $\boldsymbol{Y}_{\text{bus}}$.

The form of this equation slightly differs from the equation used in [94]. The additional matrix factor $-\boldsymbol{L}^{-1}\boldsymbol{L}_{0,\text{col}}$ in front of V_0 considers the line capacities in the system. This term cannot be neglected for grids with a high number of underground cables having high line capacities without loss of precision. Furthermore, the equation here assumes not only real-valued slack voltages.

The linear affine transformation is done with complex components to consider the load correlation between the buses and between the real and imaginary parts in the algorithm. Hence, the load distribution Φ_S is converted to complex normal form Φ_S^{C}. This is a more general solution than the restrictive assumption of independent loads and an addition to the proposed algorithm in [94]. The calculation of the complex expectation value $\boldsymbol{\mu}_S \in \mathbb{C}^N$, the complex covariance matrix $\boldsymbol{\Gamma}_S \in \mathbb{C}^{N\times N}$, and the pseudo-covariance matrix $\boldsymbol{C}_S \in \mathbb{C}^{N\times N}$ is given in Equations 3.47 to 3.49 [97].

$$\Phi_S^{\mathsf{C}} = \mathcal{N}\left(\boldsymbol{S} \mid \boldsymbol{\mu}_S, \boldsymbol{\Gamma}_S, \boldsymbol{C}_S\right) \tag{3.46}$$

$$\boldsymbol{\mu}_S = \boldsymbol{\mu}_{S,\text{re}} + j\boldsymbol{\mu}_{S,\text{im}} \tag{3.47}$$

$$\boldsymbol{\Gamma}_S = \boldsymbol{\Sigma}_{S,\text{rr}} + \boldsymbol{\Sigma}_{S,\text{ii}} + j\left(\boldsymbol{\Sigma}_{S,\text{ir}} - \boldsymbol{\Sigma}_{S,\text{ri}}\right) \tag{3.48}$$

$$\boldsymbol{C}_S = \boldsymbol{\Sigma}_{S,\text{rr}} - \boldsymbol{\Sigma}_{S,\text{ii}} + j\left(\boldsymbol{\Sigma}_{S,\text{ir}} + \boldsymbol{\Sigma}_{S,\text{ri}}\right) \tag{3.49}$$

Prior Distribution

Now, the affine transformation of the linearized power flow equation is executed to reach the voltage prior distribution. Any linear transformation of a Gaussian distribution is again Gaussian. The general form of linear affine transformation for a normal and a complex-valued normal distribution is given in Appendix A.2.1. For the transformation, the power flow Equation 3.45 is rewritten as

$$\boldsymbol{V}_{\text{ns}} = \boldsymbol{A}\boldsymbol{S}^* + \boldsymbol{b} \tag{3.50}$$

$$\text{with } \boldsymbol{A} = \frac{\boldsymbol{L}^{-1}}{V_0^*} \text{ and } \boldsymbol{b} = -\boldsymbol{L}^{-1}\boldsymbol{L}_{0,\text{col}}V_0.$$

The explicit calculation steps for the linear affine transformation of complex load distribution Φ_S^{C} to complex prior voltage distribution $\Phi_{V_{\mathrm{pr}}}^{\mathrm{C}}$ are given below.

$$\Phi_{V_{\mathrm{pr}}}^{\mathrm{C}} = \mathcal{N}\left(\boldsymbol{V} \mid \boldsymbol{\mu}_{V_{\mathrm{pr}}}, \boldsymbol{\Gamma}_{V_{\mathrm{pr}}}, \boldsymbol{C}_{V_{\mathrm{pr}}}\right) \tag{3.51}$$

$$\boldsymbol{\mu}_{V_{\mathrm{pr}}} = \boldsymbol{A}\boldsymbol{\mu}_{S^*} + \boldsymbol{b} \tag{3.52}$$

$$\boldsymbol{\Gamma}_{V_{\mathrm{pr}}} = \boldsymbol{A}\boldsymbol{\Gamma}_{S^*}\boldsymbol{A}^{\mathrm{H}} \tag{3.53}$$

$$\boldsymbol{C}_{V_{\mathrm{pr}}} = \boldsymbol{A}\boldsymbol{C}_{S^*}\boldsymbol{A}^{\mathrm{T}} \tag{3.54}$$

For the subsequent calculation step $\Phi_{z|x} \times \Phi_{V_{\mathrm{pr}}}$, the complex voltage prior distribution $\Phi_{V_{\mathrm{pr}}}^{\mathrm{C}}$ must be re-transformed to real component normal distribution $\Phi_{V_{\mathrm{pr}}}$ [97].

$$\Phi_{V_{\mathrm{pr}}} = \mathcal{N}\left(\boldsymbol{V} \mid \boldsymbol{\mu}_{V_{\mathrm{pr}}}, \boldsymbol{\Sigma}_{V_{\mathrm{pr}}}\right) \tag{3.55}$$

$$\boldsymbol{\Sigma}_{V_{\mathrm{pr}}} = \begin{pmatrix} \frac{1}{2}Re\left(\boldsymbol{\Gamma}_{V_{\mathrm{pr}}} + \boldsymbol{C}_{V_{\mathrm{pr}}}\right) & \frac{1}{2}Im\left(-\boldsymbol{\Gamma}_{V_{\mathrm{pr}}} + \boldsymbol{C}_{V_{\mathrm{pr}}}\right) \\ \frac{1}{2}Im\left(\boldsymbol{\Gamma}_{V_{\mathrm{pr}}} + \boldsymbol{C}_{V_{\mathrm{pr}}}\right) & \frac{1}{2}Re\left(\boldsymbol{\Gamma}_{V_{\mathrm{pr}}} - \boldsymbol{C}_{V_{\mathrm{pr}}}\right) \end{pmatrix} \tag{3.56}$$

Likelihood Distribution

The likelihood distribution $\Phi_{z|x} = \mathcal{N}\left(\boldsymbol{z} \mid \boldsymbol{\mu}_{z|x}(\boldsymbol{x}), \boldsymbol{\Sigma}_{z|x}\right)$ is defined by the expectation value $\boldsymbol{\mu}_{z|x} \in \mathbb{R}^M$ and the covariance matrix $\boldsymbol{\Sigma}_{z|x} \in \mathbb{R}^M$. $\boldsymbol{\Sigma}_{z|x}$ is determined by the accuracy of the given measurements. It is a diagonal matrix with squared standard deviations of the measurements $\boldsymbol{\sigma}_{\mathrm{z}} \in \mathbb{R}^{M \times M}$ for the diagonal elements. The standard deviations can be obtained from the accuracy of the installed measurement devices.

$$\boldsymbol{\Sigma}_{z|x} = (\mathrm{diag}(\boldsymbol{\sigma}_z))^2 \tag{3.57}$$

For $\boldsymbol{\mu}_{z|x}$, the measurement function $h(\boldsymbol{x})$ is linearized around $\boldsymbol{\mu}_{V_{\mathrm{pr}}}$ using Taylor series linearization (see appendix A.2.2).

$$\boldsymbol{\mu}_{z|x}(\boldsymbol{x}; \boldsymbol{\mu}_{V_{\mathrm{pr}}}) \approx h\left(\boldsymbol{\mu}_{V_{\mathrm{pr}}}\right) + \boldsymbol{H}\left(\boldsymbol{x} - \boldsymbol{\mu}_{V_{\mathrm{pr}}}\right) \tag{3.58}$$

$\boldsymbol{H} \in \mathbb{C}^{M \times 2N}$ is the Jacobian matrix of measurement function and is given by

$$\boldsymbol{H} = \begin{pmatrix} \frac{\partial h(\boldsymbol{x})_m}{\partial V_{\mathrm{re},n}} & \frac{\partial h(\boldsymbol{x}),m}{\partial V_{\mathrm{im},n}} \end{pmatrix} \tag{3.59}$$

It is received by partial deviations with respect to $V_{\mathrm{re},n}$ and $V_{\mathrm{im},n}$. In [94], $\boldsymbol{H}$ was only defined for voltage phasor measurements. In this thesis, it was extended for all measurable variables according to entries of h_{full} from Equation 3.23. The resulting entries are given in Appendix A.2.3.

Bayes Step

The product of two normal distributions results in another normal distribution [98]. Using the "completing square" operation [76], the expectation value and covariance matrix for the posterior distribution can be determined. The exponent of a normal distribution can be written in quadratic form:

$$-\frac{1}{2}\left(\boldsymbol{x}-\boldsymbol{\mu}_x\right)^{\mathrm{T}}\boldsymbol{\Sigma}_x^{-1}\left(\boldsymbol{x}-\boldsymbol{\mu}_x\right)=-\frac{1}{2}x^{\mathrm{T}}\boldsymbol{\Sigma}_x^{-1}\boldsymbol{x}+\boldsymbol{x}^{\mathrm{T}}\boldsymbol{\Sigma}_x^{-1}\boldsymbol{\mu}_x+const. \tag{3.60}$$

Here it can be seen that the second-order term in $\boldsymbol{x}$ equals the inverse of $\boldsymbol{\Sigma}_x$, and the first-order term in $\boldsymbol{x}$ equals $\boldsymbol{\Sigma}_x^{-1}\boldsymbol{\mu}_x$. Hence, for a normal distribution resulting from the product of two other normal distributions, the covariance matrix and the expectation value can be obtained from second and linear-order terms from the quadratic form of the exponent.

For this, the posterior distribution can be derived from the sum of the exponents of the likelihood and the prior distribution.

$$-\frac{1}{2}\left[\left(\boldsymbol{z}-\boldsymbol{\mu}_{z|x}\right)^{\mathrm{T}}\boldsymbol{\Sigma}_{z|x}^{-1}\left(\boldsymbol{z}-\boldsymbol{\mu}_{z|x}\right)+\left(\boldsymbol{x}-\boldsymbol{\mu}_{V_{\mathrm{pr}}}\right)^{\mathrm{T}}\boldsymbol{\Sigma}_{V_{\mathrm{pr}}}^{-1}\left(\boldsymbol{x}-\boldsymbol{\mu}_{V_{\mathrm{pr}}}\right)\right] \tag{3.61}$$

In this Equation 3.61 $\boldsymbol{\mu}_{z|x}$ is substituted by Equation 3.58. After multiplying out, there are second-order terms of $\boldsymbol{x}$ (3.62), linear $\boldsymbol{x}$ terms (3.63, 3.64) and terms independent of $\boldsymbol{x}$ (3.65).

$$\begin{aligned}
-\frac{1}{2}\Big[&\boldsymbol{H}^{\mathrm{T}}\boldsymbol{x}^{\mathrm{T}}\boldsymbol{\Sigma}_{z|x}^{-1}\boldsymbol{H}\boldsymbol{x}+\boldsymbol{x}^{\mathrm{T}}\boldsymbol{\Sigma}_{V_{\mathrm{pr}}}^{-1}\boldsymbol{x} && (3.62)\\
&-\boldsymbol{H}^{\mathrm{T}}\boldsymbol{x}^{\mathrm{T}}\boldsymbol{\Sigma}_{z|x}^{-1}(\boldsymbol{z}+\boldsymbol{H}\boldsymbol{\mu}_{V_{\mathrm{pr}}}-h(\boldsymbol{\mu}_{V_{\mathrm{pr}}}))-\boldsymbol{x}^{\mathrm{T}}\boldsymbol{\Sigma}_{V_{\mathrm{pr}}}^{-1}\boldsymbol{\mu}_{V_{\mathrm{pr}}} && (3.63)\\
&-(\boldsymbol{z}+\boldsymbol{H}\boldsymbol{\mu}_{V_{\mathrm{pr}}}-h(\boldsymbol{\mu}_{V_{\mathrm{pr}}}))^{\mathrm{T}}\boldsymbol{\Sigma}_{z|x}^{-1}\boldsymbol{H}\boldsymbol{x}-\boldsymbol{\mu}_{V_{\mathrm{pr}}}^{\mathrm{T}}\boldsymbol{\Sigma}_{V_{\mathrm{pr}}}^{-1}\boldsymbol{x} && (3.64)\\
&+(\boldsymbol{z}+\boldsymbol{H}\boldsymbol{\mu}_{V_{\mathrm{pr}}}-h(\boldsymbol{\mu}_{V_{\mathrm{pr}}}))\boldsymbol{\Sigma}_{z|x}^{-1}(\boldsymbol{z}+\boldsymbol{H}\boldsymbol{\mu}_{V_{\mathrm{pr}}}-h(\boldsymbol{\mu}_{V_{\mathrm{pr}}}))+\boldsymbol{\mu}_{V_{\mathrm{pr}}}^{\mathrm{T}}\boldsymbol{\Sigma}_{V_{\mathrm{pr}}}^{-1}\Big] && (3.65)
\end{aligned}$$

According to 3.60, the inverse of the second-order terms is equal to the new covariance matrix:

$$\begin{aligned}
\boldsymbol{\Sigma}_{V_{\mathrm{po}}}&=(\boldsymbol{H}^{\mathrm{T}}\boldsymbol{\Sigma}_{z|x}^{-1}\boldsymbol{H}+\boldsymbol{\Sigma}_{V_{\mathrm{pr}}}^{-1})^{-1} && (3.66)\\
&=\boldsymbol{\Sigma}_{V_{\mathrm{pr}}}-\boldsymbol{\Sigma}_{V_{\mathrm{pr}}}\boldsymbol{H}^{\mathrm{T}}\left(\boldsymbol{H}\boldsymbol{\Sigma}_{V_{\mathrm{pr}}}\boldsymbol{H}^{\mathrm{T}}+\boldsymbol{\Sigma}_{z|x}\right)^{-1}\boldsymbol{H}\boldsymbol{\Sigma}_{V_{\mathrm{pr}}} && (3.67)
\end{aligned}$$

With the theorem from [99], Equation 3.66 can also be written as Equation 3.67. The general form of this theorem is given in Appendix A.2.4.

According to Equation 3.60, the new expectation value for posterior distribution $\boldsymbol{\mu}_{V_{\text{po}}}$ is equal to the product of the posterior variance and the linear terms of the exponent in $\boldsymbol{x}$:

$$\boldsymbol{\mu}_{V_{\text{po}}} = \boldsymbol{\Sigma}_{V_{\text{po}}}(\boldsymbol{H}^{\text{T}}\boldsymbol{\Sigma}_{z|x}^{-1}(\boldsymbol{z} + \boldsymbol{H}\boldsymbol{\mu}_{V_{\text{pr}}} - h(\boldsymbol{\mu}_{V_{\text{pr}}})) + \boldsymbol{\Sigma}_{V_{\text{pr}}}^{-1}\boldsymbol{\mu}_{V_{\text{pr}}}) \tag{3.68}$$

Posterior Distribution

Hence, the voltage posterior density function $\Phi_{V_{\text{po}}}$ can be written as below with posterior distribution covariance $\boldsymbol{\Sigma}_{V_{\text{po}}}$ and expectation value $\boldsymbol{\mu}_{V_{\text{po}}}$:

$$\Phi_{V_{\text{po}}} = \mathcal{N}\left(\boldsymbol{V} \mid \boldsymbol{\mu}_{V_{\text{po}}}, \boldsymbol{\Sigma}_{V_{\text{po}}}\right) \tag{3.69}$$

$$\boldsymbol{\Sigma}_{V_{\text{po}}} = \boldsymbol{\Sigma}_{V_{\text{pr}}} - \boldsymbol{K}\boldsymbol{H}\boldsymbol{\Sigma}_{V_{\text{pr}}} \tag{3.70}$$

$$\boldsymbol{\mu}_{V_{\text{po}}} = \boldsymbol{\mu}_{V_{\text{pr}}} + \boldsymbol{K}\left(\boldsymbol{z} - h\left(\boldsymbol{\mu}_{V_{\text{pr}}}\right)\right) \tag{3.71}$$

$$\text{with } \boldsymbol{K} = \boldsymbol{\Sigma}_{V_{\text{pr}}}\boldsymbol{H}^{\text{T}}\left(\boldsymbol{H}\boldsymbol{\Sigma}_{V_{\text{pr}}}\boldsymbol{H}^{\text{T}} + \boldsymbol{\Sigma}_{z|x}\right)^{-1}$$

Finally, $\Phi_{V_{\text{po}}}$ is marginalized to distributions of the posterior voltage $\Phi_{V_{\text{po},n}}$ at each node $n \in \{0, ..., N\}$.

$$\Phi_{V_{\text{po},n}} = \mathcal{N}(V_{\text{po},n} \mid \mu_{V_{\text{po},n}}, \Sigma_{V_{\text{po},n}}) \tag{3.72}$$

In the last step, each $\Phi_{V_{\text{po},n}}$ is transformed to polar form. The conversion of the expectation value to magnitude and phase follows the general Equations 3.3 and 3.4, respectively.

$$\mu_{V_{\text{po},\text{mag},n}} = \sqrt{\left(\mu_{V_{\text{po},\text{re},n}}\right)^2 + \left(\mu_{V_{\text{po},\text{im},n}}\right)^2} \tag{3.73}$$

$$\mu_{V_{\text{po},\text{ang},n}} = arg\left(\mu_{V_{\text{po},n}}\right) \tag{3.74}$$

A linear Taylor series approximation is used to transform the marginalized posterior variances into polar form. Their derivation is given in Appendix A.2.5.

$$\Sigma_{V_{\text{po},\text{mag},n}} = \begin{pmatrix} \mu_{V_{\text{po},\text{re},n}} \\ \mu_{V_{\text{po},\text{im},n}} \end{pmatrix}^T \times \Sigma_{V_{\text{po},n}} \times \begin{pmatrix} \mu_{V_{\text{po},\text{re},n}} \\ \mu_{V_{\text{po},\text{im},n}} \end{pmatrix} \times \left(\mu_{V_{\text{po},\text{mag}}}\right)^{-2} \tag{3.75}$$

$$\Sigma_{V_{\text{po},\text{ang},n}} = \begin{pmatrix} -\mu_{V_{\text{po},\text{im},n}} \\ \mu_{V_{\text{po},\text{re},n}} \end{pmatrix}^T \times \Sigma_{V_{\text{po},n}} \times \begin{pmatrix} -\mu_{V_{\text{po},\text{im},n}} \\ \mu_{V_{\text{po},\text{re},n}} \end{pmatrix} \times \left(\mu_{V_{\text{po},\text{mag}}}\right)^{-4} \tag{3.76}$$

3.3.3 Summary of Bayesian Algorithm

Figure 3.3 summarizes the above-described state estimation algorithm steps in a flow chart. The algorithm output constitutes the marginalized voltage posterior distribution in polar form ($V_{\text{mag},n}, V_{\text{ang},n}$ for $n \in \mathbb{R}^N$). As mentioned in definition 1, the other state variables can be calculated from them by using Equations 3.15-3.19.

The required inputs for the Bayesian state estimation algorithm are:

- The grid topology, which includes line connections and switching states, and the grid parameters. From this, $\boldsymbol{Y}_{\text{bus}}$ can be built, which is necessary for the linearized power flow transformation to calculate $\Phi_{V_{\text{pr}}}$ (see Equation 3.45) and for possible node power measurements in $h(x)$ and H. Further, $\boldsymbol{Y}_{\text{f}}$ and $\boldsymbol{Y}_{\text{t}}$ can be calculated, which are needed for various branch measurements in $h(\boldsymbol{x})$ and $\boldsymbol{H}$.
- The real-time measurements $\boldsymbol{z}$, their uncertainties $\boldsymbol{\sigma}_z$ and the measurement type and element. Together with the bus and branch admittance matrices, the measurement uncertainties, type and element information are necessary to generate the likelihood distribution $\Phi_{z|x}$.
- The non-real-time meter data to generate the background distribution of loads Φ_S.

A dashed line frames the part for the online[7] state estimation. The prior and the measurement distribution can be calculated offline, whereas the state is updated every time new real-time measurements are available. The Bayes step is illustrated in the small exemplary graph in Figure 3.3.

Summary: The state estimation algorithm for MV grids in this thesis is set on analytic Bayesian algorithm (see Section 3.2). The algorithm has been described in detail in Section 3.3.2, and the single steps are given in an overview chart in the current section. Finally, a short section follows, where the equations of the Bayesian approach are compared to the most widely used state estimation approach for TS.

[7] "*Online estimation algorithms estimate the parameters and states of a model when new data is available during the operation of the physical system.*" [100]

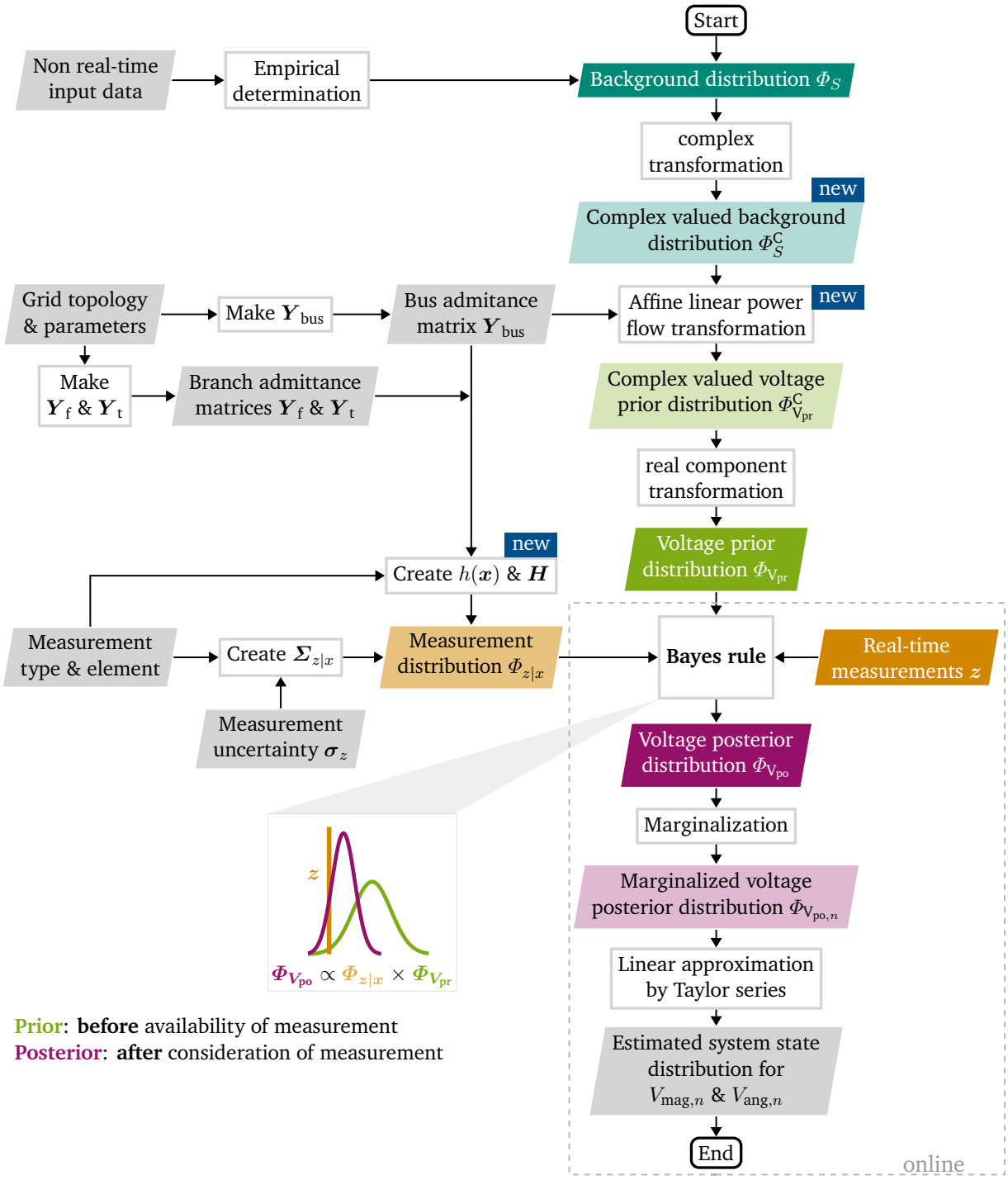

Figure 3.3: Flow chart of proposed Bayesian Linear State Estimation algorithm. The blue marked steps are added or adapted to the work of [94]. As mentioned at the beginning of section 3.3, with these adaptions it is possible to incorporate branch capacities in the linearized power flow equation, to consider load correlations, and to utilize all measurable variables from PMUs and RTUs.

3.4 Comparison of Bayesian to Benchmark State Estimation Algorithm

In this thesis, the widely used state estimation approach for TS grids is selected as benchmark state estimation algorithm. It solves the WLS objective function by using the iterative Gauss Newton algorithm. The solving scheme is given in the following Subsection. After this, the Bayesian based objective functions MAP is compared to the WLS objective function from the benchmark approach.

3.4.1 Benchmark State Estimation Algorithm

As mentioned in Section 3.2.1, the WLS objective function aims to minimize the squared sum of residuals weighted by the standard deviation of measurements. In the conventional approach, it is assumed that all measurements are uncorrelated. Hence the covariance matrix is, in fact, a diagonal matrix, i.e. $\boldsymbol{W}^{-1} = \text{diag}(\frac{1}{\boldsymbol{\sigma}_e})^2$.

$$\hat{\boldsymbol{x}}_{\text{WLS}} = \arg\min_{x} \left[(\boldsymbol{z} - h(\boldsymbol{x}))^T \boldsymbol{W}^{-1} (\boldsymbol{z} - h(\boldsymbol{x})) \right] \tag{3.77}$$

This objective function $J(\boldsymbol{x}) = \hat{\boldsymbol{x}}_{\text{WLS}}$ is solved iteratively with Gauss-Newton function [24]. To find $\boldsymbol{x}$ that minimizes J, the first-order derivation of J according to $\boldsymbol{x}$ has to be satisfied:

$$g(\boldsymbol{x}) = \frac{\partial J(\boldsymbol{x})}{\partial \boldsymbol{x}} = -\boldsymbol{H}^T \boldsymbol{W}^{-1} [\boldsymbol{z} - h(\boldsymbol{x})] \stackrel{!}{=} 0 \tag{3.78}$$

$$\boldsymbol{H} = \frac{\partial h(\boldsymbol{x})}{\partial \boldsymbol{x}} \tag{3.79}$$

Due to non-linear measurement function $h(\boldsymbol{x})$, the results can not be calculated in closed form. Hence, $g(\boldsymbol{x})$ is linearized around $\boldsymbol{x}_k$ by using linearized Taylor series (see Equation A.4 in appendix A.2.2). The Gauss-Newton iteration uses an approximated gain matrix $\boldsymbol{G}(\boldsymbol{x})$, which neglects the higher order terms[8].

$$g(\boldsymbol{x}) \approx g(\boldsymbol{x}_k) + \boldsymbol{G}(\boldsymbol{x}_k)(\boldsymbol{x} - \boldsymbol{x}_k) \stackrel{!}{=} 0 \tag{3.80}$$

$$\boldsymbol{G}(\boldsymbol{x}_k) = \frac{\partial g(\boldsymbol{x})}{\partial \boldsymbol{x}} \approx \boldsymbol{H}^T(\boldsymbol{x}_k) \boldsymbol{W}^{-1} \boldsymbol{H}(\boldsymbol{x}_k) \tag{3.81}$$

The iterative solution scheme for Gauss-Newton method with iteration index k is then given by:

$$\boldsymbol{x}_{(k+1)} = \boldsymbol{x}_k - [\boldsymbol{G}(\boldsymbol{x}_k)]^{-1} \cdot g(\boldsymbol{x}_k) \tag{3.82}$$

The algorithm converges if $\Delta \boldsymbol{x} = \mid \boldsymbol{x}_{(k+1)} - \boldsymbol{x}_k \mid$ is smaller than a given tolerance.

[8] Netwon-Raphson iterations take the second-order terms into account. For this, it has higher computational costs.

3.4.2 Comparison of Maximum-A-Posterior and Weighted Least Square Approach

Bayesian state estimation methods can generally be used to calculate a full probability distribution of system state variables. As the benchmark approach has only a deterministic output, its estimate can not be compared to the entire posterior distribution but to e.g., the Maximum-A-Posterior estimate (MAP). MAP aims to find x that maximizes the posterior probability $p(x \mid z)$. By (3.29), this is equivalent to finding x that maximizes the product of the likelihood $p(z \mid x)$ and the prior ("pr") probability $p(x)$ (3.84), since the marginal measurement probability $p(z)$ acts as a normalizing constant.

$$\hat{\boldsymbol{x}}_{\text{MAP}} = \arg\max_{x} p\left(\boldsymbol{x} \mid \boldsymbol{z}\right) \tag{3.83}$$

$$= \arg\max_{x} p\left(\boldsymbol{z} \mid \boldsymbol{x}\right) p\left(\boldsymbol{x}\right) \tag{3.84}$$

For (multivariate) normal Gaussian distributions, finding x that maximizes the posterior distribution Φ_{po} is equivalent to finding x that minimizes the negative sum of the exponents of the likelihood $(\boldsymbol{z}-\boldsymbol{\mu}_{z|x})^T \boldsymbol{\Sigma}_{z|x}^{-1}(\boldsymbol{z}-\boldsymbol{\mu}_{z|x})$ and the prior distribution $(\boldsymbol{x}-\boldsymbol{\mu}_{x_{\text{pr}}})^T \boldsymbol{\Sigma}_{x_{\text{pr}}}^{-1}(\boldsymbol{x}-\boldsymbol{\mu}_{x_{\text{pr}}})$ (see Equation 3.61).

$$\hat{\boldsymbol{x}}_{\text{MAP}} = \arg\max_{x} \Phi_{x_{\text{po}}} \tag{3.85}$$

$$= \arg\min_{x} \left[(\boldsymbol{z}-\boldsymbol{\mu}_{z|x})^T \boldsymbol{\Sigma}_{z|x}^{-1}(\boldsymbol{z}-\boldsymbol{\mu}_{z|x}) + (\boldsymbol{x}-\boldsymbol{\mu}_{x_{\text{pr}}})^T \boldsymbol{\Sigma}_{x_{\text{pr}}}^{-1}(\boldsymbol{x}-\boldsymbol{\mu}_{x_{\text{pr}}})\right] \tag{3.86}$$

Further, for normal Gaussian distributions, the MAP estimate is equal to the expectation value of the posterior distribution $\boldsymbol{\mu}_{x_{\text{po}}}$ and hence equal to the MMSE defined by

$$\hat{\boldsymbol{x}}_{\text{MMSE}} = \mathbb{E}\left[\boldsymbol{x} \mid \boldsymbol{z}\right] = \boldsymbol{\mu}_{x_{\text{po}}} = \hat{\boldsymbol{x}}_{\text{MAP}}. \tag{3.87}$$

The first multiplier of MAP is the likelihood function. The Maximum-Likelihood (ML) estimator ($\hat{\boldsymbol{x}}_{\text{ML}}$) maximizes the conditional probability for $\boldsymbol{x}$ given $\boldsymbol{z}$ (3.88).

$$\hat{\boldsymbol{x}}_{\text{ML}} = \arg\max_{x} p\left(\boldsymbol{z} \mid \boldsymbol{x}\right) \tag{3.88}$$

$$= \arg\max_{x} \left[(\boldsymbol{z}-\boldsymbol{\mu}_{z|x})^T \boldsymbol{\Sigma}_{z|x}^{-1}(\boldsymbol{z}-\boldsymbol{\mu}_{z|x})\right] \tag{3.89}$$

If in the Maximum-A-Posterior Equation 3.83, the prior distribution is assumed to be uniform and thus $p(\boldsymbol{x})$ is a constant for all x, then $\hat{\boldsymbol{x}}_{\text{MAP}} = \hat{\boldsymbol{x}}_{\text{ML}}$.

Assuming normal distributions, independence and homoscedasticity of measurement errors, and $\boldsymbol{\mu}_{z|x} = h(\boldsymbol{x})$, then the WLS objective function equals the ML objective function [101].

Hence, for the assumption of a uniform prior distribution (MAP equal ML) together with the above assumptions, the objective function of MAP is equal to WLS. Figure 3.4 compares ML, WLS and MAP for varying modeling assumptions.

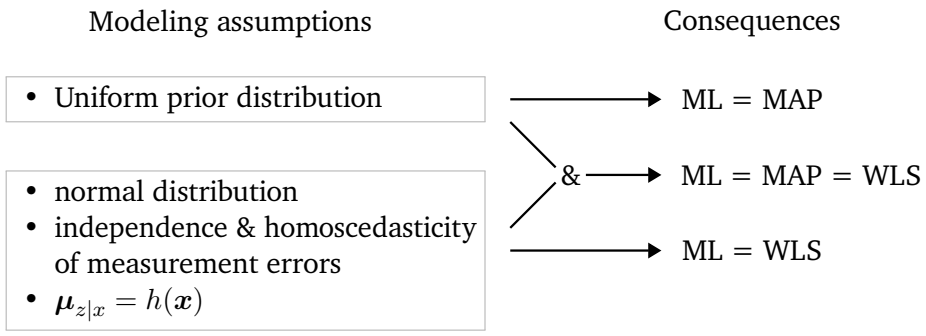

Figure 3.4: Comparing ML, MAP and WLS for different modeling assumptions

Instead of neglecting the prior distribution or assuming it uniform, the WLS objective function can also be extended to equal the MAP estimate: The Extended Kalman Filter[9] (EKF) [103] adapts the WLS by a forecast state (prior knowledge) in such a way that it is equal to the MAP estimate. Hence, MAP and the EKF can be used equivalently as objective function for state estimation algorithms.

[9]The Kalman filtering recursively updates its estimates based on new measurements [102].

4 Method - Bayesian State Estimator for MV Grids

This chapter compares the Bayesian state estimation methods from literature according to the requirements defined in research question 1. One of the requirements for the state estimation method is to consider the uncertainties of the input data and its varying temporal availability. Hence, before the literature analysis, the inputs for Bayesian state estimations must be analyzed in more detail (see Section 4.1). From the subsequent literature review, the research gaps result for Bayesian state estimation methods in MV grids. To face these research gaps, two new modules are developed here that complement the selected basis algorithm (Bayesian linear state estimation algorithm) described in the previous chapter.

4.1 Input of Bayesian State Estimation Methods for MV Grids

The inputs for the Bayesian state estimator have already been mentioned in Subsection 3.3.3. They include the grid topology and parameters, the non-real-time data for background distribution, and the real-time measurements. The real-time measurements and the non-real-time inputs are distinguished according to the following definitions:

- Real-time measurements: Measurements from the field that are available to the system operator within seconds. Each time new real-time measurements are available, a new state estimation run is performed (see online state estimation in Subsection 3.3.3).
- Non-real-time data: Data that is only available to the system operator minutes to months after the actual measurement or comes from forecasting tools or exogenous data sources such as weather measurements. This data is used in the background distribution of the Bayesian linear state estimator.

In the following, different real-time measurement devices are compared in terms of measurable values, measurement accuracy, and temporal consistency. It continues with an overview of different non-real-time inputs for the background distribution and a deep dive into its correlation properties. The last subsection concerns practice-relevant considerations for the grid topology of test grids.

4.1.1 Real-Time Measurements

In MV grids, real-time measurements are usually only taken at HV/MV substations and at central MV nodes [45]. In addition to widely used RTU data, more and more PMUs are installed in the power grids [104]–[106]. RTUs measure a set of system variables including V_{mag}, I_{mag}, P or Q measurements, while PMUs measure the complete voltage or current phasors (V, I). Due to the additional angle measurement, PMUs require an accurate time synchronization. For this, a global positioning system (GPS) receiver connected to the PMUs is required. In addition, PMU devices have high-quality sensors, for which their overall measurement accuracy is at least one order of

magnitude higher than for RTUs[1]. The highly precise PMUs are more expensive than RTUs, mainly due to the expensive high-speed core processor and GPS equipment. The main differences between RTU and PMU technologies are summarized in Table 4.1 [105], [107], [108].

Table 4.1: Comparison of RTU and PMU devices

	RTU	**PMU**
Magnitude measurement	✓	✓
Phase measurement		✓
Time synchronization		✓
Time resolution	$1\,\text{ms}$ - $1\,\text{s}$	$0.001\,\text{ms}$
Measurement device uncertainty	mostly 0.2 - $1.5\,\%$	mostly $< 0.05\,\%$
Phase deviation		0.01 - $0.05°$
Advantage	more cost effective	accurate time synchronization

In the future, so-called micro-PMUs (μ-PMU) will be promising real-time measurement devices in MV grids. They are one order of magnitude cheaper than PMUs by replacing the expensive high-speed processor with low-cost microprocessors [109], [110]. They are claimed to have standard deviations of $0.05\,\%$, and $0.01°$ and benefit from possible angle measurement if connected to a GPS receiver [111], [112]. Currently, there are only a few μ-PMUs implemented.

To generate the likelihood distribution, the uncertainty of the real-time measurements is required (see Equation 3.57). In the field, measurement devices are connected to instrument transformers, which also cause measurement uncertainties. Consequently, not only the measurement device itself (RTU or PMU) is decisive for the uncertainty of a measurement value [113]. For this, the state estimation method must consider the end-to-end uncertainty of the entire measurement chain. This is analyzed in the following.

End-to-End Real-Time Measurement Uncertainty Analysis

For the accuracy of the state estimation result, the quality of the real-time measurements plays an important role. The quality of the real-time measurements depends on the measurement accuracy and temporal consistency. The accuracy of a measured value depends on all devices in the measurement chain, which is exemplary given in Figure 4.1.

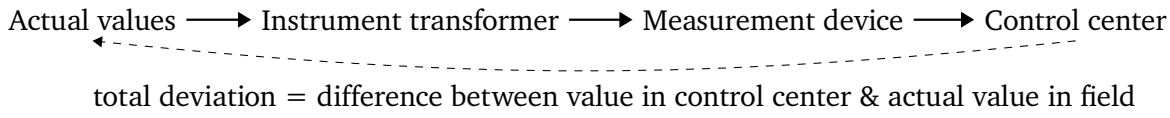

Figure 4.1: Measurement chain: from actual values to values received in the control center

[1]The high accuracy, together with the high reporting rate, allows observation of transients, which is important for frequency stability in (ultra) HV levels.

The difference between the value received in the control center and the actual value in the field is the total measurement error. Hence, for the uncertainty of a measurement value, the uncertainties of all chain elements must be considered. The resulting measurement accuracy thus includes the accuracy of the measurement device and the connected instrument transformer.

Instrument transformers are divided into current transformers (CT) [114] and voltage transformers (VT)[2] [115]. The accuracy of the instrument transformers depends on the materials of the core. Some cores are designed to provide high accuracy for measurement applications, and others are designed to be more robust for protection measures to provide reliable performance during fault conditions. The accuracy classes for instrument transformers are given in the IEC 61869 standard for current [114] and voltage [115] transformers. For measurement applications, the accuracy classes range from 0.1 to 3. The accuracy class number equals the maximum relative error for magnitude values in %[3]. The maximum relative errors for protection cores are between 1 and $3\,\%$ for CTs and 3 or $6\,\%$ for VTs, and thus are higher than with measurement core. Hence, real-time measurement devices for state estimation applications should be primarily connected to instrument transformers with measurement cores to achieve accurate results [4]. For further consideration, instrument transformers with a 0.5 measurement accuracy class are selected. In the accuracy classes, there is also a phase displacement given. For the 0.5 accuracy class, it is $0.33°$ for VT and $0.5°$ for CT.

Now, the accuracies of the **measurement devices** (RTU and PMU) are discussed. The so-called performance classes for RTUs are given in the IEC 61557-12 standard [116]. The performance class number corresponds to the maximum allowed relative deviations (equivalent to the accuracy class of instrument transformers). For voltage and current measurements, the performance classes range from 0.05 to 2. The performance classes for active power measurement lie between 0.1 and 2.5. For reactive power measurements, performance classes of 2 or 3 can be assumed. The accuracy of the PMU measurements is affected by the accuracy of the analog-to-digital converter [107], the central processing unit [117], and the GPS receiver [118]. The synchrophasor standard IEEE C37.118.1 [119] defines a maximally allowed total vector error of $1\,\%$ [120]. Hence, for zero phase deviations, the allowed magnitude deviation is $1\,\%$, and for zero magnitude deviation, the allowed phase deviation is $0.47\,°$ ($= 26\,\mu s$). In reality, none of them is zero. To not violate any of the magnitude or angle limits, the PMUs are designed to reach higher accuracies: In literature and data sheets, the standard deviation for PMUs is given between 0.01-$0.06\,\%$ for magnitude measurements and 0.01-$0.05\,°$ for phase deviation [121]–[124].

For generating the covariance matrix of the likelihood distribution for Bayesian state estimation, the standard deviations of measurement errors are necessary. For this, the standard deviation for exemplary PMU and RTU measurement chains is calculated. Each measurement chain consists of the standard deviation of the measurement device and instrument transformer. The instrument transformer is assumed to have the accuracy class 0.5 and RTU to have the performance class 0.5 for V & I and 1 for P & Q. As the values for instrument transformers and RTUs are given as maximum thresholds, they first must be transformed to standard deviation values. According to [125], [126], it is assumed that the given maximum error covers $95\,\%$ of all measured values.

[2] VTs are also called potential transformers (PT).

[3] For CT, there are higher deviations if the measured current is $< 20\,\%$ of rated primary current.

[4] If a measurement device should be installed where a protection device is already available, the measurement device is mostly connected to the existing protection instrument transformers for economic aspects.

Assuming normally distributed measurement errors, the error interval is consequently in the range of $\mu_e \pm 1.96\,\sigma_e$. For this, the maximum deviation values from the standards are divided by a factor of 1.96 to reach the value for one standard deviation. The PMUs' standard deviations are assumed to be $0.02\,\%$ and $0.02\,^\circ$ from literature analysis. The combined standard deviation for the measurement chain is calculated by the root sum of squares with the assumption of statistically independent errors. The results are rounded to one decimal place and are given in Table 4.2.

Table 4.2: Comparison of standard deviations for RTU and PMU measurement chains with 0.5 accuracy class for instrument transformer and RTU performance class 0.5 for V & I and 1 for P & Q. Standard deviation of PMU are assumed to be $0.02\,\%$ and $0.02\,^\circ$.

	PMU chain		RTU chain	
	V	I	V & I	P & Q
magnitude deviation in %	0.2	0.2	0.4	0.6
angle deviation $^\circ$	0.2	0.3	-	-

In Table 4.2, the end-to-end standard deviations for PMU and RTU measurement chains for node voltage and branch current magnitude measurements differ only by $0.2\,\%$. The reason is that the major part of the uncertainty of the PMU chain results from the instrument transformer. Hence, for actual values from the field measured by a PMU directly connected to an instrument transformer, the high accuracy of the PMU device itself is, therefore, not fully effective. In the example given in the table above, the factor of improvement for PMU over RTU from individual devices to devices within a measurement chain reduces from 10 to 2.

In addition to the measurement accuracy, the quality of the real-time measurements depends also on the temporal consistency. For PMUs, the temporal consistency is high for two reasons: once for the time stamps given to the values by the GPS receiver and twice for low latencies prescribed by communication protocols. The PMU sends data mostly via Ethernet connection to the phasor data concentrator with IEEE C37.118.2 protocol [127], and the phasor data concentrator sends the data forward to the control center with the ICCP protocol [120], [128]. The RTU transmits the data to the Supervisory Control and Data Acquisition (SCADA) system via wired (e.g., Ethernet, RS-485) or wireless (e.g., Wi-Fi, cellular) connections based on IEC 61850 and IEC 60870-5-104 standards [105], [129]. The RTU measurements do not receive time stamps in the measurement device, only when received in the control center. Hence, the delay time caused during transmitting the measured values from the measurement location to the control center is the determined value for temporal consistency. Since the exact measurement time for RTU is not known, the non-synchronized RTU data leads to problems in the temporal allocation for state estimation applications and thus to measurement uncertainties.

Summary for Real-Time Measurements

In summary, PMU devices have higher (about one order of magnitude) accuracy than RTU devices. While RTUs are more cost-effective, PMUs have the advantage of additional angle measurement and time stamps, resulting in higher temporal consistency. Another way to obtain real-time measurements is to use μ-PMUs. They offer a good balance between cost and time consistency.

Future developments and tests in the field will show their applicability for MV grid state estimation. In practice, real-time measurement devices in the field are connected to instrument transformers. The uncertainty caused by the instrument transformer is mostly the determining factor for the accuracy of the measurement chain. Hence, for state estimation, the end-to-end uncertainty of the entire measurement chain must be considered and not only the standard deviation of the measurement device. As MV grids have different real-time measurement configuration, only RTU or PMU or combined, the Bayesian state estimation method should be able to process all measurable quantities of these both devices.

4.1.2 Non Real-Time Measurements

As mentioned in 2.2, the low coverage with real-time measurement in MV grids can be partly compensated using additional data sources. The additional non-real-time data is used to generate the background distribution, which is then used to calculate the voltage prior distribution for the Bayesian state estimation algorithm.

For MV nodes, where a large customer is directly connected, usually time-resolved historical power series (German: Registrierende Leistungsmessung, RLM) are available. The RLMs are mandatory for large, mostly commercial customers whose yearly energy demand is greater than 100 MWh [130]. Their power consumption is typically recorded in 15 min intervals. Furthermore, large commercial RES plants that are directly connected to MV nodes and receive EEG remuneration[5] must provide the grid operators electricity feed-in data annually [4]. According to the EEG, the feed-in tariff in Germany is usually settled in 15-minute intervals. Therefore, the feed-ins must also be recorded in 15 min resolution.

For MV nodes with underlying LV grids, power series directly measured at the MV nodes are not available (except if a real-time measurement is placed there). However, in the underlying LV grids, there are time-resolved power series from customers equipped with a Smart-Meter (SM). A SM is a digital meter combined with a so-called SM-gateway to transmit the power measurements digitally to the system operator[6]. These are typically recorded in regular intervals, e.g., in the European Union at least every 15 minutes [132]. The recorded SM measurements can be used aggregated for estimating the power series of the connected MV nodes described in detail later. Customers connected to LV grids without SM-gateways only report annual consumption values from analog or digital meters. System operators conventionally estimate the power consumption of these non-metered grid users by standard load profiles (SLPs). SLPs are 15-minute time-resolved power time series for one year, typically representing the average of a consumer group [133]. A further source of additional input can be gained from weather measurements. The power generation from PV or wind turbines can be calculated by solar irradiation or wind velocity measurements. Further data sources can be PV converters, heat pumps or EV charging stations.

[5] The beneficial remuneration of RES plants in Germany is determined by the Renewable Energy Sources Act (EEG).

[6] In Germany, the implementation of SM gateways is mandatory until 2032 under certain conditions. This relates to grid customers with annual energy demand between 6 and 100 MWh, plant operators with an installed capacity of 7 to 100 kW, and customers with controllable loads such as HP or night storage heating [131].

The above mentioned non-real-time data sources are summarized:

- Time-resolved recorded power measurements (RLM), which are mandatory for large customers whose yearly energy demand is greater than 100 MWh. Such customers are mostly directly connected to MV nodes.
- Time-resolved feed-in measurements from large renewable energy units directly connected to MV nodes.
- Smart-Meter measurements from underlying LV grids typically recorded in regular intervals. SMs are digital meters communicating to the system operator via an SM-gateway.
- Annual energy demand from analog or digital meters from customers with no SM or RLM measurement.
- Standard load profiles (SLP), which are power time series for one year in 15 min resolution. They typically represent the average of its consumer group.
- Data from exogenous sources like solar irradiation or wind velocity measurements to estimate generation from PV or wind turbines.
- Data from PV converters, heat pumps or EV charging stations.

Depending on future technological developments this list can be further extended, e.g. data from mobile apps including social media.

In Figure 4.2, the available power measurement data for MV grid state estimation are exemplary shown. Historical power profiles can be obtained from recorded real-time measurements (orange), RLM and commercial RES measurements (blue), or from SMs (green) in underlying LV grids.

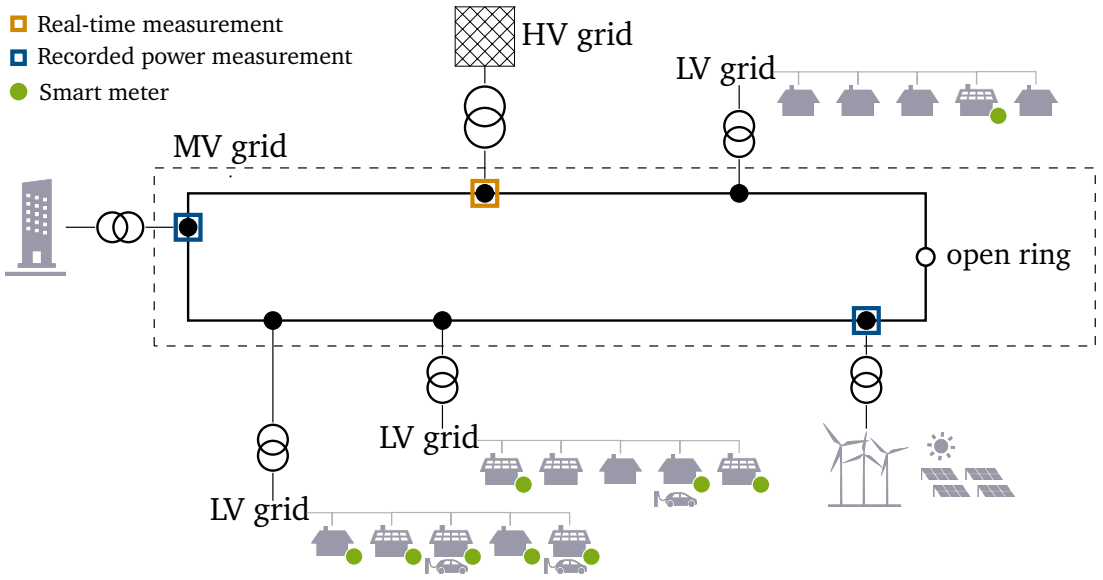

Figure 4.2: Exemplary MV nodes with different available power measurement data

The non-real-time measurement data varies strongly in its levels of detail: from 15-minute time-resolved power measurement to only annual energy values. Since most MV nodes have LV grids connected to them and their local grid transformer is usually not directly metered, the availability of time-resolved data strongly depends on the SM coverage in the underlying LV grid. To give an order of magnitude on how many customers are equipped with SM measurements, which are then available to DSOs for state estimation as background information, an overview of the SM coverage for European countries and US states is given in the following.

Smart Meter Coverage

Only a few European countries or US states have near 100 % SM coverage. With the Third Energy Package (European Union, 2009), European member states are required to implement SMs. The currently achieved SM coverage differs strongly for European countries [134], [135]. Sweden, Norway, Spain, and Italy have an extremely high SM coverage of over 97 %. Conversely, Poland, Hungary, and Slovakia have coverage smaller than 10 %. For Germany, the SM coverage ranges between 2 % and 15 % across DSOs [7]. Similarly, in the US [136], the SM coverage for Utah and New Mexico is below 20 % while California, Nevada, Georgia, and Washington State achieve high coverage over 80 %. New York State and West Virginia have rates between 20 and 40 %.

In summary, for US- and European grids, only a few countries or states have nearly 100 % SM coverage. Hence, in most countries, there is a substantial number of customers for which only annual energy consumption is known. Consequently, combined non-real-time data with varying levels of detail (from detailed readings (SM, RLM, and commercial RES) to aggregated yearly consumption only) should be considered as input for MV grid state estimation as it represents realistic conditions for data availability.

Correlations

It is important to note that state variables in a power system are not statistically independent. If, for instance, the voltage magnitude at one node increases, the voltage magnitude at the neighboring nodes often increases as well. These correlations are valuable for state estimation because they allow one to use data from one node to infer information about other nodes, particularly unmeasured ones. These node voltage correlations originate from two different causes:

1. **Physical correlation** is caused by the physical coupling of the grid, for example, by a high voltage at one grid node being transmitted via a line to another node.

2. **Load correlation** is caused by similar behavior of grid customers independent from the grid, i.e., even for electrically unconnected customers. Load correlation of grid customers includes both consumer and generation behavior. Regarding generation units, in particular, volatile RES (PV and wind) are highly correlated in space and time. An example of consumption behavior causing high load correlations: If it is a warm day, the power consumption for air conditioning will be higher than the historical average for all households simultaneously. This will cause a voltage drop in different grid segments that may not even be physically connected.

[7] The delay of German SM roll-out is due to strict data protection regulations and security issues.

The load correlations can be considered in the background distribution, i.e., the load probability distribution of the connected loads and generation units. Properly accounting for these load correlations in the state estimation process can drastically improve the accuracy of the state estimation results [137] [138]. Therefore, it is essential to consider the load correlations in the state estimation input.

Between the real-time measurements also exist correlations. However, the authors in [137] find out that incorporating the real-time measurement correlations achieves only a small benefit, particularly in comparison with load correlations.

4.1.3 Grid Topology

Another highly relevant input to Bayesian state estimation approaches is the grid topology. For a realistic scale of the grid, the number of substations should be in realistic order of magnitude (about 80-200 [139]). As most of the MV grids in Germany have ring structures (see Section 2.2), partly also operated as closed rings, a state estimation method for MV grids should be able to deal with non-radial structures. As also mentioned in Section 2.2, there are possibly phase imbalances in MV grids, for which a three-phase model would be reasonable. However, despite of some special cases, they can often be neglected for the discussed reasons, given in Section 2.2. One further point concerns the uncertainty of grid topology[8]. However, since many switching states in MV grids are not reported digitally [1], having a topology identification before the actual state estimation can be helpful [140]. With such a topology estimation preceding the actual state estimation step, the grid topology can be assumed to be known. If this is not given, the grid uncertainties should usually be considered in the input for MV grid state estimation.

4.2 Comparison of Bayesian State Estimation Methods for MV Grids in Literature

Bayesian state estimation approaches are now compared according to the method requirements defined in research question 1. First, the comparison criteria are defined. Secondly, a literature review of Bayesian state estimation methods for MV grids is given. This results in the research gaps of MV grid Bayesian state estimation methods. Thirdly, the research gaps considered in this thesis are exposed.

4.2.1 Comparison Criteria

According to research question 1, MV grid state estimation methods should be efficient, practical, and uncertainty-aware. These requirements are now reformulated as discrete comparison criteria:

Efficient

One defined requirement is to obtain the state estimation results **near real-time**. So the methods from the literature are compared according to achieve computation times **smaller than 60 s**. Another requirement is to achieve **accurate** results with a focus on detecting limit violations. For

[8] As already mentioned in 2.2, to focus on state estimation topology identification is not a topic in this thesis.

this purpose, the output must be **evaluated with respect to limit violations** and **checked for correct identification**. A detection rate of at least 90 % should be achieved.

Practical

The requirement for practical state estimation methods for MV grids demands that the method is feasible despite the low level of measurement instrumentation. Hence, the method should handle realistic available types and amounts of measurements and consider realistic MV characteristics of grid topology. For assuming practice-relevant MV grids, the Bayesian state estimation method should consider a **realistic grid-scale** (>80 buses) and be able to **deal with ring structures**. For completeness, the methods are also compared according to 3-phase modeling and uncertainty in grid topology, even if assumed negligibly small for this thesis. Concerning the real-time measurement input, the method should be able to process **all measurable variables** from both mostly implemented real-time measurement devices (PMU and RTU). Hence, the methods are compared if these are considered. The non-real-time inputs are compared for involving **smart meter data, weather data, and annual energy demand**. A further criterion in this context is if the method considers the mostly **varying temporal availability** of the non-real-time data. The literature approaches are also compared to consider load and measurement **correlations** in the non-real-time input for the background distribution.

Uncertainty-aware

The last requirement is to consider the **posterior variances for evaluation** in addition to the expectation values.

4.2.2 Literature Review of Bayesian State Estimation Methods for MV Grids

A few Bayesian state estimation methods using the Bayes rule to fuse the scarce real-time measurements with various background inputs have already been proposed in literature. For each paper, the main idea is summarized shortly. Then, the papers are compared according to the previously defined comparison criteria. Although this thesis focuses on analytical Bayesian state estimation algorithms (see Subsection 3.2.2), methods based on machine learning and iterative approaches are also included in the review. In principle, machine learning and iterative Bayesian state estimation approaches can also handle probability distributions, and thus, they are considered in this comparison for completeness.

[81], [94], [141]–[143] propose methods for analytic Bayesian state estimation methods.
In [94], the basic principle for Bayesian Linear DSSE is demonstrated for a radial, 15 buses, 11 kV grid. The authors assume full SM coverage to generate the background distribution. They analyze the accuracy of state estimation results as a function of varying numbers of PMU measurements. The calculations are executed with normal Gaussian distributions, and load correlations are not considered. [141] proposes a method that overcomes the simplification of uncorrelated customer behavior by considering the load correlations calculated from historical data. For this, the authors use the complex form of the multivariate normal distribution. They demonstrate their method for a radial 11 kV grid with 747 buses. They validate their approach with different measurement scenarios for RTU data and achieve computational time below 3 seconds. [142] developed the method to use non-Gaussian distributions for load modeling by applying model matching with

known distributions and empirical distribution fitting. The method considers load correlations of SM data by using copulas for the background distribution[9]. They assume uniformly distributed measurements and incorporate PMU and RTU measurements. They demonstrate the method on a $20\,\mathrm{kV}$ feeder with only 5 buses. In [81], the load modeling is done by Gaussian Mixture. The authors consider RTU and PMU measurements and correlations of historical load data. They tested the method for the IEEE 14, 30 and 118 bus systems. Even for the 118 bus system, they achieve computational time below 1 second. There is also a proposal for an analytic three-phase Bayesian state estimation method [143]. The authors forecast load probability distributions based on historical load data. Instead of forward/backward sweep power flow equation, which is used by [94] and also in this thesis (see Equation 3.45), they use the *LinDist3Flow* model according to [145]. For real-time measurements, they assume PMU devices. The tests were executed on 37, 142, and 8500 bus systems.

In addition to analytic Bayesian approaches, there are papers combining machine learning with the Bayes rule [95], [146]. A neural network processes input data through different layers, adjusting connection strengths called weights to learn patterns and make predictions [147]. Compared to conventional neural networks with deterministic weights, Bayesian neural networks have probability distributions as weights. The model considers the load and measurement correlations. The tests in [95] were executed with RTU measurements. The method was demonstrated for a radial 85 bus LV grid and a meshed 3120 bus grid. [146] analyzed varying PMU measurements on a radial LV grid with 13 buses.

Examples of iterative Bayesian state estimation methods are given in [83], [148]–[150]. The authors used the belief propagation algorithm, which is a message-passing algorithm[10]. It is combined with a Bayesian network, a specific type of probabilistic graphical model using factor graphs. In all four papers, RTU measurements are used. [83] used additional PMU input. [83], [148] use historical load data to calculate a prior distribution. Both other papers start with broad prior distributions and assumed all nodes with voltage phasors for 1 pu and $0°$. [148] demonstrated the method on the IEEE 4 bus test feeder, whereas the authors of the other three papers chose larger varying IEEE test systems, e.g., IEEE 14 and 118. [83] explicitly tested the model for ring structure and investigated the computational times. One recently published iterative method [82] uses a Bayesian information fusion to combine data with different sampling rates from milliseconds up to 30 minutes time intervals. They consider SM, RTU, and PMU measurements and incorporate load correlations. The method is demonstrated for IEEE 123 and 342 bus systems and simulated for a real three-phase meshed Brazilian grid with 1058 buses.

Table 4.3 compares the Bayesian state estimation methods from literature according to the defined criteria from Subsection 4.2.1. For clarity, papers whose considerations are fully covered by another paper are not separately listed.

[9] The authors use Sklar's theorem [144], which states that the joint distribution of two variables can also be represented as the product of the copula of the variables and the marginals.

[10] The algorithm iteratively passes messages between neighboring nodes. At each iteration, the messages are updated based on the incoming messages. The update process is designed to refine the beliefs about the variables.

The results of this comparison can be summarized as follows:

- All papers assume to know the grid parameters and grid topology including the switching states. None considered uncertainty in the grid topology.
- Some discuss using weather data as input, but none have done so yet.
- Further, none of them considered customers with only annual energy demand information. All papers assume the non-real-time inputs for the MV nodes to be available fully time-resolved, e.g., full smart meter coverage or historical power series at every MV node. In view of the low coverage with time-resolved measurements (e.g., SM), this should be adapted to practically relevant measurements configurations.
- Concerning the output, most of the papers only take the expectation values of their posterior distributions as the estimates; thereby, they ignore important uncertainty information of the output. Two papers ([83], [142]) plot one exemplary estimate of the posterior variance, but they consider only the expectation values for the evaluation.
- None of the papers address the probabilistic post-processing of uncertainty information, which can be easily modeled in the Bayesian framework. The results are not further analyzed, e.g. to quantify the probabilities of operational limit violations.
- Moreover, none of the papers compare the estimates with limit violations, not even the expectation values.

The method developed in this thesis is also included in the comparison review of Table 4.3. That the ticked criteria are actually fulfilled will be proven in the results and discussed afterwards.

Table 4.3: Comparing Bayesian state estimation methods from literature according to criteria resulting from requirements defined in research question 1

	Compared criteria	[142]	[81]	[143]	[95]	[146]	[83]	[82]	thesis
Practice-relevant MV grids	Realistic scale		✓	✓	✓		✓	✓	✓
	Deals with ring structure				✓		✓	✓	✓
	3 phase/unbalanced			✓				✓	
	Topology uncertainty								
Realistic available measurement inputs	PMU measurements	✓	✓	✓		✓	✓	✓	✓
	RTU measurement	✓	✓		✓		✓	✓	✓
	Smart meter data	✓			✓			✓	✓
	Weather data								
	Annual energy demand								✓
	Non-real-time data with varying levels of detail								✓
Correlation consideration	Load correlation	✓	✓		✓	✓		✓	✓
	Measurement correlation				✓	✓			
Near real-time	Calculation time $< 60\,\mathrm{s}$	✓	✓	✓	✓	✓	✓	✓	✓
Uncertainty-aware evaluation	Consider posterior variance								✓
Identification of limit violations	Compare estimates to voltage band & thermal current limits								✓

4.2.3 Addressed Research Gaps in This Thesis

This thesis addresses the following research gaps:

- Considering customers with only **annual energy demand** information in addition to time-resolved non-real-time input: This thesis proposes a new method for the use of **non-real-time input with different levels of data availability** ranging from complete time-resolved measurement sets to yearly energy consumption data only.
- Evaluating **uncertainty-aware** identification of **limit violations**: In this thesis, a new method for processing Bayesian state estimation output is proposed. It focuses on identifying operational limit violations while considering the uncertainty of the output.

Figure 4.3 compares the considerations of this thesis graphically to the approaches from literature.

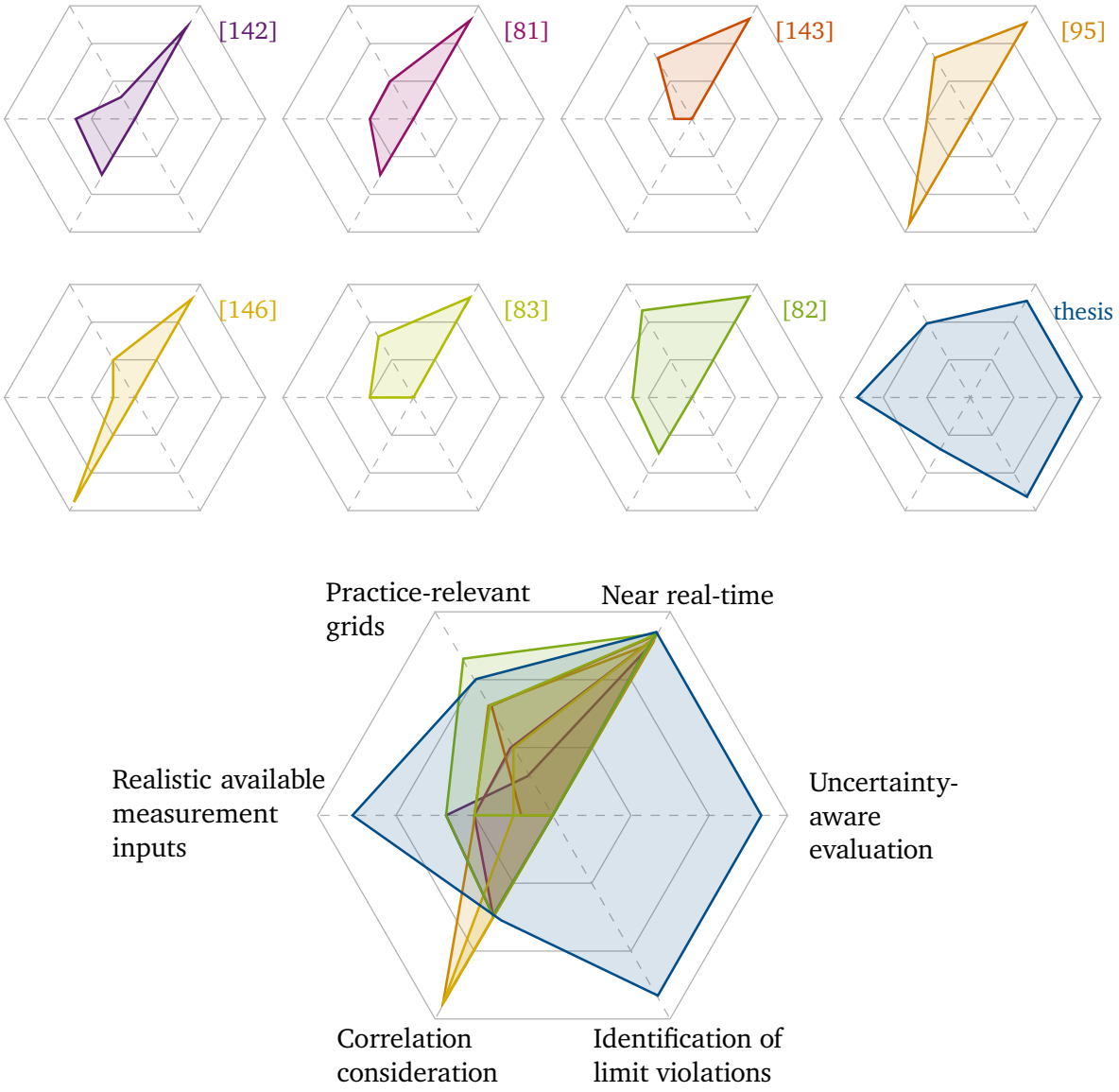

Figure 4.3: Graphical illustration of research gaps considered in this thesis

The colored areas represent the addressed topics of each paper. The corner points of the areas in Figure 4.3 derive from the comparison in Table 4.3. The compared criteria are clustered in six topics, given in the left column in Table 4.3 and put at the corners of the hexagon in Figure 4.3. The further out a corner point of a colored area reaches, the more the topic named at the corner is considered in this paper. The three levels in the hexagon represent that a topic is *partly, mostly or fully* considered.

Pre- and Post-Processing Modules

To address the above research gaps, the following two modules were developed:

- One **pre-processing module** is added, which generates the background distribution from non-real-time inputs. This statistics module is a newly proposed synthesis method for data sources with varying levels of detail. The synthesis incorporates load correlations, which significantly benefits the state estimation results.

- Further, one **post-processing module** is added after estimating the marginalized voltage posterior distribution. It calculates the probability of critical system states due to operational limit violations by using the uncertainty of the posterior variance. With this criticality analysis module a higher detection accuracy of limit violations can be achieved than with deterministic approaches.

Figure 4.4 shows the adapted Bayesian linear state estimation method. Blue rectangles mark the developed pre- and post-processing modules. The next section describes the post-processing module for calculating the probability of critical system states due to operational limit violations. The pre-processing module is proposed in the last section of this chapter. It is a correlation-aware synthesis module for input with varying levels of detail.

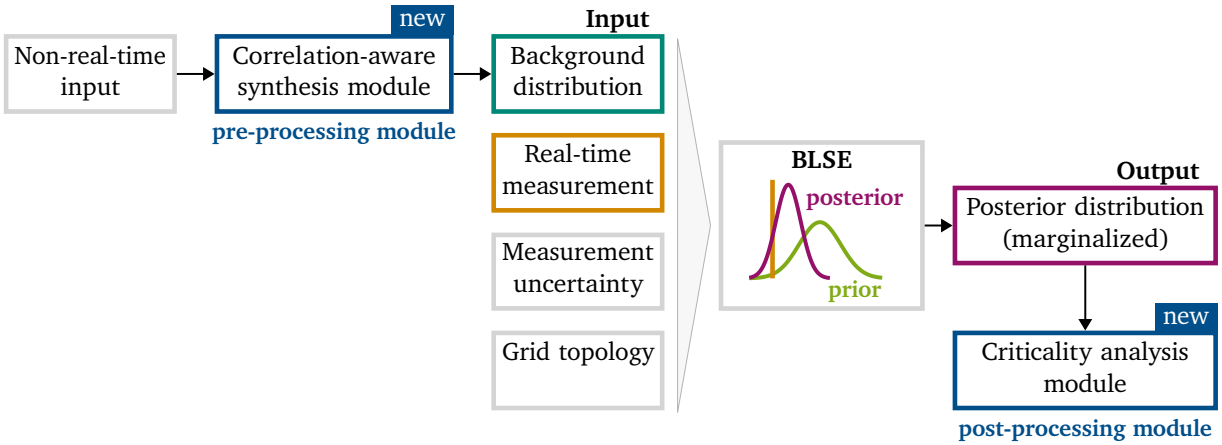

Figure 4.4: Adaption of Bayesian linear state estimation method (BLSE) with pre- and post-processing modules

4.3 Calculating the Probability of Critical System States due to Operational Limit Violations

According to research question 1, the developed MV grid state estimation method should aim to identify limit violations as accurately as possible. If an operational limit is violated, the system state is defined as critical (see Definition 2). Hence, identifying operational limit violations is assumed to be equal to identifying critical system states. Without sufficient real-time measurements, a deterministic statement about the system state is not reasonable. The methodology developed in this work therefore uses probabilistic modeling.

The new idea is to calculate the probability of critical system states to combine the uncertainty of the state estimation output with the identification of critical system states. This idea was introduced in [151], [152].

Idea: The area of a marginalized posterior distribution exceeding an operational limit equals the estimated probability of a system state being critical. This idea is illustrated in Figure 4.5.

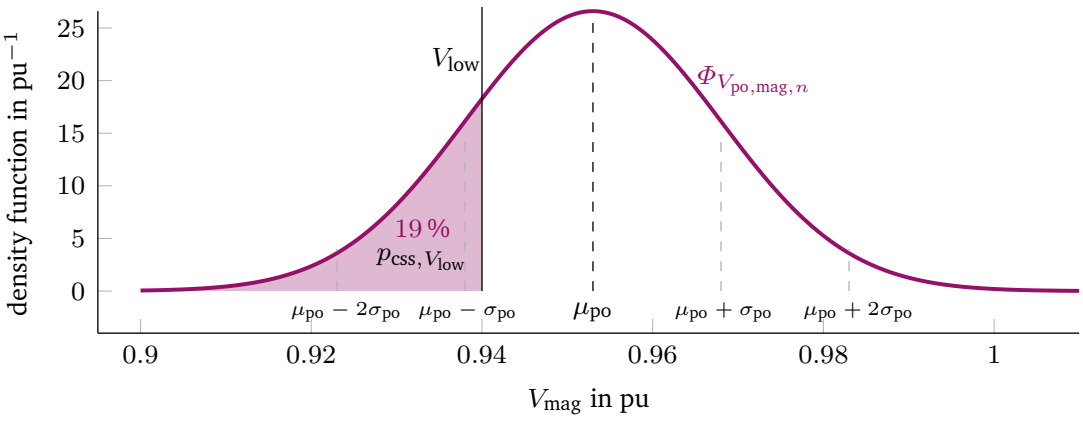

Figure 4.5: Probability of critical system state due to lower voltage limit violation

Figure 4.5 shows the critical system state regarding lower voltage band violation. The marginalized voltage magnitude posterior distribution $\phi_{\text{po},\text{V}_{\text{mag}},n}$ for bus n and a given lower voltage limit $V_{\text{low}} = 0.94\,\text{pu}$ is pictured. The colored area left to the limit is equivalent to the estimated probability of violating the given voltage limit $p_{\text{css},V_{\text{low}},n}$.

$$p_{\text{css},V_{\text{low}},n} = \int_{-\infty}^{V_{\text{low}}} \Phi_{V_{\text{po,mag},n}} dV_{\text{mag}} \cdot 100\,\% \tag{4.1}$$

This procedure can also be done for upper voltage limits. The probability of critical system states due to upper voltage limit violation $p_{\text{css},V_{\text{up}}}$ is equivalent to the area right to upper limit V_{up}. Hence,

the integral limits are set from V_{up} to ∞.

$$p_{\text{css},V_{\text{up}},n} = \int_{V_{\text{up}}}^{\infty} \Phi_{V_{\text{po,mag}},n} dV_{\text{mag}} \cdot 100\,\% \tag{4.2}$$

A critical system state can also be caused by overloading the operating equipment. Considering line and transformer thermal current limits I_{th}, it is necessary to know the posterior distribution of branch current magnitudes. An affine linear transformation by use of Equation 3.15 helps to transform the voltage to current posterior distribution $\Phi_{I_{\text{po}}}$. The resulting complex branch current posterior distribution is marginalized and transformed to polar form according to equations 3.72-3.76.

Hence, the probability of critical system state due to current thermal limit violation $p_{\text{css},I_{\text{th}},b}$ at branch b is defined by

$$p_{\text{css},I_{\text{th}},b} = \int_{I_{\text{th}}}^{\infty} \Phi_{I_{\text{po,mag}},b} dI_{\text{mag}} \cdot 100\,\% \tag{4.3}$$

The benefit of considering the entire posterior distribution instead of simply using the expectation values can be seen in Figure 4.5. In a situation where μ_{po} does not violate the given limit V_{low}, an expectation-value-based conclusion would be that there is no critical system state. Actually, there is a $19\,\%$ probability for critical system state, which is neglected by methods only considering expectation values.

Considering the entire posterior distribution is particularly important for state estimation in MV grids. To clarify the importance, a small example is given below. Figure 4.6 shows a lower voltage limit V_{low} and two voltage posterior distributions with different variances. The shown posterior variances depend on the uncertainty of the inputs. If the state estimation receives a high amount of only highly accurate measurements as the state estimators in TS, the posterior variance would be small as in Figure 4.6a. For this, the expectation value μ_{po} is a good approximation for the current state. Suppose the state estimation receives many uncertain input data, as is the case for MV grid with low real-time measurement coverage. In that case, the estimate has larger posterior variances, as exemplary shown in Figure 4.6b. For this, the single expectation value μ_{po} is no sufficient estimate.

Hence, for MV grid estimation methods with low real-time coverage and thus higher uncertainties in input and output, it is recommended to consider the posterior variances for identifying critical system states. A case study for calculating the probability of critical system states is given in Section 5.1.

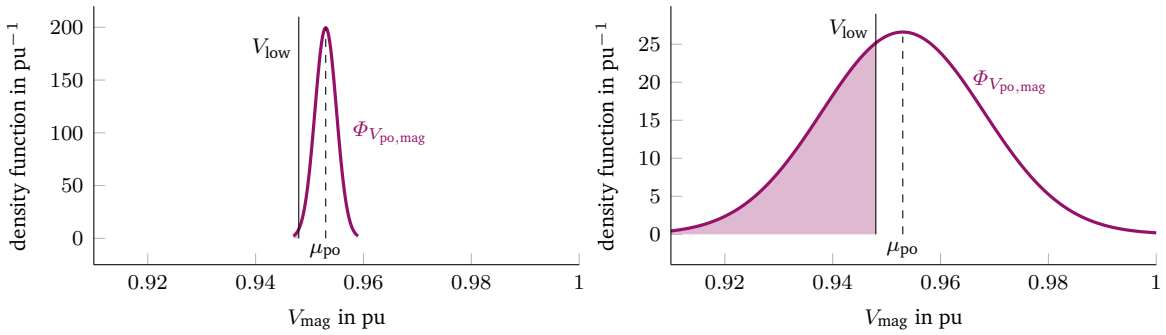

(a) Highly accurate inputs result in small posterior variances. For this, the expectation value is a good approximation for the state.

(b) Uncertain inputs result in larger posterior variances. For this, the single expectation value is no sufficient estimate.

Figure 4.6: Importance of considering the posterior variance of the Bayesian state estimation output when using uncertain input data

In the current section, the basic principle of the criticality analysis module has been described. Further, two additional points should be remarked:

1. The application of this post-processing module for calculating the probability of critical system states is not restricted to normal distributions. For generalization, it can be applied to every integrable posterior probability distribution, e.g., Gaussian Mixture or beta distributions.

2. In order to address research question 2, the probabilistic output can be processed for practical decision support. For this, a probability threshold p_{thres} is introduced. The threshold can be used to classify an element as critical, e.g., if the probability of critical system states for a node or branch element elements exceeds the given threshold. Further, multiple probability thresholds can be introduced to assign elements to warning and alert stages. This allows for greater sensitivity to near-critical conditions.

4.4 Correlation-Aware Synthesis Module for Input with Varying Levels of Detail

The pre-processing module proposed in this section aims to estimate the background distribution Φ_S for state estimation methods by combining non-real-time inputs with varying levels of detail and properly accounting load correlations. This module was introduced in [138], [153]. The following recorded non-real-time inputs are considered:

- Power measurement from real-time devices at MV nodes in 15 min resolution;
- 15 min time-resolved power measurements for large customers (RLM) and renewable generation units, which are directly connected to the MV grid;
- 15 min time-resolved SM measurements from underlying LV grids;
- Annual energy demand values for every costumer in underlying LV grid, which is not equipped with SM.

Further exogenous measurements can also be considered like solar irradiation measurements for power estimation of PV modules or wind velocity measurements for estimated power of wind turbines.

Assuming the case that time-resolved power series $S_{\text{MV},n,t}$ are available for an MV node n resp. $m \in \{1, .., N\}$ with time steps $t \in \{1, ..., T\}$, the parameters of the normal distributed background distribution $(\mu_{S_n}, \Sigma_{S_{nm}})$ can be easily calculated by the sample mean $\mu_{S,\text{samp},n}$ and sample covariance[11] $\Sigma_{S,\text{samp},nm}$.

$$\mu_{S,\text{samp},n} = \frac{1}{T} \sum_{t=1}^{T} S_{\text{MV},n,t} \tag{4.4}$$

$$\Sigma_{S,\text{samp},nm} = \frac{1}{T-1} \sum_{t=1}^{T} \left(S_{\text{MV},n,t} - \mu_{S_{\text{samp}},n}\right) \left(S_{\text{MV},m,t} - \mu_{S_{\text{samp}},m}\right) \tag{4.5}$$

Note that for normal distributions, the real and imaginary parts of the expectation value vector μ_S and the covariance matrix Σ_S are stacked as defined in Equation 3.39. In this chapter, such as in the equations above, the elements of the vector and matrix are first calculated for complex-valued apparent power for a more compact notation and divided into real and imaginary parts in the end.

Since, in reality, not every MV node has a time-resolved power series recording, the proposed module generates synthesized power series for unmeasured MV nodes. For this, the MV nodes at first differed depending on their available measurement information. They are classified into Measurement Instrumentation Scenarios (MIS). Then, for every MIS, a determination for time-resolved power series is presented. In the last step, the calculation of background distribution parameters from the power series is proposed. The steps for the correlation-aware synthesis module can be summarized as follows:

1. Classifying every MV node into a Measurement Instrumentation Scenario. The MIS scenarios are explained in detail in Subsection 4.4.1.
2. Determination of power time series for MV nodes according to their assigned MIS as described in Subsection 4.4.2.
3. Determination of background distribution parameters μ_S and Σ_S, which is explained in Subsection 4.4.3.

4.4.1 Measurement Instrumentation Scenario

In this subsection, each MV node is assigned to a Measurement Instrumentation Scenario according to the data availability. For a MV node, where no direct measurement information is available, measurements from the underlying LV grids can be taken into account. This is a justifiable assumption: if all customers in an LV grid are equipped with SMs, their summed-up demand would be approximately the demand at the connected MV node[12]. Hence, for classifying each MV node

[11] The formula for unbiased sample covariance is used: According to the Bessel's correction it must divided by $T-1$ instead of T.

[12] plus small line and transformer losses

according to its available data, further information is necessary: the assignment of connected LV nodes to their corresponding MV node given by grid topology and the smart meter coverage of the underlying LV grid. Further external information required is the type and index of measurements at the MV node. The classification for MV nodes into MIS is proposed in table 4.4.

Table 4.4: Classification of MV nodes into different Measurement Instrumentation Scenarios

Name	Description of MIS
$\mathrm{MV}_{\mathrm{meas}}$	Recorded measurement data at MV node
$\mathrm{SM}_{100\,\%}$	$100\,\%$ SM coverage in underlying LV grid
$\mathrm{SM}_{\geq \alpha_{\mathrm{thres}}}$	SM coverage $\geq \alpha_{\mathrm{thres}}$ in LV grid
$\mathrm{SM}_{< \alpha_{\mathrm{thres}}}$	SM coverage $< \alpha_{\mathrm{thres}}$ in LV grid

The first scenario ($\mathrm{MV}_{\mathrm{meas}}$) covers all MV nodes with recorded real-time measurements, with RLMs, and with feed-in measurements of commercial RES. Here, the meter devices are directly installed at the MV nodes. This usually only applies to the primary substation, central MV nodes or MV nodes with directly connected large customers. Most of the MV nodes are not equipped with a metering device, but historical data from the SMs of the underlying LV grids can be used as an information source. Three scenarios are defined for the underlying LV grids, corresponding to full, substantial, or low SM coverage. Here, a *low* SM coverage means that the set of customers with SMs cannot be assumed to be statistically representative of the behavior of all consumers. The scenario where the LV grid is fully covered with SMs is denoted by $\mathrm{SM}_{100\,\%}$. To differentiate between LV grids with *substantial* and *low* SM coverage, a threshold fraction α_{thres} is defined (e.g., $\alpha_{\mathrm{thres}} = 60\,\%$). Using this threshold fraction, the measurement instrumentation scenario $\mathrm{SM}_{\geq \alpha_{\mathrm{thres}}}$ represents grids where SM measurements are available for at least α_{thres} of all customers. Analogously, the scenario $\mathrm{SM}_{< \alpha_{\mathrm{thres}}}$ represents grids where SM measurements are available for less than α_{thres} of all customers. In Figure 4.7 each exemplary MV node from Subsection 4.1.2 is assigned to one of the proposed MISs.

As mentioned in Subsection 4.1.2, system operators conventionally use SLPs to estimate the power consumption of non-metered grid users. In this module, it is also possible to take SLPs for the LV grid profiles. However, using SLPs does not correctly reproduce correlations between groups of customers. Simply calculating the sample correlations between two MV nodes using the same SLP time series in the underlying LV grids results in an unrealistically high correlation value of $100\,\%$. One way to avoid such unrealistic correlation values is to consider correlations between comparable LV grids. By this, for non-metered grid users, exemplary synthetic power time series are generated from power profiles of comparable grids. A more detailed description is given in the following.

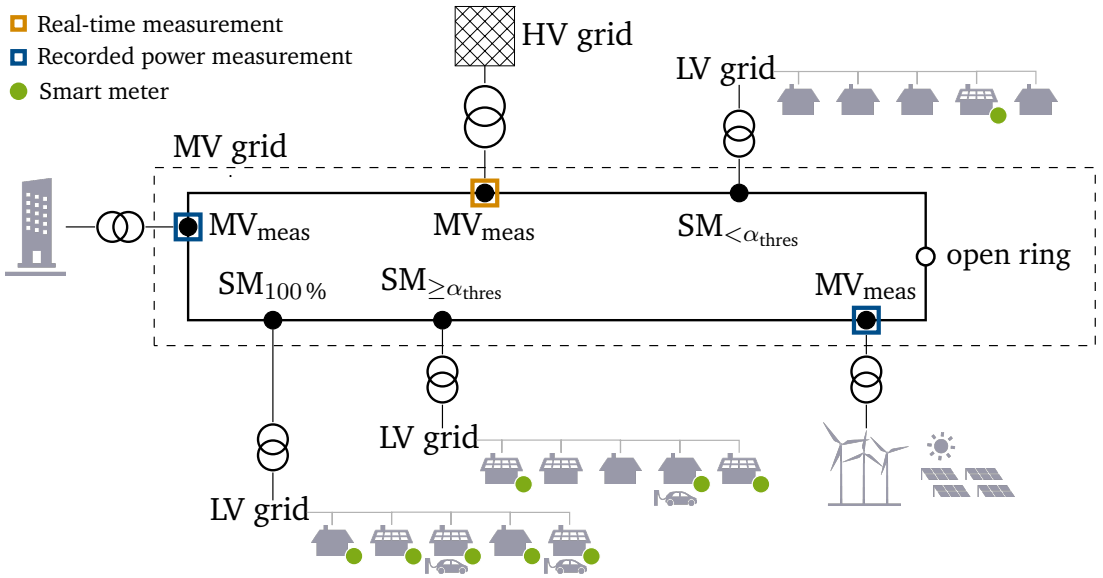

Figure 4.7: Exemplary MV nodes assigned to proposed MISs

4.4.2 Determination of Power Time Series

The MV node power series is denoted by $S_{\text{MV},n,t}$ at every MV node $n \in \{1,..,N\}$ for every time step $t \in \{1,...,T\}$. Table 4.5 shows the calculation steps for determining the power series values for each MIS. For MV nodes assigned to scenario MV$_{\text{meas}}$, the recorded measurements at the

Table 4.5: Determination of power time series $S_{\text{MV},n,t}$ for MV node n according to MIS classification

MIS	Determination of Time Series for MV nodes	
MV$_{\text{meas}}$	Recorded MV node measurements	$S_{\text{MV},n,t} = S_{\text{MV}_{\text{meas}},n,t}$
SM$_{100\,\%}$	Sum up SM-data from the underlying LV grid	$S_{\text{MV},n,t} \approx S_{\sum \text{SM},n,t} = \sum_{l=1}^{N_{\text{SM},n}} S_{\text{SM},n,l,t}$
SM$_{\geq\alpha_{thres}}$	Sum up data from SM nodes & scale up to meet total annual energy consumption	$S_{\text{MV},n,t} \approx S_{\sum \text{SM},n,t} \cdot f_{\text{scale},n}$ with $f_{\text{scale},n} = \frac{E_{\sum \text{LV},n}}{E_{\sum \text{SM},n}}$
SM$_{<\alpha_{thres}}$	Calculate K exemplary, synthetic time series from sum of SM-data for SM nodes & sum of comparable profiles for non-SM nodes	$S_{\text{MV,synth},n,t,k} = S_{\sum \text{SM},n,t} + S_{\sum \text{LV}_{\text{comp}},n,t,k}$ with $k \in \{1,...,K\}$

MV nodes $S_{\text{MV}_{\text{meas}},n,t}$ can directly be used as time series input. The other scenarios require the power time series from the SMs of the underlying LV grid. The SM power time series for LV node $l \in \{1,...,N_{\text{SM}}\}$ connected to MV node n are denoted $S_{\text{SM},n,l,t}$. $N_{\text{SM},n}$ is the number of the LV nodes equipped with smart meters connected to MV node n.

For the scenario with the assumption of $100\,\%$ SM coverage in LV grids, the SM power series of all LV nodes are summed up for the corresponding MV node n and result in a time series $S_{\sum \text{SM},n,t}$ with a quarter-hourly resolution. As the losses in LV systems are bounded by $5\,\%$ for active and $10\,\%$ for reactive power, they are neglected here to simplify the approach[13].

For LV grids with larger SM coverage than the threshold α_{thres}, it is assumed that the summed-up time series $S_{\sum \text{SM},n,t}$ of the SM measured grid users is representative for the behavior of this LV grid. To achieve correct energy demand values at the MV nodes, the aggregated SM time series are multiplied with a scaling factor $f_{\text{scale},n}$ that compensates for the missing power contributions from unmeasured customers. This factor is calculated as the ratio of the summed-up annual energy demand of all LV nodes of this grid $E_{\sum \text{LV},n}$ and the summed-up energy demand recorded by SM $E_{\sum \text{SM},n}$.

In the last scenario $\text{SM}_{<\alpha_{\text{thres}}}$, the SM information cannot be assumed to be representative for the non-SM nodes due to the small sample size. So, a set of K exemplary, synthetic time series $S_{\text{MV,synth},n,k,t}$ for $k \in \{1, ..., K\}$ is created. These exemplary time series will be used to estimate the parameters of the background distribution representing this MV node. That the use of proxy time series is justified and that correlation parameters from similar groups of customer profiles can be used is shown in Section 4.4.3. The number of power profiles K should be high enough to achieve sufficient sampling. For every LV node that is not a SM-node, a residential profile from comparable grids is randomly assigned. The profiles are scaled to the LV nodes' annual consumption. For each sampling index k, the synthesized time series $S_{\text{MV,synth},n,t,k}$ is now defined as the sum of the aggregated SM profiles $S_{\sum \text{SM},n,t}$ for the SM nodes and of the aggregated comparable profiles for the non-SM nodes $S_{\sum \text{LV}_{\text{comp}},n,t,k}$. To select suitable comparable profiles, the profiles should equal the SLP classes of the assigned customer. Hence, MV nodes assigned to $\text{SM}_{<\alpha_{\text{thres}}}$ require the SLP classes of the consumers in the underlying LV grid.

4.4.3 Determination of Background Distribution

This subsection includes the calculation steps of determining a correlation-aware background distribution from the generated power time series. For all MIS, the mean μ_S is calculated from the time series as the sample expectation value $\mu_{S_{\text{samp}}}$ (see Equation 4.4). This is equivalent to the annual energy consumption divided by the number of time steps T. As the synthetic time series are scaled to the annual consumption, the mean is always the same for every exemplary K.

$$\mu_{S,\text{samp},n} = \frac{1}{T} \cdot E_{\sum \text{LV},n} \tag{4.6}$$

The elements of background distribution covariance matrix $\Sigma_{S_{nm}}$ with $n, m \in N$ are calculated according to Table 4.6. For n, m-pairs, where none of n and m is assigned to scenario $\text{SM}_{<\alpha_{\text{thres}}}$, the covariance matrix elements are calculated as the sample covariance $\Sigma_{S_{nm,\text{samp}}}$ (see Equation 4.5).

[13] For future research, the line losses can approximated and added to the equation.

If at least one of the nodes (n or m) is classified as $\text{SM}_{<\alpha_{\text{thres}}}$ (i.e., no sufficient measurement coverage), then the sample covariance $\Sigma_{S_{nm,\text{samp},k}}$ is calculated for every k and then averaged over all k. To calculate the sample covariance for $k \in \{1...K\}$, the k-th synthesized time series $S_{\text{MV,synth}n,k,t}$ for every $n \in \text{SM}_{<\alpha_{\text{thres}}}$ and the measured time series $S_{\text{MV},n,t}$ for every $n \notin \text{SM}_{<\alpha_{\text{thres}}}$ are used. To validate this approach, a statistical analysis of an exemplary set of residential active power profiles was performed in the following Subsection 4.4.4.

Table 4.6: Determination of Σ_S element for (n, m)-pairs and included MIS

MIS of n and m	**Calculation of elements for Σ_S**
$n, m \notin \text{SM}_{<\alpha_{\text{thres}}}$	$\Sigma_{S,\text{samp},nm} = \frac{1}{T-1} \sum_{t=1}^{T} \left(S_{\text{MV},n,t} - \mu_{S_{\text{samp},n}}\right) \left(S_{\text{MV},m,t} - \mu_{S_{\text{samp},m}}\right)$
$n \in \text{SM}_{<\alpha_{\text{thres}}}$ or $m \in \text{SM}_{<\alpha_{\text{thres}}}$	$\Sigma_{S_{\text{comp}},nm} = \frac{1}{K} \sum_{k=1}^{K} \Sigma_{S,\text{samp},nm,k}$
	$\Sigma_{S,\text{samp},nm,k} = \frac{1}{T-1} \sum_{t=1}^{T} \left(S_{n,t} - \mu_{S_{\text{samp},n}}\right) \left(S_{m,t} - \mu_{S_{\text{samp},m}}\right)$
	$S_{n,t} = \begin{cases} S_{\text{MV,synth}n,k,t} & \text{, if } n \in \text{SM}_{<\alpha_{\text{thres}}} \\ S_{\text{MV},n,t} & \text{, else} \end{cases}$

The steps of the correlation-aware synthesis module for input with varying levels of detail, described in this section, are summarized in Figure 4.8. A case study for the benefits of this proposed module for Bayesian state estimation results is executed in 5.2[14].

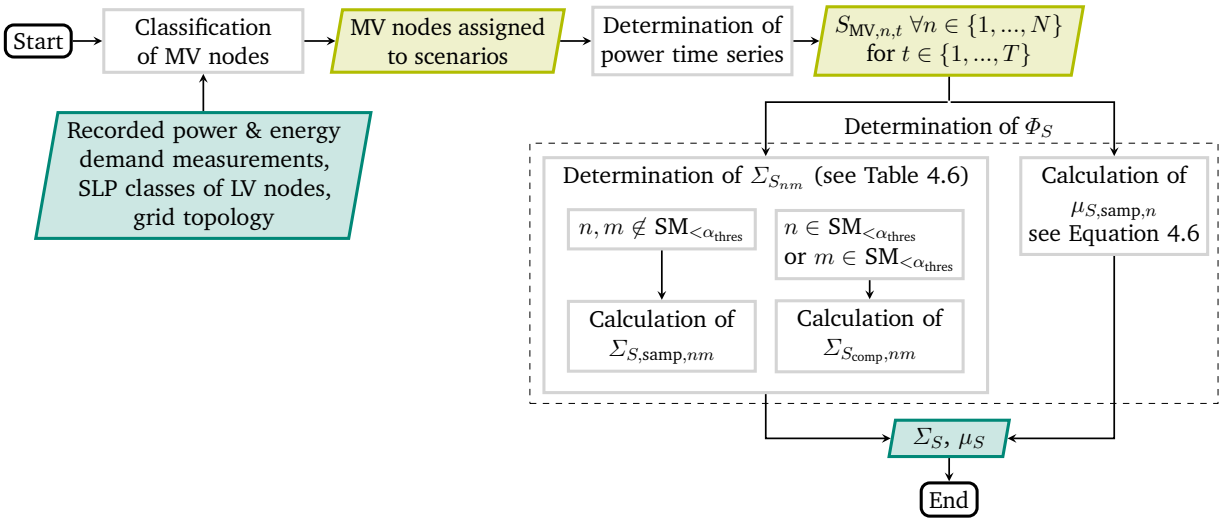

Figure 4.8: Flow Chart for Correlation-Aware Synthesis Module

[14] As a site note: The resulting background distribution can also be used to enhance the state-of-the-art state estimation approach that consider correlations between pseudo-measurements.

4.4.4 Correlation Analysis between LV grids

A statistical analysis of correlations between LV grids is performed to justify the assumption for using comparable LV grids for non sufficiently metered LV grids. For this, an exemplary set of residential active power profiles is taken from OpenEI [154]. The profiles are taken for Washington state, because of moderate climate and correlation values similar to load profiles from HTW-Berlin[15] [155]. OpenEI provides a "*publicly available dataset of calibrated and validated* 15*-minute resolution load profiles for all major residential and commercial building types and end uses, across all climate regions in the United States*" [154]. This database has previously been used by other authors for state estimation methods [142]. For Washington state, 4947 individual residential profiles are available. The correlation coefficient between these individual consumption profiles is $11\,\%$ on average. Building types with electric heating are excluded. This simplification can currently be justified for German households as less than $5\,\%$ of residential buildings are heated electrically [156]. This should be appropriately included for future scenarios with high heat pump penetration. Furthermore, the selected profiles do not include buildings with mobile home classification since these are rare in Germany.

For the analysis of correlations between subgrids with a varying number d of households, for each pair of subgrid sizes (d_1 and d_2) one thousand samples of d_1 and d_2 are randomly chosen. The required power profiles are taken from over 4900 Washington state profiles. Each subgrid is characterized by the number of households in the underlying subgrid represented by the variables d_1 respectively d_2. For each subgrid pair (d_1 and d_2) the following steps are performed:

1. For the subgrids, d_1 (or d_2) randomly chosen power profiles are summed up to obtain MV node time series (for active power $P_{\mathrm{MV},t}$).

2. A correlation coefficient is calculated for the aggregated power profiles of the subgrid pair.

These steps are performed 1000 times for each subgrid pair for statistical purposes. The resulting mean and standard deviations of the correlation coefficients for each subgrid pair, μ_ρ respectively σ_ρ, are plotted as heat maps in Figure 4.9. It can be seen, that for a small number of households (< 3) the correlations variate with standard deviations up to $14\,\%$. However, already for subgrids consisting of only 30 customers each, the variance in correlation values drops to $\sim 4\,\%$. This indicates that the correlation of two similarly sized subgrids taken from a comparable region provides a reliable estimate for the correlation coefficient of two individual subgrids. This universality of the correlations is used in the correlation aware synthesis module. Furthermore, if the size of the subgrids increases, so does the accuracy of the estimate: For a sufficiently large number of households in the subgrids (> 80), the mean of correlation coefficients μ_ρ is an accurate estimate of the correlation as the standard deviation for correlation coefficients σ_ρ is lower than 1%.

[15] HTW-Berlin supplies real measured power profiles of 74 residential customers in Germany.

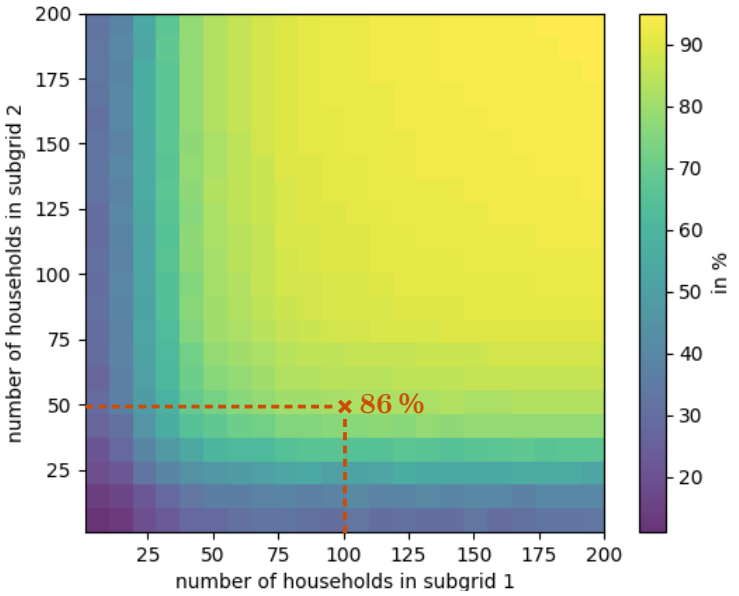

(a) Mean μ_ρ for correlation coefficients

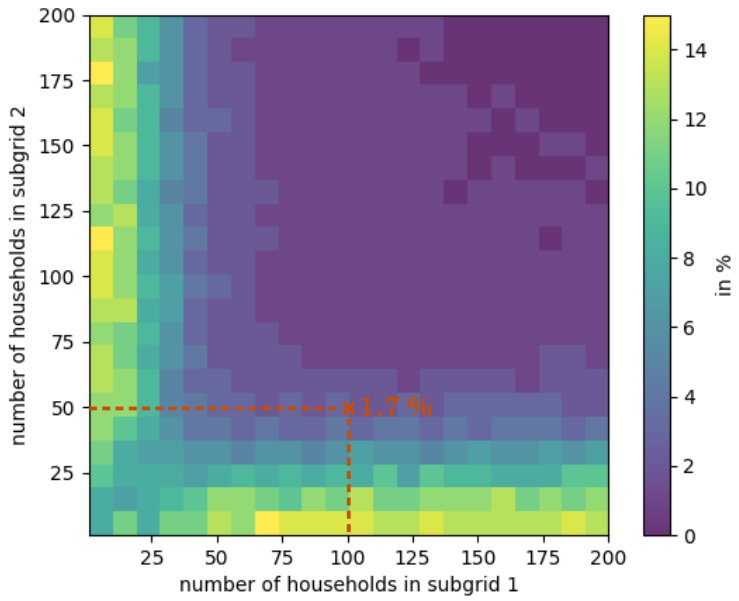

(b) Standard deviation σ_ρ for correlation coefficients

Figure 4.9: Illustrative representation of mean μ_ρ (a) and standard deviation σ_ρ (b) for correlation coefficients between two subgrids with varying number of households in %. For example: two subgrids with $d_1 = 100$ and $d_2 = 50$ households, the mean of correlation coefficient is $86\,\%$ (chart a). Furthermore, in all samples of the subgrids of these sizes, the correlation coefficient has a standard deviation of $1.7\,\%$ (chart b).

5 Results - Case Studies for the Proposed State Estimation Method

In this chapter, the proposed uncertainty-aware state estimation method is applied to different case studies. The proposed method consists of a combination of the basic linear Bayesian state estimation algorithm described in Section 3.3 and the pre- and post-processing modules from Section 4.3 and 4.4. First, in Section 5.1, the detection accuracy of critical system states is evaluated for the results obtained with the criticality analysis module. In the second step, the correlation-aware synthesis module for non-real-time input with varying levels of detail is added. Section 5.2 shows the accuracy gains from using this pre-processing module for the Bayesian linear state estimation.

Furthermore, this chapter analyses whether the proposed Bayesian state estimation method meets the requirements defined in research question 1. Finally, the strengths and limitations of the method and of the case study assumptions are discussed.

5.1 Recognition of Critical System States

This section evaluates the proposed Bayesian state estimation method for recognizing critical system states. The proposed method considers the entire posterior distribution, i.e., the expectation value and (in particular) the variance of the posterior distribution. The probability of critical system states is calculated according to the approach proposed in Section 4.3. The method is compared to a Bayesian state estimator that considers only the expectation values of the posterior distributions and with the selected WLS benchmark estimator. Hence, the following three different state estimates $\hat{x}$ are compared regarding the correct recognition of critical system states:

- The probability of critical system state $\boldsymbol{p}_{\text{css}}$ based on the entire posterior distribution (see equations 4.1-4.3);
- The expectation value of the posterior distribution $\boldsymbol{\mu}_{\text{po}}$ (see Equation 3.71);
- The estimate of the WLS state estimation approach $\hat{\boldsymbol{x}}_{\text{WLS}}$ widely used in TS (see equations in Section 3.4.1).

This section begins with an introduction to the performance metrics used for the evaluation. A description of the simulation environment follows. Then, exemplary warning and alert messages for system operators are presented graphically. Finally, the state estimation results are evaluated for correct recognition of critical system states.

5.1.1 Performance Metrics

According to Definition 2, a system state is classified as critical if any operational limit is violated. However, in the following evaluation, the criticality analysis is carried out separately for each element. This has the following reason: If, for example, one element recognizes its limit violation correctly while another element (maybe even in another feeder) does not recognize its limit violation, the state of the entire system would be assumed critical. Hence, it would be correctly recognized that there is a limit violation in this time step but not the locations of every critical element. As the location of the critical elements is highly important for the system operator to react with spatially correct mitigation measures, this separate evaluation for the elements is necessary. Consequently, the state for each element is evaluated separately at each time step with respect to criticality detection.

First, an indicator function for operational limit violations is introduced. The indicator function $\kappa_{x,\epsilon,t,lim} \in [0,1]$ is defined to be 1 if a given limit $lim \in [V_{\text{low}}, V_{\text{up}}, I_{\text{th}}]$ is violated in a state $x_{\epsilon,t}$ for time step $t \in \{1,...,T\}$ at element $\epsilon \in \{1,\dots,E\}$[1]. If no operational limit is violated, the indicator function is set to 0.

$$\kappa_{x,\epsilon,t,lim} = \begin{cases} 1 & \text{if } lim \text{ is violated in state } x_{\epsilon,t} \text{ for time step } t \text{ for element } \epsilon \\ 0 & \text{otherwise} \end{cases} \tag{5.1}$$

Simulated states resulting from a non-linear power flow calculation are used as the ground truth ($x_{\epsilon,t} = x_{\text{true},\epsilon,\text{t}}$). If $x_{\text{true},\epsilon,\text{t}}$ violates an operational limit, the state is assumed to be actually critical. For this, the indicator function is set to 1. Hence, the number of true critical states pos_{true} is equal to the sum of $\kappa_{x_{\text{true}},\epsilon,t,lim}$ over all time steps and elements. The number of all evaluated states for all time steps t and elements e equals the product of T and E. The number of non-critical states neg_{true} result from the difference between all evaluated states and the true critical states.

$$pos_{\text{true}} = \sum_{t=1}^{T} \sum_{\epsilon=1}^{E} \kappa_{x_{\text{true}},\epsilon,t,lim} \tag{5.2}$$

$$neg_{\text{true}} = T \cdot E - pos_{\text{true}} \tag{5.3}$$

The estimates of the different state estimators are given to the indicator function to obtain a criticality classification. For both deterministic state estimation results, μ_{po} and $\hat{x}_{\text{WLS}}$, the indicator function from Equation 5.1 can directly be used to classify the estimated states $\hat{x}_{\epsilon,t}$ as critical (1) or non-critical (0). For the probabilistic estimate p_{css}, an adapted indicator function is proposed (see Equation 5.4).

[1] If voltage band limit violations are considered, these elements are the grid nodes, and hence, E is equal to the number of non-slack nodes N. If thermal current limits are considered, E equals the number of branches B.

For p_{css}, an estimated state $\hat{x}_{\epsilon,t}$ is classified as critical by the indicator function $\kappa_{p_{\text{css}},\epsilon,t,lim}$ if the probability $p_{\text{css},lim,\varepsilon,t}$ for a limit violation of element ε at time t is above a chosen threshold p_{thres}.

$$\kappa_{p_{\text{css}},\epsilon,t,lim} = \begin{cases} 1 & \text{if } p_{\text{css},\epsilon,t,lim} > p_{\text{thres}} \\ 0 & \text{otherwise} \end{cases} \tag{5.4}$$

Hence, one or multiple probability thresholds must be selected for this indicator function. The following two thresholds are chosen for the evaluation:

$p_{\text{thres},\sigma}$: A state is classified as critical if any value in the range of $\mu_{\text{po}} \pm \sigma_{\text{po}}$ is critical. For normally distributed posterior estimates, this range contains $68.3\,\%$ of the estimated states. Hence, $15.85\,\%$ $((100\,\% - 68.3\,\%)/2)$ remains on each side. Consequently, the resulting threshold is set to $\sim 15.9\,\%$.

$p_{\text{thres},2\sigma}$: A state is classified as critical if any value in the range of $\mu_{\text{po}} \pm 2\sigma_{\text{po}}$ is critical. This range contains $95.45\,\%$ of the estimated states. The resulting threshold is set to $\sim 2.3\,\%$.

The thresholds $p_{\text{thres},\sigma}$ and $p_{\text{thres},2\sigma}$ are pictured in Figure 5.1.

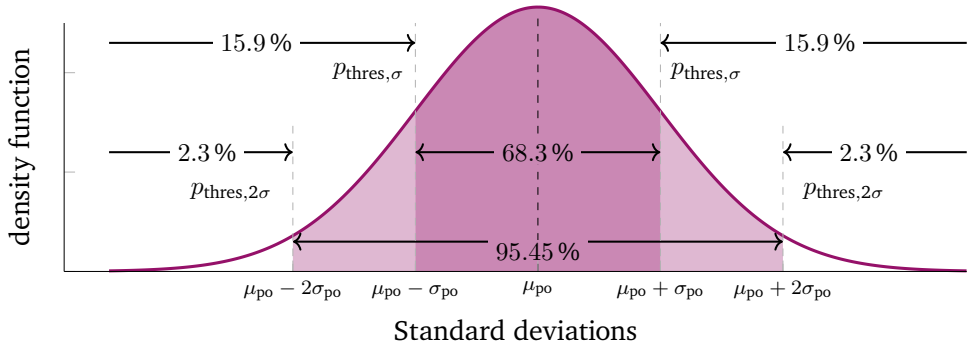

Figure 5.1: Thresholds for the indicator function of p_{css} estimate, considering the range within one standard deviation $p_{\text{thres},\sigma}$ and within two standard deviations $p_{\text{thres},2\sigma}$

Next, the classified estimates are compared to the true states. If the estimate $\hat{x}_{\epsilon,t}$ correctly recognizes a critical system state, it is set to true-positive (tp). More detailed: a correct detection is present if the indicator function classifies the true and the estimated state as critical $\left(\kappa_{x_{\text{true}},\epsilon,t,lim} = 1\right) \wedge \left(\kappa_{\hat{x}_{\epsilon,t},lim} = 1\right)$. For the correct recognition of non-critical states, the estimate is set to true-negative (tn). For this, the indicator function has to classify $\hat{x}_{\epsilon,t}$ and $x_{\text{true},\epsilon,t}$ as non-critical states, setting $\kappa_{\hat{x}_{\epsilon,t},lim}$ and $\kappa_{x_{\text{true}},\epsilon,t,lim}$ to 0.

$$tp_{\hat{x},\epsilon,t,lim} = \left(\kappa_{x_{\text{true}},\epsilon,t,lim} = 1\right) \wedge \left(\kappa_{\hat{x},\epsilon,t,lim} = 1\right) \tag{5.5}$$

$$tn_{\hat{x}_{\epsilon,t},lim} = \left(\kappa_{x_{\text{true}},\epsilon,t,lim} = 0\right) \wedge \left(\kappa_{\hat{x},\epsilon,t,lim} = 0\right) \tag{5.6}$$

Distribution system operators need to know if and where it is necessary to execute mitigation measures to ensure secure grid conditions. An indicator of whether the system operator gets the correct information about existing critical states is the aggregated true-positive rate $tpr_{\hat{x},lim}$. It is defined by the sum of all correctly recognized critical states $tp_{\hat{x},\epsilon,t,lim}$ over all elements and time steps, divided by all true critical states pos_{true}.

$$tpr_{\hat{x},lim} = \frac{1}{pos_{\text{true}}} \sum_{t=1}^{T} \sum_{\epsilon=1}^{E} tp_{\hat{x},\epsilon,t,lim} \tag{5.7}$$

A high aggregated true-positive rate indicates a high recognition rate of critical system states.

The number of critical states that are not correctly recognized, and so *missed* by the estimate, can be quantified by the aggregated false-negative rate *fnr* (see Equation 5.8). It equals the share of true critical states that are not correctly recognized.

$$fnr_{\hat{x},lim} = 1 - tpr_{\hat{x},lim}. \tag{5.8}$$

Further, it is important not to classify normal states as critical. The aggregated true-negative rate $tnr_{\hat{x},lim}$ quantifies correctly recognized non-critical states. It equals the sum of all correctly recognized normal states (non-critical) divided by all true normal states neg_{true}.

$$tnr_{\hat{x},lim} = \frac{1}{neg_{\text{true}}} \sum_{t=1}^{T} \sum_{\epsilon=1}^{E} tn_{\hat{x},\epsilon,t,lim} \tag{5.9}$$

Normal states that are incorrectly assumed to be critical are classified as false positives (*fp*). The aggregate false positive rate *fpr* is defined by

$$fpr_{\hat{x},lim} = 1 - tnr_{\hat{x},lim}. \tag{5.10}$$

To correctly classify non-critical states, the aggregated false-positive rate should be low or, equivalently, the true-negative rate possibly high.

The overall accuracy can also be aggregated for all elements and time steps. The aggregated accuracy (*ac*) is the sum of all correctly recognized states (true critical and true non-critical states) divided by the number of all evaluated states ($T \cdot E = pos_{\text{true}} + neg_{\text{true}}$).

$$ac_{\hat{x},lim} = \frac{1}{T \cdot E} \sum_{t=1}^{T} \sum_{\epsilon=1}^{E} (tp + tn)_{\hat{x},\epsilon,t,lim} \tag{5.11}$$

The aggregated rates are multiplied by $100\,\%$ so that the rates are expressed in %.

5.1.2 Simulation Environment

A practice-relevant MV grid is required for the following tests. The grid should have realistic grid parameters, e.g. line impedance and line lengths, a realistic order of magnitude of the buses, and a realistic grid topology. Simbench [139] provides four synthetic German MV grids fulfilling these requirements. One of these is selected for the following case studies. It is called *commercial* and owns 107 buses. It can be seen in Fig. 5.2. The 20 kV grid is given in pandapower data model [38][2]. It has ring structures that are operated radially (open switches) except for one ring. The wiring rate is 70 %, which is typical for MV grids (see Section 2.2). Load and generation profiles for one year with a 15-minute resolution are assigned to the MV nodes. The renewable generation plants directly connected to MV nodes include PV, wind, biomass, and hydropower units. In summary, 10 large RES units and 19 large commercial customers are connected at the MV level. Among the MV nodes, 79 have underlying LV grids. The LV grids have varying numbers of customers: 13 to 118. Different LV grid types are included: rural, urban, and semi-urban. The aggregated power profiles of the LV grids include in-feed from rooftop PVs (2 % to 31 %). Table A.2 in Appendix A.3.1 gives a more detailed breakdown of the connected grid users.

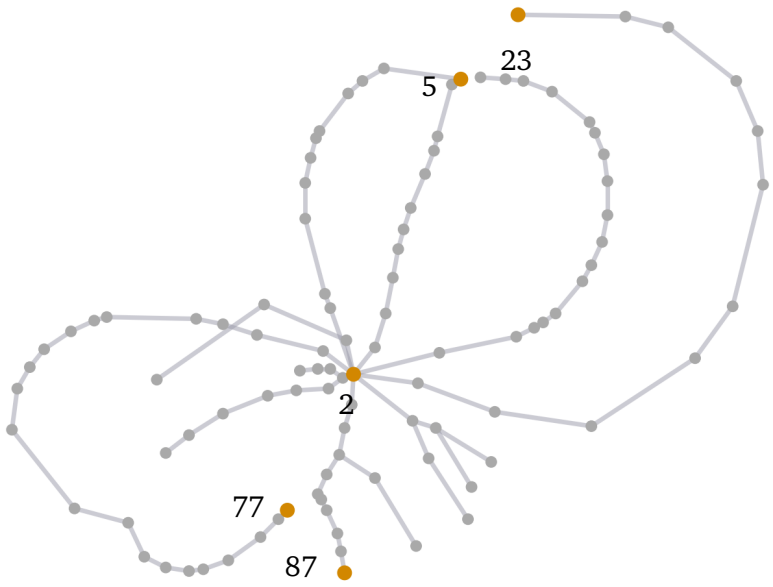

Figure 5.2: 20 kV Test grid from simbench [139]

In the simbench baseline scenario no limit violations occur. That currently still represents most of the German MV grids. However, the installed capacity of RES in German MV grids is expected to increase by a factor of three to four in the next 20 years [158] and with the expected strong increase of heat pumps and EV, the annual electricity demand of individual households could increase by a factor between 1.5 and 5 [159]. Hence, to create a simplified scenario for testing the developed algorithm, the load and generation profiles are multiplied by a factor of three. This simplified scenario includes possible future peak strains resulting in limit violations. Current violations occur in 24 % of the time steps, and voltage limit violations occur in 31 % of the time steps for at least one el-

[2]Pandapower is a Python library for power system calculation [157].

ement[3]. While this thesis focuses on algorithm development for uncertainty-aware state estimation methods, future research should include a more detailed modeling of load and generation scenarios.

For each time step, a power flow calculation is executed with the Newton Rapshon algorithm from the Matpower library [53] included in pandapower. These non-linear power flow results represent the true system states $\boldsymbol{x}_{\text{true}}$. Simulated measurements are obtained from true system states without adding synthetic errors. The proposed uncertainty-aware state estimation method is compared to the selected WLS benchmark approach. The commonly used WLS algorithm receives the same synthetic real-time measurements as the Bayesian algorithm and the background distribution parameters as pseudo-measurements. In particular, the pseudo-measurement values are equal to $\boldsymbol{\mu}_S$ and for the weights, the standard deviations $\boldsymbol{\sigma}_S$ are calculated from the diagonal elements of the background distribution covariance matrix $\sigma_{S_n} = \sqrt{\Sigma_{S_{nn}}}$ (see Equation 3.36).

The thermal branch limits for lines and transformers are given by the realistic standard line-type tables of the chosen simbench grid; different environmental conditions are not evaluated. For the voltage limits, the measurement configuration, and the measurement uncertainty, an initial setup is assumed. It is varied through the tests.

The initial setup assumes:

- Voltage limits: $\pm 6\,\%$ (see Subsection 3.1.3)
- Real-time measurement uncertainty $\boldsymbol{\sigma}_z$: $0.2\,\%$ and 0.2° (from Table 4.2)
- Measurement type and configuration: 5 voltage PMU measurements at transformer busbar and feeder ends

In Figure 5.2, the measurements of the initial setup are marked in orange: one measurement is located at the lower side of the HV/MV transformer station (2) and four at randomly chosen end feeder nodes with switches, one closed (5) and three open (23, 77 and 87). Hence, in this setup, less than $5\,\%$ of the nodes are equipped with real-time measurements.

Based on the initial setup, the following three variations are applied:

1. Stricter voltage limits: $\pm 4\,\%$
2. Higher real-time measurement uncertainty: $1.5\,\%$ and 1°
3. Higher real-time measurement coverage: voltage PMU measurements at transformer busbar and at all feeder ends ($11\,\%$ of the nodes are equipped with real-time measurements)

For each setup variant, only the explicitly mentioned parameters change; the other parameters are equal to the initial setup.

[3] The pos_{true} is 7 % and 1 % respectively

5.1.3 Warning and Alert Stages for Critical System States

According to research question 2, one aim of this work is to develop a method that outputs warning and alert messages as decision support for system operators. To address this aim, a criticality stage classification is applied to the system. An exemplary demonstration of the graphical message output is given below. One warning and one alert stage are defined. The two thresholds from Figure 5.1 are taken for the warning and alarm stages assignment. An element ε is assigned

- To a warning stage, if $p_{\text{css},\varepsilon}$ exceeds $p_{\text{thres},2\sigma}$;
- And to an alert stage, if $p_{\text{css},\varepsilon}$ exceeds $p_{\text{thres},\sigma}$.

For two exemplary time steps, the elements of the test grid from Subsection 5.1.2 are assigned to the stages according to the above definition. In Figure 5.3, the assigned buses and lines are marked with colors. Red elements are assigned to the alert stage, and orange elements are assigned to the warning stage. Further, the feeders, including the affected buses or lines, are colored in the background.

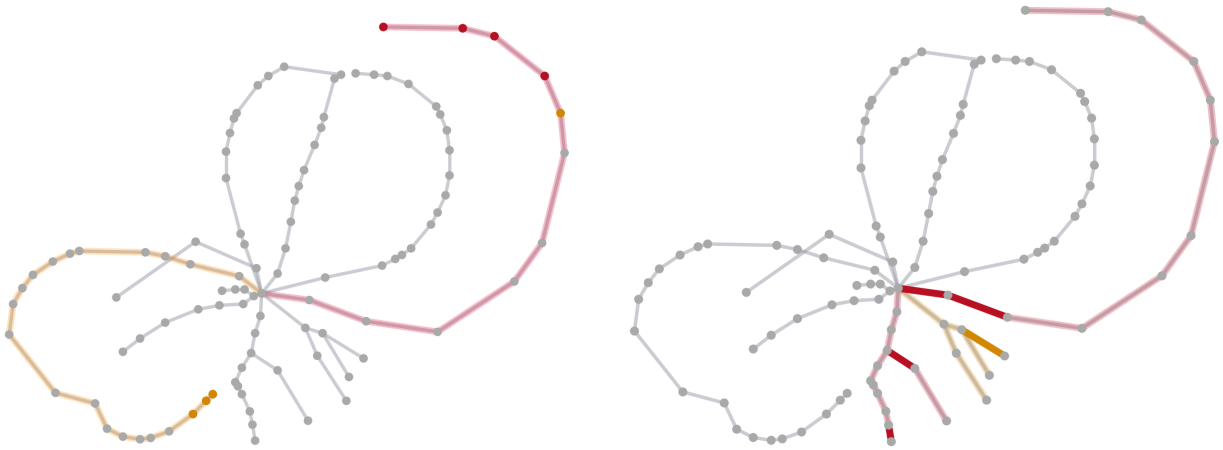

(a) Affected buses and feeders containing them

(b) Affected lines and feeders containing them

Figure 5.3: Graphical output for buses (a) and lines (b) assigned to warning (orange) and alert (red) stages

5.1.4 Test Results for Recognition of Critical System States

This section evaluates the accuracy performance of the three different state estimates $\boldsymbol{p}_{\text{css}}$, $\boldsymbol{\mu}_{\text{po}}$, and $\hat{\boldsymbol{x}}_{\text{WLS}}$ for recognition of critical system states. For this, the performance metrics described in Section 5.1.1 are applied to the different estimates for each setup described in Subsection 5.1.2.

Initial setup

For the first evaluation, the aggregated true-positive rate $tpr_{\hat{x},lim}$, the aggregated true-negative $tnr_{\hat{x},lim}$ and the aggregated accuracy $ac_{\hat{x},lim}$ are calculated for the initial setup defined in Section 5.1.2. Figure 5.4 and Figure 5.5 show the results for critical system states due to lower and upper voltage limit violations. It should be noted that in the load-dominated test case upper voltage limit violations occur only in $1\,\%$ of time steps in the test scenario.

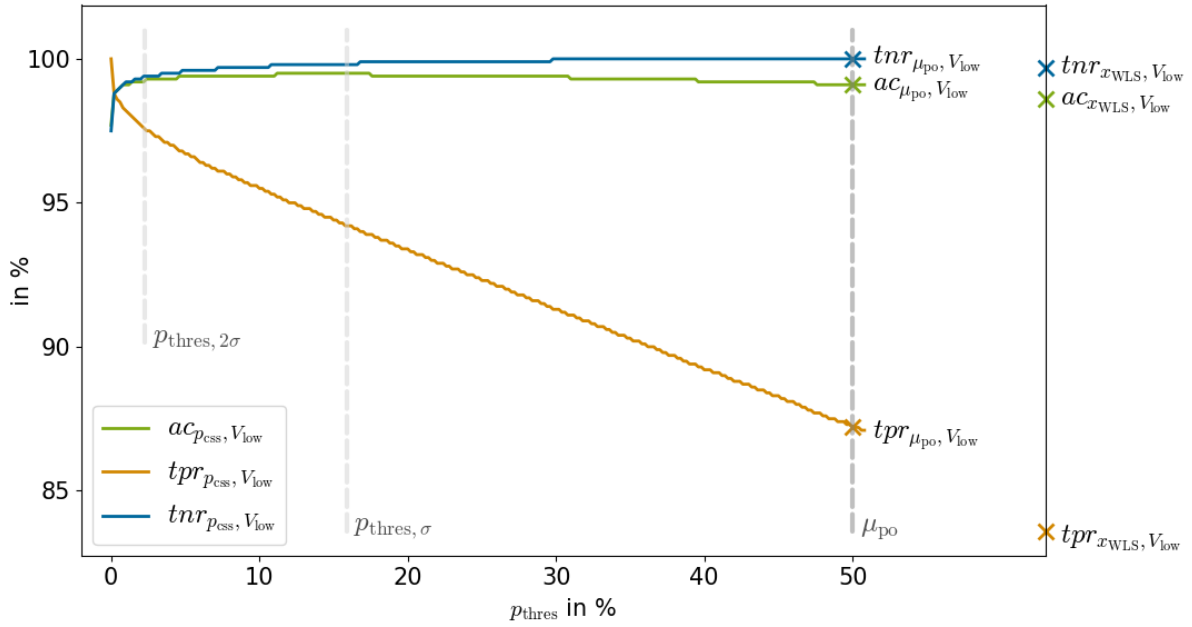

Figure 5.4: Aggregated accuracy $ac_{\hat{x},lim}$, true-positive $tpr_{\hat{x},lim}$ and true-negative rate $tnr_{\hat{x},lim}$ for the different state estimation results $\boldsymbol{p}_{\text{css}}$, $\boldsymbol{\mu}_{\text{po}}$, and $\hat{\boldsymbol{x}}_{\text{WLS}}$ for violating V_{low} (-6 %) for initial test setup . A state is classified as critical if p_{css} exceeds the given threshold p_{thres}.

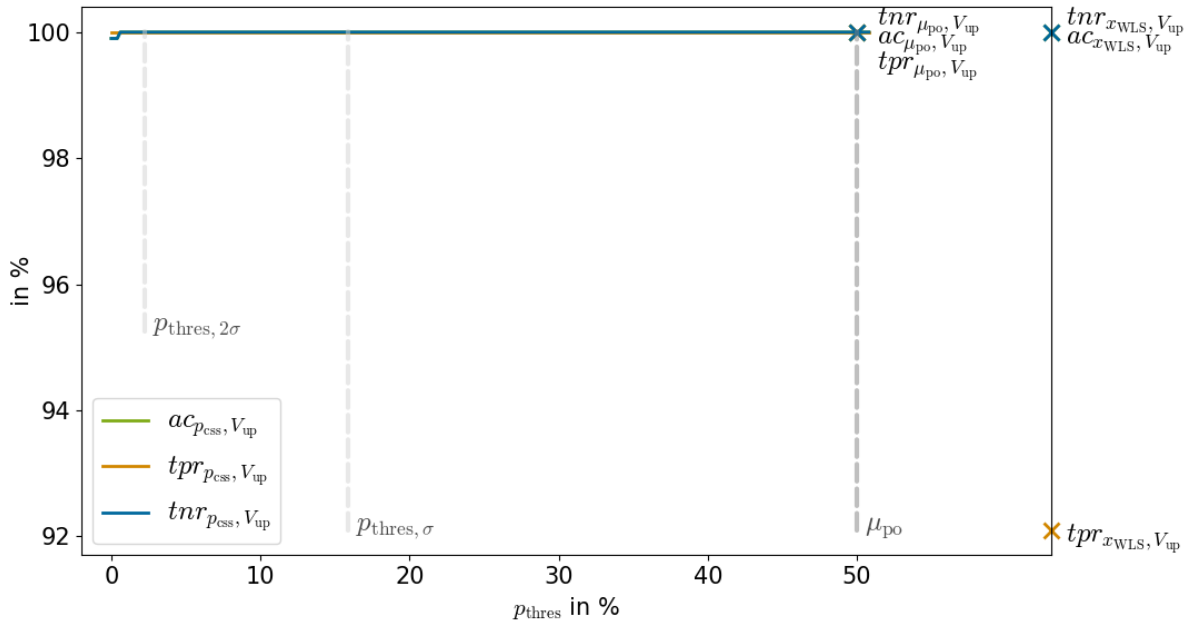

Figure 5.5: Aggregated accuracy $ac_{\hat{x},lim}$, true-positive $tpr_{\hat{x},lim}$ and true-negative rate $tnr_{\hat{x},lim}$ for the different state estimation results $\boldsymbol{p}_{\text{css}}$, $\boldsymbol{\mu}_{\text{po}}$, and $\hat{\boldsymbol{x}}_{\text{WLS}}$ for violating V_{up} (+6 %) for initial test setup

The results for critical system states due to I_{th}-violations are given in Figure 5.6.

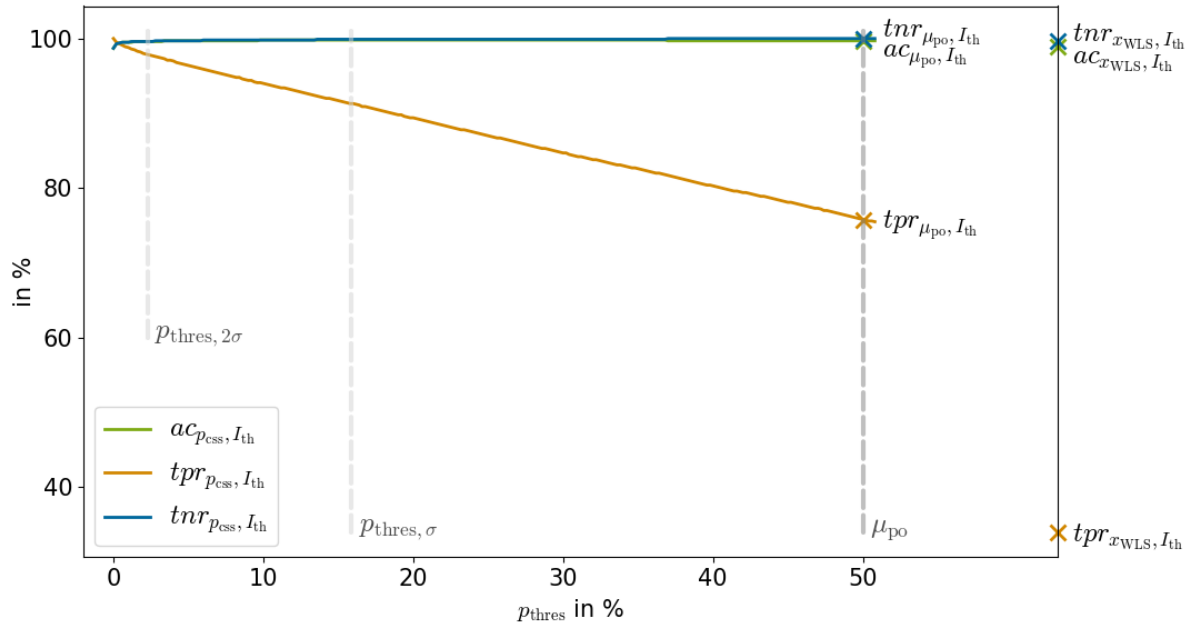

Figure 5.6: Aggregated accuracy $ac_{\hat{x},lim}$, true-positive $tpr_{\hat{x},lim}$ and true-negative rate $tnr_{\hat{x},lim}$ for the different state estimation results $\boldsymbol{p}_{\text{css}}$, $\boldsymbol{\mu}_{\text{po}}$, and $\hat{\boldsymbol{x}}_{\text{WLS}}$ for violating I_{th} for initial test setup

The results for p_{css} are plotted over different threshold values p_{thres} (see Equation 5.4 in Subsection 5.1.1), from 0 to $50\,\%$. A state is classified as critical if the probability of a critical system state p_{css} exceeds the given p_{thres}. For Gaussian distributions, the results for p_{css} with a threshold of $50\,\%$ equal the results obtained with the expectation value-based method μ_{po}. The results for the benchmark method $\hat{x}_{\text{WLS}}$ are shown on the right axis. $\hat{x}_{\text{WLS}}$ does not depend on the threshold.

For the cases where V_{low} and I_{th} violations are considered, the $tpr_{p_{\text{css}},lim}$ starts at a level near $100\,\%$ and decreases with increasing p_{thres} (since p_{css} is only classified as critical if $p_{\text{css}} > p_{\text{thres}}$). The true-negative rate $tnr_{p_{\text{css}},lim}$ shows opposite behavior. It increases with the increasing threshold. The behavior of $tpr_{p_{\text{css}},lim}$ and $tnr_{p_{\text{css}},lim}$ imply that for higher p_{thres} less states are classified as critical. The $ac_{p_{\text{css}},lim}$ first grows with increase of $tnr_{p_{\text{css}},lim}$, but then falls with the strongly decreasing $tpr_{p_{\text{css}},lim}$. As most states in the test set are actually non-critical, the true-negative estimates have a stronger impact on the aggregated accuracy than the true-positive estimates. Consequently, the *ac* curve is closer to *tnr* than to *tpr*. For the violations of the upper voltage limit V_{up}, the results of *tpr*, *tnr* and ac for p_{css} are consistently above $99.8\,\%$ for the evaluated thresholds (0 to $50\,\%$). This means that the Bayesian method accurately detects critical and non-critical states for upper voltage limit violations. For $p_{\text{thres},2\sigma}$, the $tnr_{p_{\text{css}},lim}$ and $ac_{p_{\text{css}},lim}$ are above $99\,\%$ for all evaluated limits. Hence, applying this threshold for warning stages would accurately detect (near) critical states. For $p_{\text{thres},\sigma}$, the $tpr_{p_{\text{css}},lim}$ is higher than $91\,\%$ for I_{th}, $94\,\%$ for V_{low}, and $99\,\%$ for V_{up}. Hence, by using $p_{\text{thres},\sigma}$ as an alarm stage, the detection rate for all types of operational limit violation is above $90\,\%$ as required by definition in 1.

Comparing the results of the p_{css} method to the deterministic results of $\boldsymbol{\mu}_{\text{po}}$ and $\hat{\boldsymbol{x}}_{\text{WLS}}$, shows following:

- Processing the entire posterior distribution and assuming a threshold $p_{\text{thres}} < 50\,\%$, instead of considering only the expectation value $\boldsymbol{\mu}_{\text{po}}$ (equivalently $p_{\text{thres}} = 50\,\%$), can lead to a significantly higher true positive rate (up to $12\,\%$ for V_{low}, and $24\,\%$ for I_{th}).
- The *tpr* for $\hat{x}_{\text{WLS}}$ is below the *tpr* for p_{css} and $\boldsymbol{\mu}_{\text{po}}$ for all considered limit violations. For V_{low} it is up to $16\,\%$, for V_{up} up to $8\,\%$, and for I_{th} even up to $65\,\%$ below the true-positive rates of p_{css} results.
- The lower true-positive rates of $\hat{x}_{\text{WLS}}$ imply that the conventional WLS benchmark method is more likely to miss critical states.

Stricter Voltage Limits

A test scenario with a stricter voltage limit of $\pm 4\,\%$ was chosen to analyze the sensitivity of the estimates to different share of true critical system states in the evaluated states. For the voltage limit of $\pm 4\,\%$, the percentage of time steps in the test set, which are true critical due to lower and upper voltage limit violation, rise to $58.7\,\%$ respectively $6\,\%$[4]. Changing the voltage limits does not change the results for violating the thermal current limits. They are identical to the initial setup (see Figure 5.6). Figure 5.7 and Figure 5.8 show the calculated performance metrics *tpr*, *tnr*, and *ac* for violating V_{low} $(-4\,\%)$ respectively V_{up} $(-4\,\%)$.

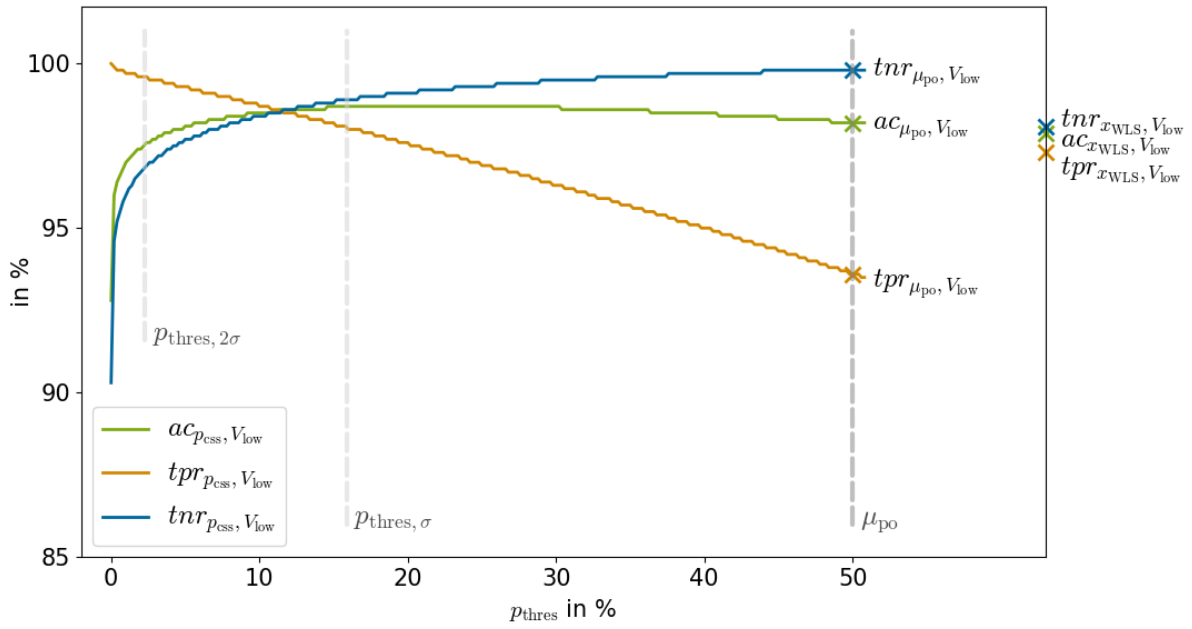

Figure 5.7: Aggregated accuracy $ac_{\hat{x},lim}$, true-positive $tpr_{\hat{x},lim}$ and true-negative rate $tnr_{\hat{x},lim}$ for the different state estimation results $\boldsymbol{p}_{\text{css}}$, $\boldsymbol{\mu}_{\text{po}}$, and $\hat{\boldsymbol{x}}_{\text{WLS}}$ for violating stricter voltage limits V_{low} $(-4\,\%)$

[4]The pos_{true} is 26 % for V_{low} respectively 2 % for V_{up}.

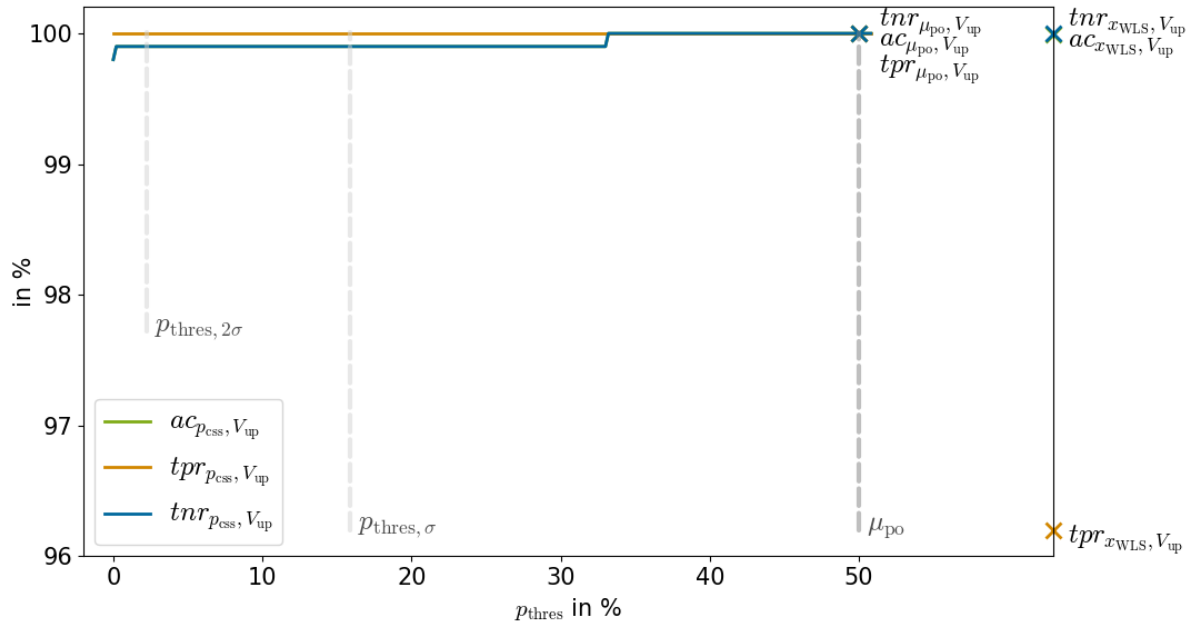

Figure 5.8: Aggregated accuracy $ac_{\hat{x},lim}$, true-positive $tpr_{\hat{x},lim}$ and true-negative rate $tnr_{\hat{x},lim}$ for the different state estimation results $\boldsymbol{p}_{\text{css}}$, $\boldsymbol{\mu}_{\text{po}}$, and $\hat{\boldsymbol{x}}_{\text{WLS}}$ for violating stricter voltage limits V_{up} $(+4\,\%)$

The behavior of $tpr_{p_{\text{css}},V_{\text{low}}}$, $tnr_{p_{\text{css}},V_{\text{low}}}$ and $ac_{p_{\text{css}},V_{\text{low}}}$ show similar behavior for the $4\,\%$ voltage limits as for the $6\,\%$. However, for $p_{\text{thres}} = 0\,\%$ the values for $ac_{p_{\text{css}},V_{\text{low}}}$ and $tnr_{p_{\text{css}},V_{\text{low}}}$ are significantly lower for the stricter limit than for $6\,\%$. This implies that for very small thresholds, e.g., $p_{\text{thres}} < p_{\text{thres},2\sigma}$, the number of critical states is overestimated. The $tpr_{p_{\text{css}},V_{\text{low}}}$ shows a flatter decreasing profile until $92\,\%$. Hence, also with $4\,\%$ voltage limit, the proposed method reaches the aim of $> 90\,\%$ detecting rate. Limit violations due to V_{up} are recognized by all three estimates with true-positive rates above $96\,\%$. The aggregated true-negative rates for V_{up} $(+4\,\%)$ lie above $99.8\,\%$. In this setup, the $\boldsymbol{p}_{\text{css}}$ results for $p_{\text{thres},2\sigma}$ and $p_{\text{thres},\sigma}$ achieve higher *tpr* than for $\hat{x}_{\text{WLS}}$ and $\boldsymbol{\mu}_{\text{po}}$ method. However, the advantage of this setup is reduced in comparison to the initial setup. This implies that the p_{css} method is particularly advantageous when the true critical states are less frequent (as in the initial setup). Since grids should be properly designed, critical states should be rare. For this, the proposed method is a good option to accurately detect rare violations. The differences between the true-negative rates of $\boldsymbol{p}_{\text{css}}$ for the both thresholds, $\boldsymbol{\mu}_{\text{po}}$, and $\hat{\boldsymbol{x}}_{\text{WLS}}$ are only $3\,\%$ in maximum.

Higher Measurement Uncertainties

To evaluate the influence of measurement uncertainties, the third setup assumes higher real-time measurement uncertainties with $\boldsymbol{\sigma}_z$ of $1.5\,\%$ for magnitude and 1° for phase. The $ac_{p_{\text{css}},lim}$ and $tnr_{p_{\text{css}},lim}$ start for $p_{\text{thres}} = 0\,\%$ at a lower percentage value than for lower measurement uncertainties but rise until $p_{\text{thres},2\sigma}$ over $96\,\%$ for all operational limit violations. The $tpr_{p_{\text{css}},lim}$ decreases steeply until $p_{\text{thres}} = 50\,\%$ $(\boldsymbol{\mu}_{\text{po}})$ to $49.7\,\%$ for V_{low}, $45.2\,\%$ for V_{up}, and $43.2\,\%$ for I_{th}. Hence, the improvement of considering the entire posterior distribution over expectation value-based approaches rises to over $50\,\%$.

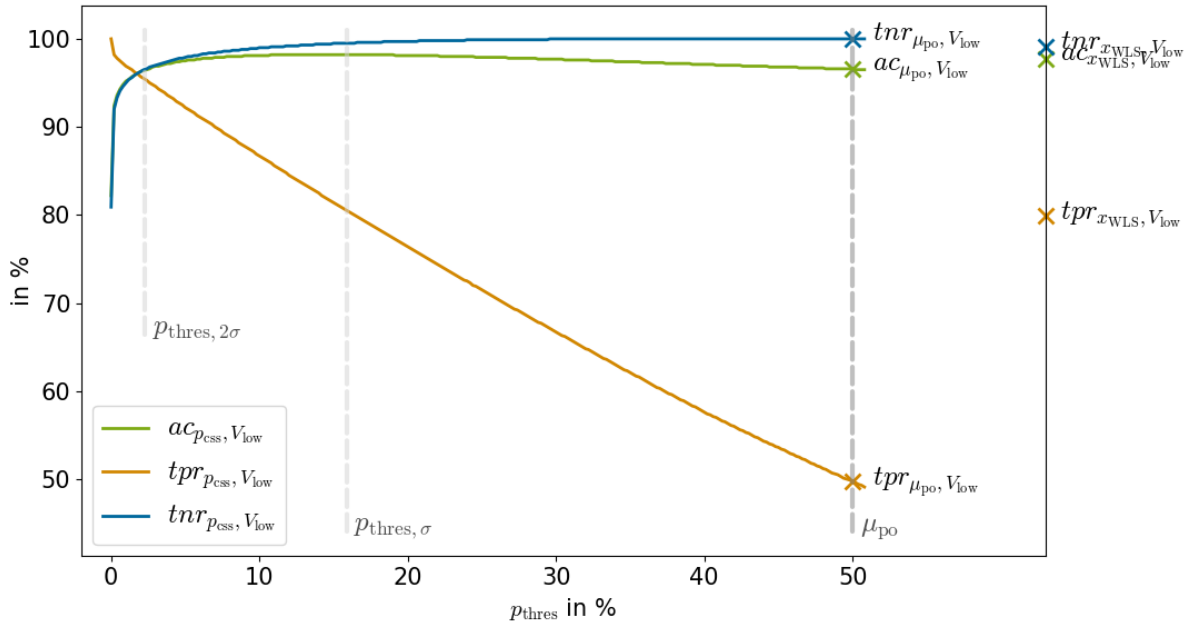

Figure 5.9: Aggregated accuracy $ac_{\hat{x},lim}$, true-positive $tpr_{\hat{x},lim}$ and true-negative rate $tnr_{\hat{x},lim}$ for the different state estimation results $\boldsymbol{p}_{\text{css}}$, $\boldsymbol{\mu}_{\text{po}}$, and $\hat{\boldsymbol{x}}_{\text{WLS}}$ for violating V_{low} ($-6\,\%$) for higher measurement uncertainty

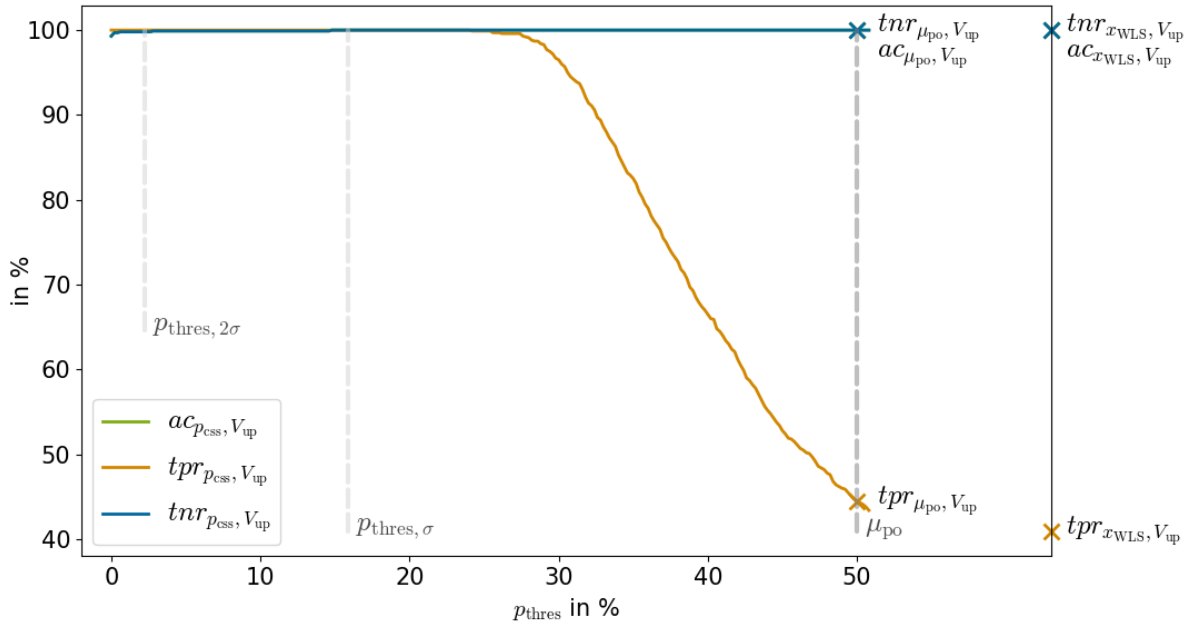

Figure 5.10: Aggregated accuracy $ac_{\hat{x},lim}$, true-positive $tpr_{\hat{x},lim}$ and true-negative rate $tnr_{\hat{x},lim}$ for the different state estimation results $\boldsymbol{p}_{\text{css}}$, $\boldsymbol{\mu}_{\text{po}}$, and $\hat{\boldsymbol{x}}_{\text{WLS}}$ for violating V_{up} ($+6\,\%$) for higher measurement uncertainty

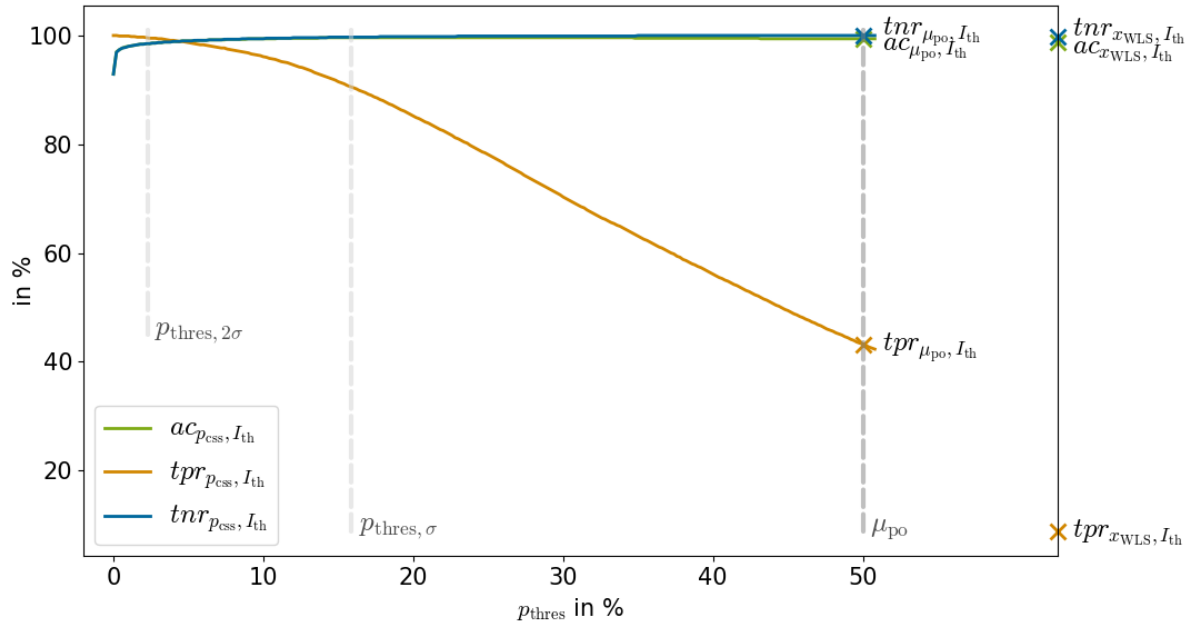

Figure 5.11: Aggregated accuracy $ac_{\hat{x},lim}$, true-positive $tpr_{\hat{x},lim}$ and true-negative rate $tnr_{\hat{x},lim}$ for the different state estimation results $\boldsymbol{p}_{\text{css}}$, $\boldsymbol{\mu}_{\text{po}}$, and $\hat{\boldsymbol{x}}_{\text{WLS}}$ for violating I_{th} for higher measurement uncertainty

This again shows the importance of considering the entire posterior distribution instead of the single expectation values. Large posterior variances can result from high measurement uncertainties and high uncertainties in the background input. For larger uncertainties, the p_{css} method (with $p_{\text{thres}} < 50\,\%$) is more accurate in detecting limit violations than the expectation value-based approach. Hence, these results confirm the graphical example from Figure 4.6 in Section 4.3 for different posterior uncertainties. For the WLS benchmark estimator, the aggregated true-positive rate for V_{low} limit detection changes only marginally for the different real-time measurement uncertainties. However, V_{up} and I_{th} violations are hardly recognized at the higher real-time measurement uncertainties ($< 40\,\%$ for V_{up} and $< 10\,\%$ for I_{th}). The high *tnr* and the extremely low *tpr* for the $\hat{\boldsymbol{x}}_{\text{WLS}}$ estimate support the assumption that the benchmark estimator is more likely to miss a critical state than to miss-classify non-critical states.

Higher Measurement Coverage

In order to evaluate the improvements that can be achieved by additional real-time measurements, a setup with voltage measurements placed at all branch ends is investigated. In the initial setup, only $1/3$ of all feeder ends are measured. With the additional real-time measurements, the *tpr* and *tnr* and thus *ac* of all estimates could be improved (up to $8\,\%$, see Appendix A.3.3). The results for this setup show the same trends as for the initial setup. Consequently, the conclusions are the same; therefore, the results will not be discussed in detail. The only additional finding from this setup is that the state estimation results, and thus the detection rates, benefit from additional accurate real-time measurements.

Overview and Summary

The results of the previous case study for detecting limit violations are given in Tables 5.1, 5.2, and 5.3. The aggregated true-positive and true-negative rates are compared for lower and upper voltage band and thermal current limit violations. They are calculated for the different state estimation results $\boldsymbol{p}_{\text{css}}$, $\boldsymbol{\mu}_{\text{po}}$, and $\hat{\boldsymbol{x}}_{\text{WLS}}$ for the varying setups. For $\boldsymbol{p}_{\text{css}}$, the results are given for thresholds $p_{\text{thres},\sigma}$ and $p_{\text{thres},2\sigma}$, which are described in 5.1.1.

Table 5.1: Aggregated true-positive $tpr_{\hat{x},V_{\text{low}}}$ and true-negative $tnr_{\hat{x},V_{\text{low}}}$ rates for the different state estimation results $\boldsymbol{p}_{\text{css}}$, $\boldsymbol{\mu}_{\text{po}}$, and $\hat{\boldsymbol{x}}_{\text{WLS}}$ for violating V_{low} in varying setups

	$\boldsymbol{p}_{\text{css}}$ & $p_{\text{thres},2\sigma}$		$\boldsymbol{p}_{\text{css}}$ & $p_{\text{thres},\sigma}$		$\boldsymbol{\mu}_{\text{po}}$		$\hat{\boldsymbol{x}}_{\text{WLS}}$	
Setup	*tpr*	*tnr*	*tpr*	*tnr*	*tpr*	*tnr*	*tpr*	*tnr*
Initial setup	97.6	99.4	94.2	99.8	87.2	99.9	83.6	99.7
Stricter voltage limits	99.6	96.8	98.9	99.0	93.5	99.8	97.3	98.1
Higher RTM* uncertainty	95.5	96.5	80.6	99.5	49.7	99.9	79.2	99.0
Higher RTM* coverage	98.2	99.4	96.1	99.8	90.6	99.9	89.5	99.8

*Real-Time Measurement

Table 5.2: Aggregated true-positive rates $tpr_{\hat{x},V_{\text{up}}}$ for the different state estimation results $\boldsymbol{p}_{\text{css}}$, $\boldsymbol{\mu}_{\text{po}}$, and $\hat{\boldsymbol{x}}_{\text{WLS}}$ for violating V_{up} in varying setups, $tnr_{\hat{x},V_{\text{up}}}$ is for all setups and estimates $> 99.9\,\%$

Setup	$\boldsymbol{p}_{\text{css}}$ & $p_{\text{thres},2\sigma}$ resp. $p_{\text{thres},\sigma}$	$\boldsymbol{\mu}_{\text{po}}$	$\hat{\boldsymbol{x}}_{\text{WLS}}$
Initial setup	99.9	99.9	92.1
Stricter voltage limits	99.9	99.9	96.2
Higher RTM* uncertainty	99.9	43.4	41.0
Higher RTM* coverage	99.9	99.9	97.5

*Real-Time Measurement

Table 5.3: Aggregated true-positive $tpr_{\hat{x},I_{\text{th}}}$ and true-negative $tnr_{\hat{x},I_{\text{th}}}$ rates for the different state estimation results $\boldsymbol{p}_{\text{css}}$, $\boldsymbol{\mu}_{\text{po}}$, and $\hat{\boldsymbol{x}}_{\text{WLS}}$ for violating I_{th} in varying setups

	$\boldsymbol{p}_{\text{css}}$ & $p_{\text{thres},2\sigma}$		$\boldsymbol{p}_{\text{css}}$ & $p_{\text{thres},\sigma}$		$\boldsymbol{\mu}_{\text{po}}$		$\hat{\boldsymbol{x}}_{\text{WLS}}$	
Setup	*tpr*	*tnr*	*tpr*	*tnr*	*tpr*	*tnr*	*tpr*	*tnr*
Initial setup	97.8	99.6	91.3	99.9	75.5	99.9	34.0	99.6
Higher RTM* uncertainty	99.6	98.5	90.6	99.7	43.2	99.9	8.8	99.8
Higher RTM* coverage	99.4	99.6	95.8	99.9	83.3	99.9	46.1	99.8

*Real-Time Measurement

The results from the tables can be summarized as follows[5]:

- By considering the entire posterior distribution, a more accurate critical state detection can be achieved than for the widely used WLS benchmark estimator ($tpr_{p_{\text{css}},lim} > tpr_{\hat{x}_{\text{WLS}},lim}$) and expectation value-based approaches ($tpr_{p_{\text{css}},lim} > tpr_{\mu_{\text{po}},lim}$). Instead of taking single estimated values as true representatives for state variables, the new method beneficially considers the uncertainties of the output.

- With the p_{css} method, it is possible to choose multiple thresholds to be more sensitive to (near) critical states.

- For stricter voltage limits, the *tpr* increase and the *tnr* decrease for every estimate. Hence, more critical system states can be detected, but more normal states are also assumed to be critical. Further, the p_{css} method is more advantageous when the true critical states are less frequent. Hence, this method is more suitable for properly designed grids and, thus, for practical applications.

- For higher measurement uncertainties, the *tpr* gets mostly smaller. The lower measurement accuracy particularly deteriorate results for $\boldsymbol{\mu}_{\text{po}}$ and $\hat{\boldsymbol{x}}_{\text{WLS}}$. Better results can be achieved by p_{css}. Hence, it becomes even more important to consider the output variances by using the p_{css} method for state estimation methods with higher real-time measurements or higher background input uncertainties.

- A higher real-time measurement coverage improves all *tpr* results, and the aggregated true-negative rates retain their high values. This implies that the recognition rates benefit from additional real-time measurements. Hence, an economical optimal meter placement allows a more accurate state detection.

5.2 Usage of Non-Real-Time Input with Varying Levels of Detail for State Estimation

This section uses the correlation-aware synthesis module from Section 4.4 to estimate the background distribution for Bayesian linear state estimation. The pre-processing module enables estimating a background distribution, including load correlations for non-real-time data with varying levels of detail. The state estimation results are evaluated for recognizing critical system states. It can be shown that considering load correlations can strongly improve the Bayesian state estimation results for detecting limit violations. Furthermore, it is shown that good results can be obtained even for MV nodes with no time-resolved historical power series available. The section starts with describing adjusted test conditions. It presents the used test cases for different smart meter coverage and load correlation assumptions. Then, the results for the recognition of limit violations are discussed. Further, the accuracy of the estimated voltage prior distribution is analyzed to get a more detailed view of the improved state estimation accuracy achieved by using the proposed synthesis module.

[5]The results for $\boldsymbol{p}_{\text{css}}$ are compared for assumption $p_{\text{thres},2\sigma} < p_{\text{thres}} \leq p_{\text{thres},\sigma}$.

5.2.1 Adjusted Test Conditions

To evaluate the effect of load correlations, and thus the benefit of the correlation-aware synthesis module, the approach from Section 4.4 is tested in a simulation study. The $20\,\text{kV}$ grid presented in 5.1.2 is chosen as a test system. In order to study correlations, a test case with a more detailed modeling of the statistical properties of individual loads had to be created. Since the original simbench data set allocates load and generation profiles from a limited set of profiles, some MV nodes are assigned to the same profiles. This results in unrealistically high correlations of $100\,\%$ between these nodes. Since the load correlations significantly impact the assessment of the effectiveness of the correlation-aware synthesis module, it is crucial for this test system to realistically replicate the correlations among power profiles of different MV nodes. Therefore, only the static specification of the grid topology and the load types is retained from the original simbench data set. The load profiles are synthesized using a bottom-up method. For MV nodes with underlying LV grids dominated by household profiles, every LV node is assigned a new, unique residential profile from an independent pool of 7000 OpenEI load profiles for New York state [154]. The commercial profiles from simbench are replaced by commercial profiles from OpenEI of the same SLP type. The PV and wind profiles are taken from simbench, with careful attention to avoid duplicate assignments and, thus, unrealistic correlations. To estimate the background distribution for subgrids with low smart meter coverage, the load profiles from OpenEI for Washington state are employed as comparable profiles as outlined in Subsection 4.4.4. This procedure prevents the comparable load profiles from being unrealistically similar to the actual load profiles in the test data. For the calculation of the reactive power profiles, a constant power factor $\frac{P}{S} = \cos(\varphi) = 0.95$ is assumed. Hence, the reactive power can be calculated by $Q = P\tan(\varphi)$ from the active power profiles.

The performance of the correlation-aware synthesis module is evaluated to identify critical system states correctly. To obtain a representative number of true critical system states for testing detection accuracy, the load and generation profiles are multiplied by a factor of three. With the synthesized power profiles, a power flow calculation is executed for every time step. The results represent the true system state (ground truth). Simulated measurements are obtained from true system states without adding synthetic measurement errors. The initial voltage limit and measurement setup from 5.1.2 is assumed. In the following, different scenarios with varying SM coverage and correlation assumptions are introduced for the evaluation. On the one hand, they aim to show the importance of considering load correlations. On the other hand, they show the benefit of the correlation-aware synthesis module for estimating the background distribution, particularly for customers with only annual energy demand information.

5.2.2 Test Cases with Varying SM Coverage and Load Correlation Assumptions

According to Subsection 4.4.1, the MV nodes of the test set are assigned to the following MISs.

- The 5 MV nodes with real-time measurements and the 21 MV nodes with RLMs (large commercial consumers and RES) are assigned to MV_{meas}.
- The 79 MV nodes with underlying LV grids can be assigned to $\text{SM}_{100\,\%}$, $\text{SM}_{\geq \alpha_{\text{thres}}}$, or $\text{SM}_{< \alpha_{\text{thres}}}$ depending on the SM coverage. The following tests consider the two extreme SM coverage scenarios of $0\,\%$ and $100\,\%$.

Four test cases with varying SM coverage and load correlation assumptions are defined. The test cases that consider load correlations (correlation-aware) are denoted by cor. Test cases that neglect load correlation (correlation-unaware) are denoted by cor_0. Each test case is defined by two parameters: the SM coverage given in % and the correlation assumption (cor or cor_0).

Test case 1: $100\,\%$ & cor
The SM coverage of all underlying LV grids is assumed to be $100\,\%$, i.e., 15 min time-resolved measured power profiles at every load are available for the estimation. Hence, the MV nodes with underlying LV grids are assigned to $\text{SM}_{100\,\%}$. The sample background distribution covariance $\Sigma_{S,\text{samp},nm}$ is calculated according to the description in Subsection 4.4.3. Hence, this test case considers the load correlations (correlation aware).

Test case 2: $100\,\%$ & cor_0
The SM coverage is also assumed to be $100\,\%$, but the load correlations are not considered (correlation-unaware). This results in a diagonal covariance matrix of the background distribution.

Test case 3: $0\,\%$ & cor
A SM coverage of 0 % is assumed for all LV grids, i.e., only the annual energy demand is available for the estimation approach. For this, the MV nodes with underlying LV grids are assigned to $\text{SM}_{<\alpha_{\text{thres}}}$. The background distribution is calculated according to the approach described in Subsection 4.4.3, using a value of $K = 1000$. The comparable profiles for non-SM nodes (in this case, all nodes in the LV grid) are drawn from the pool of 4947 OpenEI power profiles of Washington state described in Subsection 4.4.4. Hence, this test case considers the load correlations (correlation aware).

Test case 4: $0\,\%$ & cor_0
The same SM coverage (0 %) as for the third test is assumed, but the load correlations are neglected (correlation-unaware).

5.2.3 Limit Violation Detection after Applying the Correlation-Aware Synthesis Module

The background distribution is estimated according to the procedure described in Section 4.4. Then, for each time step $t \in \{1, ..., t\}$, the Bayesian linear state estimation algorithm is performed according to Section 3.3, resulting in a posterior distribution. Subsequently, from the resultant posterior distribution, the probability of critical system states p_{css} is calculated as presented in Subsection 4.3. The results are evaluated for threshold $p_{\text{thres},\sigma}$ for each test case described above. The performance metrics from Section 5.1.1 are applied to measure how well critical system states are recognized.

Table 5.4 shows the aggregated true-positive rate in % for recognizing critical system states due to low voltage and thermal current limit violations. In the adjusted test case, no violations of the upper voltage limit are to be evaluated. The aggregated true-negative rate, which gives the percentage of correctly recognized non-critical system states, is for all four test cases and considered limit violations (V_{low}, I_{th}) larger than $99.6\,\%$.

Table 5.4: Aggregated true-positive rates in % for recognition of critical system states due to low voltage limit (6 %) and thermal current limit violation by Bayesian linear state estimation for different SM coverage with (cor) and without (cor_0) considering load correlation

Test case	1: 100 % & cor	2: 100 % & cor_0	3: 0 % & cor	4: 0 % & cor_0
$tpr_{p_{\text{css}},V_{\text{low}}}$	98.0	82.1	98.0	80.7
$tpr_{p_{\text{css}},I_{\text{th}}}$	97.6	76.7	95.2	72.8

The results from Table 5.4 are discussed first for considering and neglecting load correlations and then for considering different SM coverage.

Benefit of Considering Load Correlation

First, the results of the test cases with 100 % SM coverage are compared (test cases one and two). Considering load correlations in the background distribution improves the true-positive rate $tpr_{x_{\text{est}},lim}$ by 15.9 % for voltage limit violations and by 20.9 % for thermal current limit violations. A similar result is found for the 0 % SM coverage (test cases three and four): Here, $tpr_{x_{\text{est}},lim}$ improves by 17.3 percentage points for voltage limit violations and by 22.4 percentage points for thermal current limit violations.

The benefit of considering load correlations becomes even more striking when viewed from the perspective of critical system states that are *missed* (i.e., not correctly recognized). This is given by the aggregated false-negative rate fnr (see Equation 5.8). Table 5.5 shows the aggregated false-negative rates for recognizing critical system states in the four test cases.

Table 5.5: Aggregated false-negative rates in % for recognition of critical system states due to low voltage limit (6 %) and thermal current limit violation by Bayesian linear state estimation for different SM coverage with (cor) and without (cor_0) considering load correlation

Test case	1: 100 % & cor	2: 100 % & cor_0	3: 0 % & cor	4: 0 % & cor_0
$fnr_{p_{\text{css}},V_{\text{low}}}$	2.0	17.9	2.0	19.3
$fnr_{p_{\text{css}},I_{\text{th}}}$	2.4	23.3	4.8	27.2

Where no smart meter measurements are available (0 % SM coverage), the approach that neglects the load correlations (cor_0) *misses* 19.3 % of critical system states caused by voltage limit violations. Using the correlation-aware estimation of background distributions (cor), that fraction drops to 2 %, a reduction by a factor of 9.7. Analogously, a reduction of the fnr by a factor of 5.7 is observed for thermal current limit violations. For 100 % SM coverage, the improvement of the false-negative rate achieved by considering load correlation is a factor of 9 for voltage limit violations and a factor of 9.7 for current limit violations. The factor reduction of fnr by considering load correlation for background distribution calculation can be seen graphically in Figure 5.12. These findings confirm the importance of considering load correlations in MV grid state estimation algorithms.

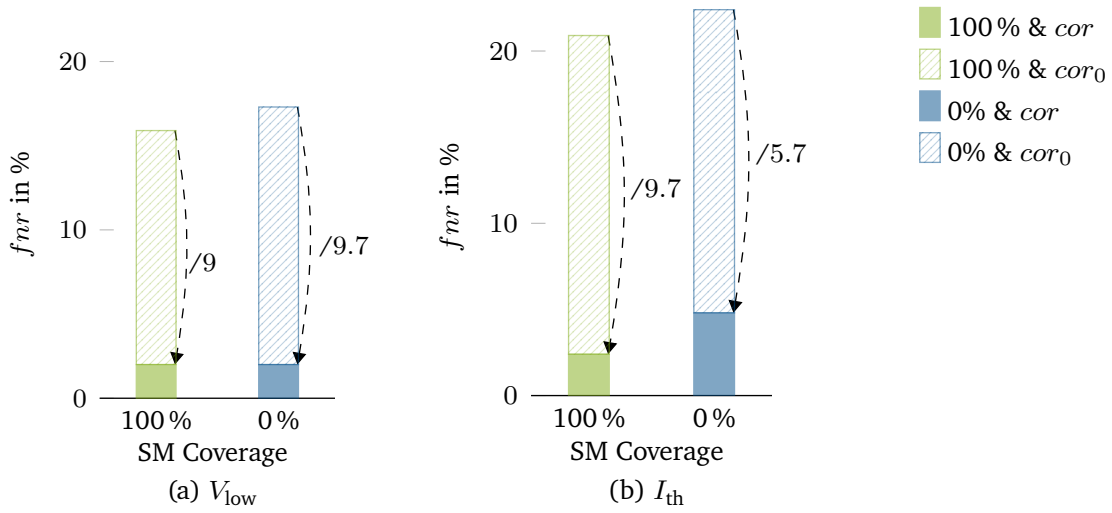

Figure 5.12: Factor reduction of aggregated false-negative rates by considering load correlation for recognition of critical system states due to (a) low voltage limit (6 %) and (b) thermal current limit violation by Bayesian linear state estimation for 0 % and 100 % SM coverage

Non-Real-Time Data with Varying Levels of Detail

The high *tpr* ($> 95\,\%$) of test case three in Table 5.4 shows that by using the correlation-aware synthesis module, critical system states can be reliably detected even for $0\,\%$ SM coverage. The first and third test cases ($100\,\%$ vs. $0\,\%$ SM coverage, each with correlation awareness) lead to similar true-positive rates. This means that the estimation of background distribution for non-metered customers is sufficiently accurate to detect limit violations. Furthermore, test case three shows a significantly higher *tpr* than test case two. This implies that even without smart meter coverage ($0\,\%$), the accuracy by incorporating load correlation (cor) is much better than what can be achieved without considering load correlation, even with full SM coverage ($100\,\%$ & cor_0). Hence, for accurate detection of limit violation, it is essential to properly estimate the load correlation between the MV nodes, e.g., by using the proposed correlation-aware synthesis module.

It is important to note that the proposed approach only uses *comparable* load profiles to estimate correlations for the test cases with $0\,\%$ SM coverage. These give an approximate indication of the true load correlation between loads in the system. The estimated correlation values differ from the empirical correlation in the ground truth by $12\,\%$ on average, with a maximum value of $39\,\%$. However, as the results above show, this approximation is good enough to improve the accuracy of the resulting state estimation substantially and, consequently, the recognition of critical system states ($tpr_{p_{\text{CSS}},lim} > 95\,\%$).

Summarized Benefit for Recognition Accuracy

In summary, considering load correlations allows for substantially more accurate recognition of critical system states in the context of Bayesian linear state estimation. Therefore, using the correlation-aware synthesis module can be beneficial even in cases where no smart meter measurements are available that would allow an empirical estimation of load correlations. Instead, knowledge extracted from a set of comparable (but different) load profiles from an entirely different

geographical region can be used to achieve accuracy levels comparable to the case where full smart meter coverage is available. Future research should include a selection of the most suitable comparison region.

The following subsection analyzes the accuracy of the estimated prior distributions for the test cases defined in Subsection 5.2.2 to gain a more detailed insight into the benefits of the correlation-aware synthesis module for Bayesian linear state estimation results.

5.2.4 Accuracy of Estimated Voltage Prior Distribution

The varying assumptions for SM coverage and load correlation change only the elements of the background distribution covariance $\boldsymbol{\Sigma}_S$ (see Table 4.6), $\boldsymbol{\mu}_S$ is not affected (see Equation 4.6). According to equations 3.51-3.54, changes in $\boldsymbol{\Sigma}_S$ only change the covariance matrix of the voltage prior distribution $\Sigma_{V_{\text{pr}}}$ [6]. For this, the varying assumptions for generating the background distribution change the elements of the voltage prior covariance matrix.

To achieve a high detection rate of critical system states, the *estimated* voltage prior distribution $\Phi_{V_{\text{pr}}}$ should represent the *true* voltage prior distribution $\Phi_{V_{\text{pr,true}}}$ as accurately as possible. To illustrate this fact, the Bayesian linear state estimation based on true, empirical voltage prior $\Phi_{V_{\text{pr,true}}}$ is performed. The approximated true prior distribution is obtained by fitting a Gaussian distribution to the voltage time series from the simulated ground truth states. By using the fitted true prior distribution and $p_{\text{thres},\sigma}$, the recognition rate of critical system states is $> 99\,\%$: The $tpr_{p_{\text{css}}lim}$ for V_{low} violation results in $99.9\,\%$ and for I_{th} violation in $99.0\,\%$.

To assess the impact of changes in background distribution covariances on the estimated prior voltage distribution, the calculated voltage prior covariance matrices $\boldsymbol{\Sigma}_{V_{\text{pr}}}$ (for each test set) are compared to the true empirical covariance matrix $\boldsymbol{\Sigma}_{V_{\text{prtrue}}}$. The following two characteristics of the prior voltage distribution are evaluated:

- Standard deviation $\boldsymbol{\sigma}_{V_{\text{pr}}}$ (overall variation of voltage values for each node);
- Correlation coefficient $\boldsymbol{\rho}_{V_{\text{pr}}}$ (correlation between voltage values at different nodes).

The normalized Root-Mean-Square-Error $NRMSE$ is used as an error metric to evaluate the accuracy of the estimated prior distribution. It is defined by the $RMSE$ between true y_{true} and estimated $\hat{y}$ values, normalized to the mean of the true values:

$$NRMSE = \frac{RMSE}{\frac{1}{N}\sum_{n=1}^{N} y_{\text{true},n}} \cdot 100\% \qquad \text{with } RMSE = \sqrt{\sum_{n=1}^{N}(y_{\text{true},n} - \hat{y}_n)^2}. \tag{5.12}$$

First, the standard deviations are discussed and then the correlation coefficients.

[6] $\boldsymbol{\mu}_{V_{\text{pr}}}$ depends only on $\boldsymbol{\mu}_S$ and not on $\boldsymbol{\Sigma}_S$.

Standard Deviations

The marginalized true and estimated prior distribution for voltage magnitude and angle is shown in Figure 5.13 for an exemplary bus (97). It illustrates the effects of load correlation and SM coverage assumptions on the variances of the estimated prior distribution.

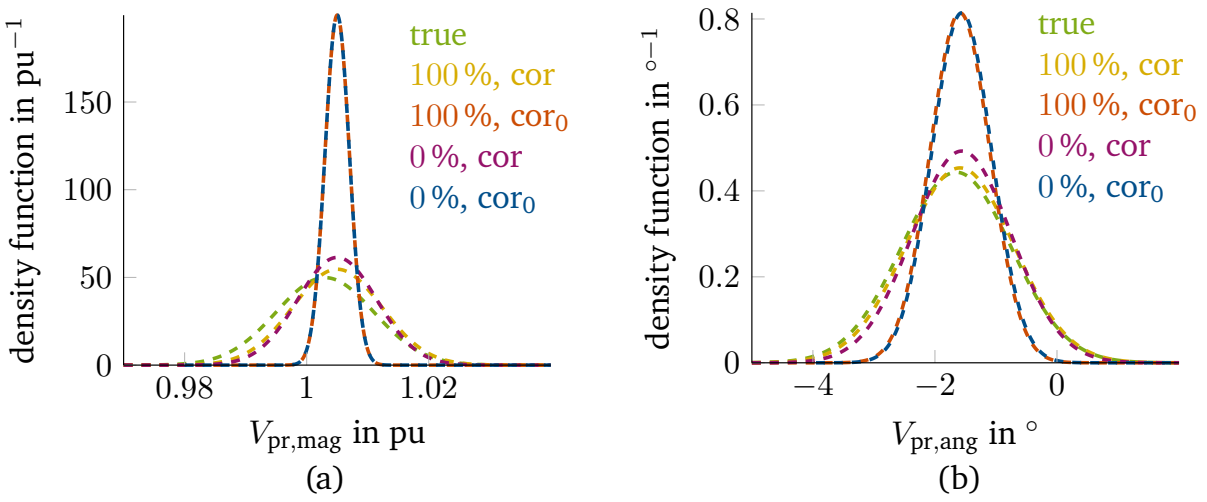

Figure 5.13: The marginalized true and estimated node voltage distribution $\Phi_{V_{\text{pr}}}$ for voltage magnitude (a) and angle (b) at the exemplary bus (97) are shown. The colors represent the true empirical values and the four test cases described in Subsection 5.2.2, covering different SM coverage and load correlation assumptions.

On a qualitative level, the standard deviation of the voltage prior distribution calculated without considering load correlations (cor_0) always substantially underestimates the true standard deviation. Thus, $\boldsymbol{\sigma}_{V_{\text{pr}}}$ for cor_0 assumes a much lower variation of voltage values in the prior distribution. This observation is also valid for every other bus in the grid. On the other hand, if load correlations are considered (cor), the resulting standard deviation is very close to the true empirical values. There are only small deviations with a maximum of $\pm\,2.7\,\%$ relative to the mean.

Table 5.6 shows the $NRMSE$ (see Equation 5.12) for $\boldsymbol{\sigma}_{V_{\text{pr}}}$ for each of the four test cases from Subsection 5.2.2, separately for magnitude and angle components of V_{pr}. If load correlations are not considered (cor_0 columns), relatively high $NRMSE$ values ($\sim 72\,\%$ for voltage magnitude and $\sim 45\,\%$ for voltage angle) are observed independently of the level of smart meter coverage. This confirms the qualitative observation from Figure 5.13. Considering load correlations reduces that error. In the case of full smart meter coverage, the error levels are reduced to $\sim 1/5$ for voltage magnitude ($15.5\,\%$ vs. $71.9\,\%$) and to $\sim 1/30$ for voltage angle ($1.5\,\%$ vs. $44.7\,\%$). Even in the case where no smart meter measurements are available as non-real-time input, using the correlation-aware synthesis module can reduce the error levels from neglecting load correlations to $\sim 1/3$ for $V_{\text{pr,mag}}$ ($27.6\,\%$ vs. $72.3\,\%$) and $\sim 1/4$ for $V_{\text{pr,ang}}$, ($1.6\,\%$ vs. $44.8\,\%$).

Table 5.6: $NRMSE$ in % for the standard deviation of the voltage prior distribution $\boldsymbol{\sigma}_{V_{\text{pr}}}$ for calculated and true voltage prior covariance depending on SM coverage and load correlation assumptions

Test case	1: 100 % & cor	2: 100 % & cor_0	3: 0 % & cor	4: 0 % & cor_0
$V_{\text{pr,mag}}$	15.5	71.9	27.6	72.3
$V_{\text{pr,ang}}$	1.5	44.7	11.6	44.8

Correlation Coefficient

Now, the correlation coefficients of the voltage prior distribution for the different test cases are analyzed. Table 5.7 shows the $NRMSE$ for the correlation coefficient of voltage prior distribution $\boldsymbol{\rho}_{V_{\text{pr}}}$ for each of the four test cases from Subsection 5.2.2, separately for magnitude and angle components of V_{pr}. Regarding the $NRMSE$ for the correlation coefficients of the prior distribution, a strong improvement can also be observed when considering load correlation in the background distribution covariance matrix. If load correlations are neglected the $NRMSE$ is $\sim 41\,\%$ for voltage magnitude and $\sim 36\,\%$ for voltage angle. When considering load correlations the error reduction for $100\,\%$ SM coverage is $\sim 1/20$ and for $0\,\%$ SM coverage $\sim 1/9$ for $V_{\text{pr,mag}}$ and $V_{\text{pr,ang}}$.

Table 5.7: $NRMSE$ in % for the correlation coefficient of the voltage prior distribution $\boldsymbol{\rho}_{V_{\text{pr}}}$ for calculated and true voltage prior covariance depending on SM coverage and load correlation assumptions

Test case	1: 100 % & cor	2: 100 % & cor_0	3: 0 % & cor	4: 0 % & cor_0
$V_{\text{pr,mag}}$	2.1	40.9	4.8	41.3
$V_{\text{pr,ang}}$	1.6	36.4	3.8	36.6

Summarized Analysis of Prior Variance Accuracy

The results from Subsection 5.2.3 and 5.2.4 for the different test cases show that a more accurate estimation of the voltage prior distribution $\Phi_{V_{\text{pr}}}$ translates into a more accurate recognition of critical system states. By considering load correlation for generating the background distribution, the $NRMSE$ for true and estimated standard deviation of the voltage prior distribution $\boldsymbol{\sigma}_{V_{\text{pr}}}$ can be reduced to at least $\sim 1/3$ and the correlation coefficient of the voltage prior distribution $\boldsymbol{\rho}_{V_{\text{pr}}}$ to $\sim 1/9$. This shows that load correlation consideration for the background distribution in Bayesian linear state estimation strongly improves the estimation of the prior distribution $\Phi_{V_{\text{pr}}}$. Further, the above results show that even without any SM measurements as non-real-time background input, the proposed correlation-aware synthesis module impressively improves the accuracy of the prior voltage distribution by accounting for the load correlations.

5.2.5 Summary for Applying Correlation-Aware Synthesis Module

Calculating a background distribution with load correlations was previously only demonstrated for a complete set of time-resolved power measurements at all MV grid nodes (e.g., historical measurements MV_{meas} or SM from underlying LV grids $\text{SM}_{100\,\%}$). With the correlation-aware

synthesis module, a background distribution incorporating load correlation can be estimated for MV grids with different MIS, including $SM_{>\alpha_{thres}}$ and $SM_{\leq\alpha_{thres}}$. The pre-processing module enables an accurate estimation of correlation-aware background distribution, even for MV nodes with underlying LV grids with less or without SM measurements.

It was shown that the background distributions for MV nodes with underlying LV grids having low SM coverage ($SM_{\leq\alpha_{thres}}$) can be accurately synthesized with properties of comparable LV grids. Section 5.2.3 highlights the importance of accurately modeling load correlations in Bayesian linear state estimation. It was demonstrated that using the correlation-aware synthesis module for estimating the background distribution and thus considering load correlation substantially improves the recognition accuracy of critical system states. Even for cases with no or very limited data availability, up to $98\,\%$ of the true critical system states are correctly identified. The fraction of *missed* critical system states can be reduced by a factor of up to 9 compared to neglecting the load correlations.

The results emphasize the importance of accurately modeling the statistical properties of customer behavior in distribution system state estimation. The correlation-aware synthesis module can adequately account for such load correlations. Further, using the pre-processing module, the recognition rate calculated with non-real-time data assuming $0\,\%$ SM coverage is nearly as high as with full-time-resolved SM coverage.

5.3 Strengths and Limitations of the Proposed Method and the Case Study

This section provides an overview of the strengths and limitations of the proposed Bayesian state estimation method for MV grids, including the modules presented. It also points out the limitations arising from the assumptions of the case study. Before discussing the strengths and limitations, the proposed uncertainty-aware state estimation method is analyzed according to the fulfillment of the requirements defined in research question 1.

5.3.1 Requirement Fulfillment of the Proposed State Estimation Method

In Section 4.2, the Bayesian state estimation methods from literature have been compared according to achieve the defined requirements from Section 2.2. For this, comparison criteria have been defined (see Subsection 4.2.1). The comparison criteria concerning the inputs are now inserted on the left-hand side in Table 5.8. On the right-hand side of the table, it is discussed whether the proposed state estimation method fulfills these criteria.

Three more requirements are analyzed in the comparison study of Section 4.2. They also result from research question 1: near-real-time condition, uncertainty-aware evaluation, and identification of limit violations. Now, it is discussed whether they are considered in the proposed uncertainty-aware state estimation method.

Table 5.8: Relevant inputs considered in this thesis

Assertion	Evidence
Practice-relevant grids realistic scale and partly closed ring structure	The test grid from Subsection 5.1.2 was chosen for the simulations in this chapter. It has 107 buses and thus fulfills the requirements for a realistic scale of a test grid with over 80 buses. Further, it has one exemplary ring structure. The tests show that the chosen model can handle this non-radial structure.
Heterogeneous meter input including PMU & RTU measurements, SM data, annual energy demand, and non-real-time data with varying levels of detail	Concerning the heterogeneous meter input, first, the real-time measurements are considered. As shown in Section 3.3, the model for Bayesian Linear state estimation from [94] was extended by using the Jacobi Matrix of measurements (see Equation 3.59). This allows handling all measurable variables from PMU and RTU measurements. The correlation-aware synthesis module developed in this thesis is used to generate the background distribution. It incorporates Smart Meter data and annual energy demand from non-metered customers. Thus, it can process non-real-time data with varying levels of detail (see Subsection 5.2).
Load correlation	The pre-processing module is explicitly beneficial for accounting for load correlations. Thus, load correlations can be considered for every MV node, even if the node is not directly metered.

In order to achieve low computation times for the near-real-time requirement, an analytical Bayesian state estimation approach was chosen (see Subsection 3.2.2). This non-iterative approach is very time-saving. Tests with different numbers of real-time measurements are evaluated to prove the near-real-time property of the method. All simulations are obtained using Python on an Intel Core i7-9850H CPU with 16 GB RAM.

- The computation time for calculation of the posterior distribution (only the online state estimation part) never exceeds 12 ms (see Figure A.1a).

- With the subsequent calculation of the probability of critical system states, the algorithm needs maximal $1/4$ s in total (see Figure A.1b).

Hence, the computation time for the proposed state estimation method is less under the requirement of 60 s.

The two other requirements, namely the consideration of the output uncertainty in the evaluation and the detection of limit violations, are covered by using the post-processing module for calculating the probability of critical system states (see Section 5.1). The criticality analysis module uses the uncertainty of the output to give a probabilistic estimate of the criticality of a system state. It was evaluated for accurate detection of limit violations and achieved the required detection rate of > 90 %.

5.3.2 Strengths

The strengths of the proposed method are summarized below. First, the benefits resulting from algorithm choice are discussed. Since the chosen Bayesian linear state estimation algorithm is non-iterative, there are no convergence issues for ring structures or a low amount of accurate real-time measurements, which is typical for MV grids. Further, as it is an analytical approach, the computation times are short, as previously evaluated in Subsection 5.3.1. The linearized power flow equation used to estimate the voltage prior distribution from the background distribution only approximates the actual non-linear power flow. Thus, the results include deviations. However, the magnitude and angle deviations of voltage prior expectation values are less than $0.5\,\%$ respectively $0.001\,°$. Hence, compared to Monte Carlo simulations or machine learning algorithms, this approximation is a suitable and time-saving tool for appropriately estimating the prior distribution. Further, compared to the widely used WLS estimator and many other deterministic approaches, the Bayesian method does not assume a single estimated value as "true and only" representative for the state. Due to the low level of measurement instrumentation, the input has uncertainties, and thus does the output. Hence, it is better to be aware of the uncertainties of the output than ignore them.

The proposed additions to the algorithm from [94] developed in this thesis (see Subsection 3.29) include further strengths. The method is no longer limited to any specific measurement type. This is achieved by incorporating the Jacobi matrix of measurement function into the approach (see Section 3.3). Further, by using the complex form of normal distribution to transform the background distribution to voltage prior distribution, the method can incorporate the load correlation of the background input. This option to consider load correlation is a massive strength of the proposed state estimation method, as it enables more accurate detection of limit violations even with a small amount ($< 5\,\%$) of real-time measurements (see Section 5.2.3).

This paragraph summarizes the benefits of the criticality analysis module. By using the entire posterior distribution, i.e., the covariance in addition to the expectation value, high recognition rates for identifying critical system states are achieved. The module for calculating the probability of critical system states is not limited to normal distributions. It can evaluate every integrable posterior probability. Further, the proposed method can output warning and alert messages in case of (near) critical system states. This has two advantages: First, if the grid expansion does not proceed fast enough and the expected high number of limit violations actually occurs, the grid operators know where to act in the critical case. Second, newly planned grids no longer have to meet the strict connection regulations calculated for the worst-case scenario. In the normal case, the grids can be loaded higher, and the grid operator is warned when a limit value is in danger of being violated.

Last, the strengths resulting from using the correlation-aware synthesis module are pointed out. The module generates background distributions for realistic availability assumptions of non-real-time data as it incorporates non-real-time data with varying levels of detail. It considered time-resolved smart meter data and customers with only annual energy demand information. Further, the method accounts for load correlations, even for non-metered customers. Thus, the method takes advantage of correlated consumer behavior and highly spatial and temporal correlated volatile energy sources.

5.3.3 Limitations

The main limitations of the method and the case study result from the model assumptions made at the beginning. Possible uncertainties in grid topology and phase imbalances are assumed to be negligibly small because of the reasons given in Section 2.2. Hence, this method does not consider uncertain switching states, and the modeling is only done for three-phase symmetrical systems. The assumption for normal distributed loads is an additional limitation of the approach. Even if the load distributions at MV nodes are often statistically close to Gaussian [160], several consumption and generations units could be modeled more appropriately by non-normally distribution, e.g., Gaussian Mixture [161], [162] or beta and log-normal distribution [163]. A further limitation is that measurement errors are not simulated so far.

Subsection 5.2.4 shows the benefits of an accurately estimated prior distribution. However, this also implies a strong dependency on the estimation accuracy of prior distributions for the state estimation results. This means that if the prior distribution does not include critical states that will occur in the future, it is more difficult to recognize them. So far, in the correlation analysis study, only LV grids with residential profiles are considered. They are the predominant type of customers, but there are also small rural and commercial customers. Hence, the correlation analysis does not distinguish between rural, semi-urban, and urban grids, thus limiting the application. However, the same concept can be straightforwardly extended to more diverse classes of customers and LV grid types. Further research should be carried out on the detailed modeling of scenarios for grids with higher penetration of heat pumps, EV and RES. A further limitation of the case study is that no optimal meter placement was applied for the location of real-time measurements.

5.3.4 Summary of Strengths and Limitations

The discussed strengths and limitations of the proposed state estimation method and the case study are summarized in Table 5.9.

Table 5.9: Summarized strengths and limitations of the proposed state estimation method and of the simulation study

Strengths	Limitations
• No convergence issues for ring structures or a low amount of accurate real-time measurements • Short computation times • Time-saving linearized power flow equation for prior estimation • Consideration of input & output uncertainties • No limitation to any specific measurement type • Incorporating load correlation • High recognition of critical system states • No limitation to normal distribution for post-processing module • Output warning and alert messages as decision support for operators • Higher grid utilization possible • Possibly incorporating non-real-time-data with varying levels of detail • Accounting for load correlations, even for non-metered customers	• Assumption of known grid topology and symmetrical phases required • Normal distributed modeling of algorithm • Neglecting simulation of measurement errors • Dependency on accurate estimation of prior distribution • Lack of correlation analysis for different LV grid types • No detailed scenario modeling • No application of optimal meter placement

6 Conclusion and Outlook

6.1 Conclusion

This thesis focuses on the objective of deploying a state estimation method adapted to the characteristics of MV grids to meet the upcoming challenges of changing system conditions. To reach this objective, a new method for medium-voltage grid state estimation was developed and evaluated through multiple simulation test cases. The following research question results from an analysis of the today's requirements and challenges for medium-voltage grid state estimation, caused by an increasing share of photovoltaic, heat pumps and electrical vehicles.

1. Which method is efficient & practical for uncertainty-aware state estimation for MV grids?

To address this question, a probabilistic Bayesian approach was chosen for the state estimation algorithm. Since it considers the uncertainties of the input and output, it enables an uncertainty-aware state estimation. To fulfill the requirements of efficiency and practicality, this algorithm was extended by one statistics module parameterizing the background distribution and one criticality analysis module evaluating the probability of limit violations. The evaluated tests show that the proposed method is highly efficient in detecting voltage band and thermal current limit violations. In case studies, the proposed state estimation method achieves a higher detection accuracy of criticality than the widely used Weighted-Least-Squares state estimation approach used for transmission systems and performs also better than expectation value-based approaches. With short computation times for realistically sized grids, faster than a second, the new method allows timely intervention by grid operators.

The selected test grid reproduces typical properties of MV grids, such as a realistic number of buses and partially closed ring structures. It also has a typically low share of buses receiving real-time measurements (5 %) and so the tests demonstrate the feasibility of the method with low measurement instrumentation. The pre-processing module developed in this thesis allows to parameterize the background load distributions for all practically relevant measurement availability scenarios while accounting for load correlations. The module can process time-resolved smart meter measurements as well as non-metered customers with only annual energy demand information. Tests were performed for non-real-time data with varying levels of detail using a new developed correlation-aware synthesis module. The results show the importance of considering load correlations by achieving substantially higher accuracy of state estimation results and, thus, higher recognition rates of critical system states than if correlations are neglected. Further, using comparable but different load profiles to estimate the behavior of unmetered customers shows that the detection rate of critical system states is nearly as high as with full smart meter coverage.

Since the proposed method is accurate in recognizing limit violations with detection rates over 90 % and as the results are available in near-real time, it meets the defined requirements for MV grid state estimation methods resulting from the requirement analysis performed in this thesis.

The usability of the result of the proposed state estimation method for system operators is addressed in a second research question:

2. How can the probabilistic state information be utilized for practical decision support in grid operation?

The output of the proposed uncertainty-aware state estimation method is the probability of critical system states. This can be used to classify the grid elements into warning and alert stages based on configurable probability thresholds. This differentiation into criticality stages provides practical decision support for grid operators. In particular, stages with low, conservative thresholds can be used for early warning. The probabilistic method with stage differentiation can be highly beneficial to the grid operators, as it is more sensitive to (near) critical system states than deterministic approaches. With this information, the grids can be better utilized, and the technical connection regulations do not have to be as strict.

6.2 Outlook

Several limitations of the proposed method and the case study were identified that should be addressed in future research.

Grid topology uncertainties and topology identification were excluded in this thesis to focus on the state estimation task. However, the grid topology uncertainties could play a major role, especially for medium-voltage grids with non-digitally monitored switching states. Therefore, the combination of grid topology estimation and state estimation is an interesting and important research area. Together with the authors from [140], a new idea for probabilistic topology and state estimation was developed during this thesis [164], which is able to provide state estimates in uncertain topologies and is promising to develop further.

The modeling in this thesis is done for a symmetrical, balanced three-phase grid. This is suitable for most European-type medium-voltage grids. However, when it is necessary to include phase imbalances, e.g., for specific applications or for US-type grids, the method could be extended to three-phase calculation in future research [143].

Furthermore, the load profiles are assumed to be normally distributed in this thesis. However, in some cases, other distribution types are more suitable than the normal distribution for modeling the behavior of grid users. To address this challenge, the given state estimation algorithm could also be modeled for Gaussian Mixture distribution similar to [81] or for log-normal distribution.

In the current case study, no tests for (gross) measurement errors were evaluated. Additional tests with measurement errors would further confirm the realistic application of the proposed method.

So far, the correlation analysis study has considered only low-voltage grids with residential load profiles. For future research, the correlation analysis could be evaluated for different types of low-voltage grids. The distinction between rural, semi-urban, and urban grids could open a broader application scope for the proposed method. For future decarbonization scenarios, further research would be needed to determine load correlations between low-voltage grids with high photovoltaic, electric vehicles, and heat pump penetrations.

The locations of the real-time measurements in this thesis were selected based on experience and exchange with system operators, but no optimal meter placement approach was applied. With an optimal meter placement for a given number of measurements, the best possible information gain can be achieved. [167] proposes an optimal meter placement approach based on a sensitivity analysis of the posterior variance.

The accuracy of the Bayesian linear state estimation can be further improved if a more accurate background distribution is available. An example would be distinguishing between weekdays and weekends or different seasons, using a separate background distribution for each setting. In addition, new input sources, such as weather data, time-varying tariffs, and penetration rates of heat pumps or wall boxes, are promising exogenous inputs for future research.

In response to the increasing need for efficiency and reliability within the distribution grid, there is a pressing demand for the continuous development of system monitoring and smart grid operation. The proposed uncertainty-aware state estimation method is suitable for dealing with the uncertainties arising with the changing system conditions. The use of artificial intelligence and the creation of flexibility options will also play a central role in future energy systems. The overall goal is to minimize congestion and limit violations, optimize load consumption, and thus ensure a sustainable, reliable, and flexible electricity supply.

Nomenclature

Variable	Description	Units
$\Gamma_S/\Gamma_{V_{\text{pr}}}$	Complex-valued covariance of background/prior distribution	
$\mu_S/\mu_{V_{\text{pr}}}/\mu_{V_{\text{po}}}/\mu_{x\|z}$	Expectation value of background/ voltage prior/ voltage posterior/ likelihood distribution	
$\mu_{S,\text{samp}}$	Sample mean of background distribution	
$\Sigma_S/\Sigma_{V_{\text{pr}}}/\Sigma_{V_{\text{po}}}/\Sigma_{x\|z}$	Real-valued covariance of background/ voltage prior/ voltage posterior/ likelihood distribution	
$\Sigma_{S_{\text{samp}}}/\Sigma_{S_{\text{comp}}}$	Sample/synthesized covariance of background distribution	
$\kappa_{x,lim}/\kappa_{p_{\text{css}},lim}$	Indicator functions	[0,1]
$\sigma_e/\sigma_z/\ \sigma_{V_{\text{pr}}}$	Standard deviation of measurement error/ measurement/ voltage prior distribution	
$\Phi_S/\Phi_{V_{\text{pr}}}/\Phi_{V_{\text{po}}}/\Phi_{x\|z}/\Phi_{I_{\text{po}}}$	Density function of background/ voltage prior/ voltage posterior/ likelihood / branch current posterior distribution	
$\Phi_S^C/\Phi_{V_{\text{pr}}}^C$	Complex-valued density function of background/prior/posterior/likelihood distribution	
$\rho_{V_{\text{pr}}}$	Correlation coefficient of prior distribution	%
τ	Transformer ratio	
ζ	Function included in GML estimator	
$ac_{\hat{x},lim}$	Accuracy for $\hat{x}$ and given limit lim	
$C_S/C_{V_{\text{pr}}}$	Pseudo-covariance of background/prior distribution	
e	Measurement error	
$E_{\sum \text{SM}}/E\sum_{\text{SM}}$	Summed up energy demand of all customers/customers with SM in LV grid	MWh
f_{scale}	Scaling factor for energy demand	
$fnr_{\hat{x},lim}/fpr_{\hat{x},lim}$	False-negative/-positive rate for $\hat{x}$ and given limit *lim*	
$\boldsymbol{G}$	Gain matrix	
$\boldsymbol{H}$	Jacobi matrix of measurement function	
h/h_{full}	Measurement function/ fully occupied measurement function	
$I_{\text{bus}}/I_{\text{f}}/I_{\text{t}}$	Current flow into bus/Branch current at “from”/“to” side	kA

I_{ph}	Single phase current	kA
I_0/ I_{ns}	Slack and non-slack currents	kA
J	Objective function	
$\boldsymbol{L}$	Admittance matrix without slack row and column	Ω^{-1}
$L_{0,0}/\boldsymbol{L}_{0,\text{col}}/\boldsymbol{L}_{0,\text{row}}$	Slack variance/Slack column/row of admittance matrix	Ω^{-1}
$S_{\text{bus}}/S_{\text{f}}/S_{\text{t}}$	Apparent power at bus/ apparent power at "from"/"to" side of branch	MVA
$S_{\text{gen}}/S_{\text{load}}$	Apparent power of generation/consumption unit	MVA
S_{loss}	Apparent power of transmission losses	MVA
S_{3ph}	Three-phase apparent power	MVA
$S_{\text{MV,synth}}/S_{\text{MV,meas}}/S_{\text{MV}}$	Synthesized/ measured/ apparent power at MV node	MVA
$S_{\sum \text{SM}}/S_{\text{SM}}$	Summed up/ apparent power of Smart Meter	MVA
$S_{\sum \text{LV}_{\text{comp}}}$	Summed up apparent power of comparable LV grid	MVA
$P_{\text{bus}}/P_{\text{f}}/P_{\text{t}}$	Active power at bus/ active power at "from"/"to" side of branch	MW
$p_{\text{css,lim}}$	Probability of critical system states for given limit lim	%
$p_{\text{thres},\sigma}/p_{\text{thres},2\sigma}$	Probability threshold for range $\mu \pm \sigma_{\text{po}}/\mu \pm 2\sigma_{\text{po}}$	
$Q_{\text{bus}}/Q_{\text{f}}/Q_{\text{t}}$	Reactive power at bus/ reactive power at "from"/"to" side of branch	MW
R	Line resistance	Ω
$r/r_{(m)}$	Residual/m-th ordered residual	
$tnr_{\hat{x},lim}/tpr_{\hat{x},lim}$	True-negative/positive rate for $\hat{x}$ and given limit *lim*	%
$V/V_{\text{f}}/V_{\text{t}}$	Node voltage at bus/ node voltage at buses of "from"/"to" side of a branch	kV
V_{ph}	Single phase voltage	kV
V_0/ V_{ns}	Slack and non-slack voltages	kV
$\boldsymbol{W}$	Weight matrix	
X	Line reactance	Ω
x	State variable	
$x_{\text{true}}/\hat{x}$	True/estimated state variable	
$\hat{x}_{\text{MAP}}/\hat{x}_{\text{ML}}/\hat{x}_{\text{MMSE}}$ $\hat{x}_{\text{LS}}/\hat{x}_{\text{WLS}}$	Estimated state variable for MAP/ML/MMSE/LS/WLS estimator	
$Y_{\text{bus}}/Y_{\text{f}}/Y_{\text{t}}$	Bus admittance/branch admittances for "from"/"to" side	Ω^{-1}
$Y_{\text{s}}/Y_{\text{sh}}/Y_{\text{bsh}}$	Series branch/ shunt branch/ shunt bus admittance	Ω^{-1}
z	Measurement variable	
Z	Branch impedance	Ω

Parameters	Description	
α_{thres}	Threshold for Smart Meter Coverage	%
θ	Phase shift	°
B	Number of branches	
$\boldsymbol{C}_{\text{f}}/\boldsymbol{C}_{\text{t}}$	Connectivity matrix for “from”/“to” side of branch	
E	Number of node or branch elements	
I_{th}	Thermal current limit	kA
K	Number of simulation runs	
M	Number of real-time measurements	
M_{trim}	Trimming constant	
N	Number of non-slack buses	
N_{SM}	Number of Smart meters	
p_{thres}	Probability threshold	%
T	Number of time steps	
$V_{\text{low}}/V_{\text{up}}$	Lower/Upper voltage band limit	kV
w	Ratio of primary to secondary windings	

Symbols	Description
MV_{meas}, $\text{SM}_{100\,\%}$/ $\text{SM}_{\geq\alpha_{\text{thres}}}/\text{SM}_{<\alpha_{\text{thres}}}$	Measurement instrumentation scenarios (see Table 4.4)
cor/cor_0	Considering/neglecting correlations

Bibliography

[1] H. Seidl, S. Mischinger, and R. Heuke. “Beobachtbarkeit und Steuerbarkeit im Energiesystem. Handlungsbedarfsanalyse der dena-Plattform Systemdienstleistungen.”, Deutsche Energie-Agentur GmbH (dena). (2016), [Online]. Available: https://www.dena.de/fileadmin/dena/Dokumente/Pdf/9184_Beobachtbarkeit_und_Steuerbarkeit_.pdf (visited on 07/20/2023).

[2] BMWK. “Zeitreihen zur Entwicklung der erneuerbaren Energien in Deutschland”. (2023), [Online]. Available: https://www.erneuerbare-energien.de/EE/Redaktion/DE/Standardartikel/zeitreihen.html (visited on 08/02/2023).

[3] A. J. Schwab, “Elektroenergiesysteme, Verbundsysteme”, in *Elektroenergiesysteme: Erzeugung, Transport, Übertragung und Verteilung elektrischer Energie*. Berlin, Heidelberg: Springer Berlin Heidelberg, 2022, pp. 9–38, ISBN: 978-3-662-64774-5. DOI: 10.1007/978-3-662-64774-5_2.

[4] “Gesetz für den Ausbau erneuerbarer Energien”, Bundesministerium der Justiz. (2014), [Online]. Available: https://www.gesetze-im-internet.de/eeg_2014/ (visited on 04/18/2023).

[5] “Veröffentlichung Zu- und Rückbau”, Bundesnetzagentur. (2022), [Online]. Available: https://www.bundesnetzagentur.de/DE/Fachthemen/ElektrizitaetundGas/Versorgungssicherheit/Erzeugungskapazitaeten/Kraftwerksliste/start.html (visited on 04/25/2023).

[6] R. Bansal, *Handbook of Distributed Generation: Electric Power Technologies, Economics and Environmental Impacts*. Springer International Publishing, 2017, ISBN: 9783319513430.

[7] (2022), [Online]. Available: https://www.iea.org/energy-system/renewables (visited on 05/19/2023).

[8] “Erneuerbare Energien”, BMWK. (2022), [Online]. Available: https://www.bmwk.de/Redaktion/DE/Dossier/erneuerbare-energien.html (visited on 07/26/2023).

[9] “Netzentwicklungsplan 2035 (2021)”, NEP. (2021), [Online]. Available: https://www.netzentwicklungsplan.de/archiv/netzentwicklungsplan-2035-2021 (visited on 04/25/2023).

[10] “Gesetz zur Reduzierung und zur Beendigung der Kohleverstromung”, Bundesministerium der Justiz. (2020), [Online]. Available: https://www.gesetze-im-internet.de/kvbg/ (visited on 04/18/2023).

[11] “Paris Agreement”, European Commission. (2015), [Online]. Available: https://climate.ec.europa.eu/eu-action/international-action-climate-change/climate-negotiations/paris-agreement_en (visited on 03/20/2023).

[12] “Der Atomausstieg in Deutschland”, Bundesamt für die Sicherheit der nuklearen Entworgung. (2011), [Online]. Available: https://www.base.bund.de/DE/themen/kt/ausstieg-atomkraft/ausstieg (visited on 04/18/2023).

[13] “EEG in Zahlen”, Deutsche Bundesnetzagentur. (2020), [Online]. Available: https://www.bundesnetzagentur.de/DE/Fachthemen/ElektrizitaetundGas/ErneuerbareEnergien/ZahlenDatenInformationen/start.html (visited on 06/27/2023).

[14] “Elektromobilität: Ausbau der Ladeinfrastruktur”, BDEW. (2022), [Online]. Available: https://www.bdew.de/service/daten-und-grafiken/elektromobilitaet-ausbau-der-ladeinfrastruktur/ (visited on 04/18/2023).

[15] “Wärmepumpenabsatz 2022: Wachstum von 53 Prozent gegenüber dem Vorjahr”, Bundesverband Wärmepumen e.V. (2023), [Online]. Available: https://www.waermepumpe.de/presse/zahlen-daten/absatzzahlen/ (visited on 03/14/2023).

[16] J. Figgener, P. Stenzel, K.-P. Kairies, J. Linßen, D. Haberschusz, O. Wessels, G. Angenendt, M. Robinius, D. Stolten, and D. U. Sauer, “The development of stationary battery storage systems in Germany – A market review”, *Journal of Energy Storage*, vol. 29, p. 101 153, 2020, ISSN: 2352-152X. DOI: https://doi.org/10.1016/j.est.2019.101153. [Online]. Available: https://www.sciencedirect.com/science/article/pii/S2352152X19309442.

[17] “Kurzinformation Elektromobilität bzgl. Strom- und Ressourcenbedarf”, Bundesministerium für Umwelt (BMU). (2022), [Online]. Available: https://www.bmu.de/fileadmin/Daten_BMU/Download_PDF/Verkehr/emob_strom_ressourcen_bf.pdf (visited on 06/27/2023).

[18] “Der Fahrzeugbestand im Überblick am 1. Januar 2023 gegenüber 1. Januar 2022”, Kraftfahrt-Bundesamt (KBA). (2023), [Online]. Available: https://www.kba.de/DE/Statistik/Fahrzeuge/Bestand/Jahrebilanz_Bestand/fz_b_jahresbilanz_node.html (visited on 06/27/2023).

[19] “Ladeinfrastruktur in Zahlen (Stand:1. januar 2023”, Bundesnetzagentur. (2023), [Online]. Available: https://www.bundesnetzagentur.de/DE/Fachthemen/ElektrizitaetundGas/E-Mobilitaet/start.html (visited on 06/30/2023).

[20] “Branchenstudie 2023: Marktentwicklung – Prognose –Handlungsempfehlungen”, Bundesverband Wärmepumpe e.V. (2022), [Online]. Available: https://www.waermepumpe.de/fileadmin/user_upload/waermepumpe/05_Presse/01_Pressemitteilungen/BWP_Branchenstudie_2023_DRUCK.pdf (visited on 04/25/2023).

[21] “Entwurf eines Gesetzes zur Änderung des Gebäudeenergiegesetzes, zur Änderung der Heizkostenverordnung und zur Änderung der Kehr- und Überprüfungsordnung”. (Jul. 20, 2022), [Online]. Available: https://www.bundesregierung.de/breg-de/aktuelles/neues-gebaeudeenergiegesetz-2184942 (visited on 07/12/2023).

[22] "Energiewende: Unzureichender Netzausbau als Risiko für die Versorgungsicherheit", Bundesrechnungshof. (2019), [Online]. Available: https://www.bundesrechnungshof.de/SharedDocs/Pressemitteilungen/DE/2019/energiewende-netzausbau.html (visited on 08/02/2023).

[23] "Bericht zum Zustand und Ausbau der Verteilernetze 2022", Deutsche Bundesnetzagentur. (2022), [Online]. Available: https://www.bundesnetzagentur.de/DE/Fachthemen/ElektrizitaetundGas/NetzentwicklungSmartGrid/Zustand_VN/start.html (visited on 04/18/2023).

[24] A. Abur and A. Gomez-Exposito, *Power System State Estimation: Theory and Implementation*. Mar. 2004, vol. 24, ISBN: 0-8247-5570-7. DOI: 10.1201/9780203913673.

[25] 50hertz. "Exploiting Instead of Curtailing: First Power-to-Heat Units Now Operational in Northern Germany", www.50hertz.com. (Nov. 29, 2021), [Online]. Available: https://www.50hertz.com/en/News/Details/11600/exploiting-instead-of-curtailing-first-power-to-heat-units-now-operational-in-northern-germany (visited on 07/10/2023).

[26] K. Rauma, A. Funke, T. Simolin, P. Järventausta, and C. Rehtanz, "Electric Vehicles as a Flexibility Provider: Optimal Charging Schedules to Improve the Quality of Charging Service", *Electricity*, vol. 2, no. 3, pp. 225–243, 2021, ISSN: 2673-4826. DOI: 10.3390/electricity2030014. [Online]. Available: https://www.mdpi.com/2673-4826/2/3/14.

[27] C. Rehtanz, N. Voropai, and U. Häger, "Requirements for Monitoring, Control and Operation", in *Monitoring, Control and Protection of Interconnected Power Systems*. Berlin, Heidelberg: Springer Berlin Heidelberg, 2014, pp. 3–17, ISBN: 978-3-642-53848-3. DOI: 10.1007/978-3-642-53848-3_1. [Online]. Available: https://doi.org/10.1007/978-3-642-53848-3_1.

[28] F. C. Schweppe, "Power System Static-State Estimation, Part I, II and III", *IEEE Transactions on Power Apparatus and Systems*, vol. PAS-89, no. 1, pp. 130–135, 1970. DOI: 10.1109/TPAS.1970.292680.

[29] "Bericht zum Zustand und Ausbau der Verteilernetze 2021", Deutsche Bundesnetzagentur. (2021), [Online]. Available: https://www.bundesnetzagentur.de/DE/Fachthemen/ElektrizitaetundGas/NetzentwicklungSmartGrid/Zustand_VN/start.html (visited on 04/18/2023).

[30] B. Hayes and M. Prodanovic, "State Estimation Techniques for Electric Power Distribution Systems", en, in *2014 European Modelling Symposium*, Pisa, Italy: IEEE, Oct. 2014, pp. 303–308, ISBN: 978-1-4799-7412-2. DOI: 10.1109/EMS.2014.76. [Online]. Available: http://ieeexplore.ieee.org/document/7154016/ (visited on 02/02/2021).

[31] J. Vijaychandra, B. R. V. Prasad, V. K. Darapureddi, B. V. Rao, and Ł. Knypiński, "A Review of Distribution System State Estimation Methods and Their Applications in Power Systems", *Electronics*, vol. 12, no. 3, 2023, ISSN: 2079-9292. [Online]. Available: https://www.mdpi.com/2079-9292/12/3/603.

[32] A. Gulati, "Overview of State Estimation Technique for Power System Control", *IOSR Journal of Electrical and Electronics Engineering*, vol. 8, pp. 51–55, Jan. 2013. DOI: 10.9790/1676-0855155.

[33] "Beschluss Az. BK6-20-061", Deutsche Bundesnetzagentur. (2021), [Online]. Available: https://www.bundesnetzagentur.de/DE/Beschlusskammern/1_GZ/BK6-GZ/2020/BK6-20-061/BK6-20-061_beschluss_vom_23.03.21.pdf?__blob=publicationFile&v=2 (visited on 09/18/2023).

[34] K. Heuck, K.-D. Dettmann, and D. Schulz, *Elektrische Energieversorgung: Erzeugung, Übertragung und Verteilung elektrischer Energie für Studium und Praxis*, 9th ed. Springer Vieweg Wiesbaden, 2010, ISBN: 978-3-8348-2174-4.

[35] D. Oeding and B. R. Oswald, *Elektrische Kraftwerke und Netze*, 8th ed. Springer Vieweg Berlin, Heidelberg, 2016, ISBN: 978-3-662-52703-0.

[36] "Moderne Verteilernetze für Deutschland (Verteilernetzstudie)", BMWI. (2014), [Online]. Available: https://www.bmwk.de/Redaktion/DE/Publikationen/Studien/verteilernetzstudie.html (visited on 06/30/2023).

[37] "Versorgungszuverlässigkeit, Spannungsqualität und Kosten", OFATE DFBEW. (2019), [Online]. Available: https://energie-fr-de.eu/de/systeme-maerkte/nachrichten/leser/versorgungszuverlaessigkeit-spannungsqualitaet-und-kosten-betrachtung-der-stromnetze-in-deutschland-und-frankreich.html (visited on 04/06/2023).

[38] L. Thurner, A. Scheidler, F. Schafer, J. Menke, J. Dollichon, F. Meier, S. Meinecke, and M. Braun, "pandapower - an Open Source Python Tool for Convenient Modeling, Analysis and Optimization of Electric Power Systems", *IEEE Transactions on Power Systems*, 2018, ISSN: 0885-8950. DOI: 10.1109/TPWRS.2018.2829021. [Online]. Available: https://arxiv.org/abs/1709.06743.

[39] K. Dehghanpour, Z. Wang, J. Wang, Y. Yuan, and F. Bu, "A Survey on State Estimation Techniques and Challenges in Smart Distribution Systems", en, *IEEE Trans. Smart Grid*, vol. 10, no. 2, pp. 2312–2322, Mar. 2019, arXiv: 1809.00057, ISSN: 1949-3053, 1949-3061. DOI: 10.1109/TSG.2018.2870600. [Online]. Available: http://arxiv.org/abs/1809.00057 (visited on 05/29/2020).

[40] T. Driesen Johan und van Craenenbroeck. "Spannungsstörungen - Einführung in die Unsymmetrie". (2004), [Online]. Available: https://kupfer.de/fileadmin/user%5C_upload/kupferinstitut.de/de/Documents/Shop/Verlag/Downloads/Anwendung/Elektrotechnik/Leonardo/5.1.3%5C_Unsymmetrie.pdf (visited on 07/26/2023).

[41] G. Müller and B. Ponick, *Kapitel 1: Transformatoren*. WILEY-VCH Verlag GmbH and Co. KGaA, Weinheim, 2006, ISBN: 3-527-40524-0.

[42] J. Watitwa and K. Awodele, "A Review on Active Distribution System State Estimation", en, in *2019 Southern African Universities Power Engineering Conference/Robotics and Mechatronics/Pattern Recognition Association of South Africa (SAUPEC/RobMech/PRASA)*, Bloemfontein, South Africa: IEEE, Jan. 2019, pp. 726–731, ISBN: 978-1-72810-369-3. DOI: 10.1109/RoboMech.2019.8704833. [Online]. Available: https://ieeexplore.ieee.org/document/8704833/ (visited on 10/29/2020).

[43] M. Majdoub, J. Boukherouaa, and B. Cheddadi, "A Review on Distribution System State Estimation Techniques", en, p. 6, 2018.

[44] S. Bhela, V. Kekatos, and S. Veeramachaneni, "Enhancing Observability in Distribution Grids Using Smart Meter Data", *IEEE Transactions on Smart Grid*, vol. 9, no. 6, pp. 5953–5961, 2018. DOI: 10.1109/TSG.2017.2699939.

[45] "Studie: Wie heizt Deutschland 2019?", bdew. (2019), [Online]. Available: https://www.bdew.de/energie/studie-wie-heizt-deutschland/ (visited on 08/21/2023).

[46] J. Peppanen, S. Grijalva, M. J. Reno, and R. J. Broderick, "Distribution system low-voltage circuit topology estimation using smart metering data", en, in *2016 IEEE/PES Transmission and Distribution Conference and Exposition (TandD)*, Dallas, TX: IEEE, May 2016, pp. 1–5, ISBN: 978-1-5090-2157-4. DOI: 10.1109/TDC.2016.7519985. [Online]. Available: http://ieeexplore.ieee.org/document/7519985/ (visited on 07/03/2023).

[47] H. Li, Y. Weng, Y. Liao, B. Keel, and K. E. Brown, "Distribution grid impedance & topology estimation with limited or no micro-PMUs", *International Journal of Electrical Power & Energy Systems*, vol. 129, p. 106 794, 2021, ISSN: 0142-0615. DOI: https://doi.org/10.1016/j.ijepes.2021.106794. [Online]. Available: https://www.sciencedirect.com/science/article/pii/S014206152100034X.

[48] A. Mabrouk, "Distribution Grid Topology Estimation: A New Approach-based on Bayesian Network Models", Sep. 2022. DOI: 10.1109/BigDataService55688.2022.00027.

[49] Y. Liao, Y. Weng, G. Liu, and R. Rajagopal, "Urban MV and LV Distribution Grid Topology Estimation via Group Lasso", *IEEE Transactions on Power Systems*, vol. 34, no. 1, pp. 12–27, 2019. DOI: 10.1109/TPWRS.2018.2868877.

[50] A. von Meier, E. Stewart, A. McEachern, M. Andersen, and L. Mehrmanesh, "Precision Micro-Synchrophasors for Distribution Systems: A Summary of Applications", en, *IEEE Trans. Smart Grid*, vol. 8, no. 6, pp. 2926–2936, Nov. 2017, ISSN: 1949-3053, 1949-3061. DOI: 10.1109/TSG.2017.2720543. [Online]. Available: https://ieeexplore.ieee.org/document/7961200/ (visited on 06/16/2020).

[51] V. Crastan, *Elektrische Energieversorgung 1: Netzelemente, Modellierung, stationäres Verhalten, Bemessung, Schalt- und Schutztechnik* (Elektrische Energieversorgung). Springer Berlin Heidelberg, 2012, ISBN: 9783642223464.

[52] K. F. Schäfer, *Netzberechnung: Verfahren Zur Berechnung Elektrischer Energieversorgungsnetze*. Springer Fachmedien Wiesbaden GmbH, 2019, ISBN: 9783658408763.

[53] R. D. Zimmerman and C. E. Murillo-Sánchez, *MATPOWER*, version 7.0, Jun. 2019. DOI: 10.5281/zenodo.3251119. [Online]. Available: https://doi.org/10.5281/zenodo.3251119.

[54] G. Herold, *Elektrische Energieversorgung I - Drehstromsysteme, Leistungen, Wirtschaftlichkeit*. J. Schlembach, 2011, ISBN: 9783935340465.

[55] D. Goswami, *The CRC Handbook of Mechanical Engineering* (Handbook Series for Mechanical Engineering). CRC Press, 2004, ISBN: 9781420041583. [Online]. Available: https://books.google.de/books?id=%5C_wlZ5LHTyBIC.

[56] M. Albach, *Elektrotechnik* (Always learning). Pearson, 2011, ISBN: 9783863265724. [Online]. Available: https://books.google.de/books?id=6GsTvwEACAAJ.

[57] L. Schmidt, G. Schaller, and S. Martius, *Grundlagen der Elektrotechnik: Netzwerke* (Et Elektrotechnik). Pearson Studium, 2006, ISBN: 9783827371072. [Online]. Available: https://books.google.de/books?id=AYaDNwAACAAJ.

[58] R. E. Kalman, “A new approach to linear filtering and prediction problems”, *Trans. ASME, D*, vol. 82, pp. 35–44, 1960.

[59] J. Lunze, *Regelungstechnik 1 - Systemtheoretische Grundlagen, Analyse und Entwurf einschleifiger Regelungen*. Springer Berlin, Heidelberg, 2010, ISBN: 978-3-642-13808-9. DOI: https://doi.org/10.1007/978-3-642-13808-9.

[60] J. R. Taylor, *Introduction To Error Analysis: The Study of Uncertainties in Physical Measurements*, 2nd ed. University Science Books Mill Valley, 1997.

[61] P. Dattalo, *Analysis of Multiple Dependent Variables*. Oxford University Press, Feb. 2013, ISBN: 9780199773596. DOI: 10.1093/acprof:oso/9780199773596.001.0001. [Online]. Available: https://doi.org/10.1093/acprof:oso/9780199773596.001.0001.

[62] “Voltage characteristics of electricity supplied by public distribution networks”, Deutsches Institut für Normung, Standard, 2011.

[63] “Technische Richtlinie-Erzeugungsanlagen am Mittelspannungsnetz (Richtlinie für Anschluss und Parallelbetrieb von Erzeugungsanlagen am Mittelspannungsnetz) z”. (2008), [Online]. Available: https://www.bdew.de/media/documents/20080601_BDEW-Mittelspannungsrichtlinie.pdf (visited on 04/09/2023).

[64] “Technische Anschlussbedingungen Mittelspannung”. (2019), [Online]. Available: https://www.westnetz.de/content/dam/revu-global/westnetz/documents/fuer-partnerfirmen/strom-infothemen-fuer-installationsunternehmen/190401-tab-mittelspannung-westnetz-2019.pdf (visited on 07/26/2023).

[65] “TAB Mittelspannung: Technische Anschlussbedingungen für den Anschluss an das Mittelspannungsnetz”. (2019), [Online]. Available: https://www.netze-bw.de/partner/elektroinstallateure (visited on 07/26/2023).

[66] “Technische Anschlussbedingungen für den Anschluss an das Mittelspannungsnetz (TAB Mittelspannung) der Rheinischen NETZGesellschaft mbH”. (2019), [Online]. Available: https://www.rng.de/bedingungen-und-verordnungen (visited on 07/26/2023).

[67] “Netzoptimierung mit regelbaren Ortsnetztransformatoren (rONT)”. (2016), [Online]. Available: https://www.vde.com/de/fnn/arbeitsgebiete/innovation/hinweis-ront.

[68] J. Hanson, “Netzplanung und Netzberechnung”, in *Elektrische Energieversorgung 3: Dynamik, Regelung und Stabilität, Versorgungsqualität, Netzplanung, Betriebsplanung und -führung, Leit- und Informationstechnik, FACTS, HGÜ*. Berlin, Heidelberg: Springer Berlin Heidelberg, 2018, pp. 239–276, ISBN: 978-3-662-49021-1. DOI: 10.1007/978-3-662-49021-1_6. [Online]. Available: https://doi.org/10.1007/978-3-662.

[69] C. Lu, J. TAng, and W. Liu, “Distribution system state estimation”, *IEEE Transactions on Power Systems*, vol. 10, no. 1, pp. 229–240, 1995.

[70] H. Wang and N. Schulz, “A revised branch current-based distribution system state estimation algorithm and meter placement impact”, *IEEE Transactions on Power Systems*, vol. 19, no. 1, pp. 207–213, 2004. DOI: 10.1109/TPWRS.2003.821426.

[71] M. E. Baran and A. W. Kelley, “A branch-current-based state estimation method for distribution systems”, *IEEE Transactions on Power Systems*, vol. 10, pp. 483–491, 1995.

[72] Y. Deng, Y. He, and B. Zhang, “A branch-estimation-based state estimation method for radial distribution systems”, *IEEE Transactions on Power Delivery*, vol. 17, no. 4, pp. 1057–1062, 2002. DOI: 10.1109/TPWRD.2002.803800.

[73] S. Thrun, W. Burgard, and D. Fox, *Probabilistic Robotics* (Intelligent Robotics and Autonomous Agents series). MIT Press, 2005, ISBN: 9780262201629. [Online]. Available: https://books.google.de/books?id=2Zn6AQAAQBAJ.

[74] “Lineare Programmierung”. (2021), [Online]. Available: https://www.ibm.com/docs/de/icos/20.1.0?topic=programming-linear (visited on 04/21/2023).

[75] T. Bayes and R. Price, “An Essay towards Solving a Problem in the Doctrine of Chances. By the Late Rev. Mr. Bayes, F. R. S. Communicated by Mr. Price, in a Letter to John Canton, A. M. F. R. S”, vol. 53, pp. 370–418, 1763.

[76] C. M. Bishop, 1st ed. Springer Science+Business Media, LLC, 2006, ISBN: 978-0387-31073-2.

[77] M. E. Baran and A. W. Kelley, “State estimation for real-time monitoring of distribution systems”, *IEEE Transactions on Power Apparatus and Systems*, vol. 9, no. 3, pp. 1601–1609, 1994. DOI: 10.1109/59.336098.

[78] L. Mili, M. Cheniae, and P. Rousseeuw, “Robust state estimation of electric power systems”, *IEEE Transactions on Circuits and Systems I: Fundamental Theory and Applications*, vol. 41, no. 5, pp. 349–358, 1994. DOI: 10.1109/81.296336.

[79] M. Gol and A. Abur, “LAV Based Robust State Estimation for Systems Measured by PMUs”, *Smart Grid, IEEE Transactions on*, vol. 5, pp. 1808–1814, Jul. 2014. DOI: 10.1109/TSG.2014.2302213.

[80] J. Zhao, L. Mili, and F. Milano, “Robust Frequency Divider for Power System Online Monitoring and Control”, *IEEE Transactions on Power Systems*, vol. PP, Dec. 2017. DOI: 10.1109/TPWRS.2017.2785348.

[81] H. Bilil and H. Gharavi, “MMSE-Based Analytical Estimator for Uncertain Power System With Limited Number of Measurements”, en, *IEEE Trans. Power Syst.*, vol. 33, no. 5, pp. 5236–5247, Sep. 2018, ISSN: 0885-8950, 1558-0679. DOI: 10.1109/TPWRS.2018.2801121. [Online]. Available: https://ieeexplore.ieee.org/document/8279475/ (visited on 08/23/2022).

[82] J. A. D. Massignan, J. B. A. London, M. Bessani, C. D. Maciel, R. Z. Fannucchi, and V. Miranda, “Bayesian Inference Approach for Information Fusion in Distribution System State Estimation”, *IEEE Transactions on Smart Grid*, vol. 13, no. 1, pp. 526–540, 2022. DOI: 10.1109/TSG.2021.3128053.

[83] Y. Weng, R. Negi, and M. D. Ilic, “Probabilistic Joint State Estimation for Operational Planning”, en, *IEEE Trans. Smart Grid*, vol. 10, no. 1, pp. 601–612, Jan. 2019, ISSN: 1949-3053, 1949-3061. DOI: 10.1109/TSG.2017.2749369. [Online]. Available: https://ieeexplore.ieee.org/document/8026175/ (visited on 03/22/2021).

[84] P. Rousseeuw, “Least Median of Squares Regression”, *Journal of The American Statistical Association*, vol. 79, pp. 871–880, Dec. 1984. DOI: 10.1080/01621459.1984.10477105.

[85] E. Handschin, M. Langer, and E. Kliokys, “An interior point method for state estimation with current magnitude measurements and inequality constraints”, en, in *Proceedings of Power Industry Computer Applications Conference*, Salt Lake City, UT, USA: IEEE, 1995, pp. 385–391, ISBN: 978-0-7803-2663-7. DOI: 10.1109/PICA.1995.515268. [Online]. Available: http://ieeexplore.ieee.org/document/515268/ (visited on 03/22/2021).

[86] M. Ferdowsi, A. Löwen, P. McKeever, A. Monti, F. Ponci, and A. Benigni, “New monitoring approach for distribution systems”, in *2014 IEEE International Instrumentation and Measurement Technology Conference (I2MTC) Proceedings*, 2014, pp. 1506–1511. DOI: 10.1109/I2MTC.2014.6860997.

[87] A. Bernieri, G. Betta, C. Liguori, and A. Losi, “Neural networks and pseudo-measurements for real-time monitoring of distribution systems”, *IEEE Transactions on Instrumentation and Measurement*, vol. 45, no. 2, pp. 645–650, 1996. DOI: 10.1109/19.492803.

[88] S. Naka, T. Genji, T. Yura, and Y. Fukuyama, “A hybrid particle swarm optimization for distribution state estimation”, *IEEE Transactions on Power Systems*, vol. 18, no. 1, pp. 60–68, 2003. DOI: 10.1109/TPWRS.2002.807051.

[89] T. Niknam, A. M. Ranjbar, A. R. Shirani, and A. Ostadi, “A new approach based on ant colony algorithm to distribution management system with regard to dispersed generation”, in *CIRED 2005 - 18th International Conference and Exhibition on Electricity Distribution*, 2005, pp. 1–5. DOI: 10.1049/cp:20051242.

[90] M. V. Likith Kumar, H. A. Maruthi Prasanna, and T. Ananthapadmanabha, “An Artificial Bee Colony algorithm based distribution system state estimation including Renewable Energy Sources”, en, in *2014 International Conference on Circuits, Power and Computing Technologies [ICCPCT-2014]*, Nagercoil, Tamil Nadu, India: IEEE, Mar. 2014, pp. 509–515, ISBN: 978-1-4799-2397-7. DOI: 10.1109/ICCPCT.2014.7054948. [Online]. Available: http://ieeexplore.ieee.org/document/7054948/ (visited on 07/02/2023).

[91] U. Sur and G. Sarkar, “Hybrid firefly algorithm based distribution state estimation with regard to renewable energy sources”, en, in *2016 International Conference on Microelectronics, Computing and Communications (MicroCom)*, Durgapur, India: IEEE, Jan. 2016, pp. 1–6, ISBN: 978-1-4673-6621-2. DOI: 10.1109/MicroCom.2016.7522497. [Online]. Available: http://ieeexplore.ieee.org/document/7522497/ (visited on 07/02/2023).

[92] R. K. Pavão and F. A. B. Lemos, “Fuzzy State Estimation Applied to Smart Distribution Network Automation Functions”, en, 2015.

[93] A. Saric and R. Ciric, “Integrated fuzzy state estimation and load flow analysis in distribution networks”, *IEEE Transactions on Power Delivery*, vol. 18, no. 2, pp. 571–578, 2003. DOI: 10.1109/TPWRD.2003.809680.

[94] L. Schenato, G. Barchi, D. Macii, R. Arghandeh, K. Poolla, and A. Von Meier, “Bayesian linear state estimation using smart meters and PMUs measurements in distribution grids”, en, in *2014 IEEE International Conference on Smart Grid Communications (SmartGridComm)*, Venice, Italy: IEEE, Nov. 2014, pp. 572–577, ISBN: 978-1-4799-4934-2. DOI: 10.1109/SmartGridComm.2014.7007708. [Online]. Available: http://ieeexplore.ieee.org/document/7007708/ (visited on 06/26/2020).

[95] K. R. Mestav, J. Luengo-Rozas, and L. Tong, "Bayesian State Estimation for Unobservable Distribution Systems via Deep Learning", en, *IEEE Trans. Power Syst.*, vol. 34, no. 6, pp. 4910–4920, Nov. 2019, ISSN: 0885-8950, 1558-0679. DOI: 10.1109/TPWRS.2019.2919157. [Online]. Available: https://ieeexplore.ieee.org/document/8723114/ (visited on 04/08/2021).

[96] U. Eminoglua and M. Hocaoglub, "Distribution systems forward/backward sweep-based power flow algorithms: A review and comparison study", vol. 37, pp. 91–110, 2008.

[97] B. Picinbono, "Second-order complex random vectors and normal distributions", *IEEE Transactions on Signal Processing*, vol. 44, no. 10, pp. 2637–2640, 1996. DOI: 10.1109/78.539051.

[98] P. Bromiley, "Products and convolutions of Gaussian probability density functions", *Tina-Vision Memo*, vol. 3, no. 4, p. 1, 2003.

[99] J. R. Schott, 3rd ed. John Wiley and Sons, Inc., Hoboken, New Jersey, 2017.

[100] T. M. Inc., *MATLAB version: 9.13.0 (R2022b)*, Natick, Massachusetts, United States, 2022. [Online]. Available: https://www.mathworks.com.

[101] E. L. Bradley, "The Equivalence of Maximum Likelihood and Weighted Least Squares Estimates in the Exponential Family", *Journal of the American Statistical Association*, vol. 68, pp. 199–200, 1973.

[102] S. Sarri, M. Paolone, R. Cherkaoui, A. Borghetti, F. Napolitano, and C. A. Nucci, "State estimation of Active Distribution Networks: Comparison between WLS and iterated kalman-filter algorithm integrating PMUs", Oct. 2012, pp. 1–8, ISBN: 978-1-4673-2595-0. DOI: 10.1109/ISGTEurope.2012.6465871.

[103] M. Brown Do Coutto Filho and J. de Souza, "Forecasting-Aided State Estimation—Part I: Panorama", en, *IEEE Trans. Power Syst.*, vol. 24, no. 4, pp. 1667–1677, Nov. 2009, ISSN: 0885-8950, 1558-0679. DOI: 10.1109/TPWRS.2009.2030295. [Online]. Available: http://ieeexplore.ieee.org/document/5233865/ (visited on 02/17/2021).

[104] Z. Jia, J. Chen, and Y. Liao, "State estimation in distribution system considering effects of AMI data", in *2013 Proceedings of IEEE Southeastcon*, 2013, pp. 1–6. DOI: 10.1109/SECON.2013.6567406.

[105] H. Bentarzi, M. Tsebia, and A. Abdelmoumene, "PMU based SCADA enhancement in smart power grid", in *2018 IEEE 12th International Conference on Compatibility, Power Electronics and Power Engineering (CPE-POWERENG 2018)*, 2018, pp. 1–6. DOI: 10.1109/CPE.2018.8372580.

[106] P. E. D. C. Bundoc and J. R. C. Orillaza, "PMU-based Distribution System State Estimation", in *TENCON 2018 - 2018 IEEE Region 10 Conference*, 2018, pp. 0993–0998. DOI: 10.1109/TENCON.2018.8650416.

[107] S. Chakrabarti, E. Kyriakides, and M. Albu, "Uncertainty in Power System State Variables Obtained Through Synchronized Measurements", *IEEE Transactions on Instrumentation and Measurement*, vol. 58, no. 8, pp. 2452–2458, 2009. DOI: 10.1109/TIM.2009.2016387.

[108] M. Zahedi, "Review on Micro-PMU Applications in Active Distribution Network", in *2020 28th Iranian Conference on Electrical Engineering (ICEE)*, Aug. 2020.

[109] A. Delle Femine, D. Gallo, C. Landi, and M. Luiso, "The Design of a Low Cost Phasor Measurement Unit", *Energies*, vol. 12, no. 14, 2019, ISSN: 1996-1073. DOI: 10.3390/en12142648. [Online]. Available: https://www.mdpi.com/1996-1073/12/14/2648.

[110] A. Singh and S. K. Parida, "Power System Frequency and Phase Angle Measurement using Raspberry Pi", in *2019 21st European Conference on Power Electronics and Applications (EPE '19 ECCE Europe)*, 2019, P.1–P.7. DOI: 10.23919/EPE.2019.8915049.

[111] A. von Meier, E. Stewart, A. McEachern, M. Andersen, and L. Mehrmanesh, "Precision Micro-Synchrophasors for Distribution Systems: A Summary of Applications", *IEEE Transactions on Smart Grid*, vol. 8, no. 6, pp. 2926–2936, 2017. DOI: 10.1109/TSG.2017.2720543.

[112] E. Dusabimana and S.-G. Yoon, "A Survey on the Micro-Phasor Measurement Unit in Distribution Networks", *Electronics*, vol. 9, no. 2, 2020, ISSN: 2079-9292. DOI: 10.3390/electronics9020305. [Online]. Available: https://www.mdpi.com/2079-9292/9/2/305.

[113] B. Appasani and D. K. Mohanta, "Chapter 3 - Uncertainty analysis and risk assessment for effective decision-making using wide-area synchrophasor measurement system", in *Decision Making Applications in Modern Power Systems*, S. H. Abdel Aleem, A. Y. Abdelaziz, A. F. Zobaa, and R. Bansal, Eds., Academic Press, 2020, pp. 63–88, ISBN: 978-0-12-816445-7. DOI: https://doi.org/10.1016/B978-0-12-816445-7.00003-7. [Online]. Available: https://www.sciencedirect.com/science/article/pii/B9780128164457000037.

[114] "IEC Standard for Instrument Transformers, Instrument tranformers-Part 2: Additional requirements for current transformers", International Electrotechnical Commission, Standard, May 2012.

[115] "IEC Standard for Instrument Transformers, Instrument transformers-Part 3: Additional requirements for inductive voltage transformers", International Electrotechnical Commission, Standard, 2011.

[116] "Elektrische Sicherheit in Niederspannungsnetzen bis AC 1 000 V und DC 1 500 V – Geräte zum Prüfen, Messen oder Überwachen von Schutzmaßnahmen - Teil 12: Geräte zur Energiemessung und -überwachung (PMD)", International Electrotechnical Commission, Standard, Sep. 2023.

[117] S. Chakrabarti and E. Kyriakides, "PMU Measurement Uncertainty Considerations in WLS State Estimation", *IEEE Transactions on Power Systems*, vol. 24, no. 2, pp. 1062–1071, 2009. DOI: 10.1109/TPWRS.2009.2016295.

[118] A. Gomez-Exposito, A. Abur, P. Rousseaux, A. De, L. Villa, and C. Gomez-Quiles, "On the Use of PMUs in Power System State Estimation", Jan. 2011.

[119] "IEEE Standard for Synchrophasor Measurements for Power Systems", *IEEE Std C37.118.1-2011 (Revision of IEEE Std C37.118-2005)*, pp. 1–61, 2011. DOI: 10.1109/IEEESTD.2011.6111219.

[120] "IEEE Standard for Synchrophasor Measurements for Power Systems", *IEEE Std C37.118.1-2011 (Revision of IEEE Std C37.118-2005)*, pp. 1–61, 2011. DOI: 10.1109/IEEESTD.2011.6111219.

[121] "SIEPROTEC 5 - Schutz, Steuerung, Automatisierung, Überwachung, Power Quality – Basis, Katalog Edition 7". (2023), [Online]. Available: https://cache.industry.siemens.com/dl/files/143/109792143/att_1054749/v1/SIDG-C10059-00_SIPROTEC_5_Katalog_DE.pdf (visited on 07/20/2023).

[122] "Phasor Measurement Unit (PMU) - Datasheet". (2018), [Online]. Available: https://www.vizimax.com/amu-pmu/%5C#pmu (visited on 07/20/2023).

[123] "Model 1133A Power Sentinel - Phasor Measurement Unit". (2018), [Online]. Available: https://www.arbiter.com/catalog/category/synchronized-power-measurements.php (visited on 07/20/2023).

[124] A. Jovicic, M. Jereminov, L. Pileggi, and G. Hug, "A Linear Formulation for Power System State Estimation including RTU and PMU Measurements", in *2019 IEEE PES Innovative Smart Grid Technologies Europe (ISGT-Europe)*, 2019, pp. 1–5. DOI: 10.1109/ISGTEurope.2019.8905561.

[125] M. Asprou, E. Kyriakides, and M. Albu, "The Effect of Variable Weights in a WLS State Estimator Considering Instrument Transformer Uncertainties", *IEEE Transactions on Instrumentation and Measurement*, vol. 63, no. 6, pp. 1484–1495, 2014. DOI: 10.1109/TIM.2013.2292138.

[126] M. Asprou, E. Kyriakides, and M. Albu, "The effect of PMU measurement chain quality on line parameter calculation", in *2017 IEEE International Instrumentation and Measurement Technology Conference (I2MTC)*, 2017, pp. 1–6. DOI: 10.1109/I2MTC.2017.7969757.

[127] "IEEE Standard for Synchrophasor Data Transfer for Power Systems", *IEEE Std C37.118.2-2011 (Revision of IEEE Std C37.118-2005)*, pp. 1–53, 2011. DOI: 10.1109/IEEESTD.2011.6111222.

[128] P. M. Joshi and H. Verma, "Synchrophasor measurement applications and optimal PMU placement: A review", *Electric Power Systems Research*, vol. 199, p. 107 428, 2021, ISSN: 0378-7796. DOI: https://doi.org/10.1016/j.epsr.2021.107428. [Online]. Available: https://www.sciencedirect.com/science/article/pii/S0378779621004090.

[129] M. Hojabri, U. Dersch, A. Papaemmanouil, and P. Bosshart, "A Comprehensive Survey on Phasor Measurement Unit Applications in Distribution Systems", *Energies*, vol. 12, no. 23, 2019, ISSN: 1996-1073. DOI: 10.3390/en12234552. [Online]. Available: https://www.mdpi.com/1996-1073/12/23/4552.

[130] "Stromnetzzugangsverordnung", BMWK. (2017), [Online]. Available: https://www.bmw.de/Redaktion/DE/Gesetze/Energie/StromNZV.html (visited on 04/12/2023).

[131] "Gesetz zum Neustart der Digitalisierung der Energiewende BGBl. 2023 I Nr. 133 vom 26.05.2023". (2023), [Online]. Available: https://www.recht.bund.de/bgbl/1/2023/133/VO.html (visited on 08/31/2023).

[132] "2012/148/EU: Commission Recommendation of 9 March 2012 on preparations for the roll-out of smart metering systems", 2012. [Online]. Available: https://eur-lex.europa.eu/eli/reco/2012/148/oj (visited on 07/20/2023).

[133] "Standardlastprofile Strom". (2017), [Online]. Available: https://www.bdew.de/energie/standardlastprofile-strom/ (visited on 07/20/2023).

[134] G. Prettico, M. Flammini, N. Andreadou, S. Vitiello, G. Fulli, and M. Masera, "Distribution System Operators Observatory 2018—Overview of the Electricity Distribution System in Europe", pp. 142–149, 2019. DOI: 10.2760/2690.

[135] F. Tounquet and C. Alaton, "Benchmarking Smart Metering Deployment in the EU-28: Final Report.", 2020. DOI: 10.2833/492070.

[136] Y. Gao, C. Fang, and J. Zhang, "A Spatial Analysis of Smart Meter Adoptions: Empirical Evidence from the U.S. Data", *Sustainability*, vol. 14, no. 3, 2022, ISSN: 2071-1050. DOI: 10.3390/su14031126. [Online]. Available: https://www.mdpi.com/2071-1050/14/3/1126.

[137] C. Muscas, M. Pau, P. A. Pegoraro, and S. Sulis, "Effects of Measurements and Pseudomeasurements Correlation in Distribution System State Estimation", en, *IEEE Trans. Instrum. Meas.*, vol. 63, no. 12, pp. 2813–2823, Dec. 2014, ISSN: 0018-9456, 1557-9662. DOI: 10.1109/TIM.2014.2318391. [Online]. Available: http://ieeexplore.ieee.org/document/6814319/ (visited on 06/30/2023).

[138] E. Buchta, M. Duckheim, M. Metzger, P. Stursberg, and S. Niessen, "Leveraging behavioral correlation in distribution system state estimation for the recognition of critical system states", *Energies*, vol. 16, no. 20, 2023, ISSN: 1996-1073. DOI: 10.3390/en16207180. [Online]. Available: https://www.mdpi.com/1996-1073/16/20/7180.

[139] S. Meinecke, D. Sarajlić, S. R. Drauz, A. Klettke, L.-P. Lauven, C. Rehtanz, A. Moser, and M. Braun, "SimBench—A Benchmark Dataset of Electric Power Systems to Compare Innovative Solutions based on Power Flow Analysis", *Energies*, vol. 13, no. 12, p. 3290, Jun. 2020. DOI: https://doi.org/10.3390/en13123290.

[140] D. Tomaselli, P. Stursberg, M. Metzger, and F. Steinke, "Representing Topology Uncertainty for Distribution Grid Expansion Planning", en, Rome, Italy: CIRED 2023, Jun. 2023. [Online]. Available: https://ieeexplore.ieee.org/document/10267489.

[141] A. Arefi, G. Ledwich, and B. Behi, "An Efficient DSE Using Conditional Multivariate Complex Gaussian Distribution", en, *IEEE Trans. Smart Grid*, vol. 6, no. 4, pp. 2147–2156, Jul. 2015, ISSN: 1949-3053, 1949-3061. DOI: 10.1109/TSG.2014.2385871. [Online]. Available: http://ieeexplore.ieee.org/document/7010936/ (visited on 06/29/2021).

[142] P. A. Pegoraro, A. Angioni, M. Pau, A. Monti, C. Muscas, F. Ponci, and S. Sulis, "Bayesian Approach for Distribution System State Estimation With Non-Gaussian Uncertainty Models", en, *IEEE Trans. Instrum. Meas.*, vol. 66, no. 11, pp. 2957–2966, Nov. 2017, ISSN: 0018-9456, 1557-9662. DOI: 10.1109/TIM.2017.2728398. [Online]. Available: http://ieeexplore.ieee.org/document/8008784/ (visited on 05/29/2020).

[143] R. Dobbe, W. van Westering, S. Liu, D. Arnold, D. Callaway, and C. Tomlin, "Linear Single- and Three-Phase Voltage Forecasting and Bayesian State Estimation With Limited Sensing", en, *IEEE Trans. Power Syst.*, vol. 35, no. 3, pp. 1674–1683, May 2020, ISSN: 0885-8950, 1558-0679. DOI: 10.1109/TPWRS.2019.2955893. [Online]. Available: https://ieeexplore.ieee.org/document/8913505/ (visited on 09/17/2021).

[144] R. B. Nelsen, *An Introduction to Copulas*. Springer New York, NY, 2010, ISBN: 978-1-4419-2109-3. DOI: https://doi.org/10.1007/0-387-28678-0.

[145] M. Sankur, R. Dobbe, E. Stewart, D. Callaway, and D. Arnold, "A Linearized Power Flow Model for Optimization in Unbalanced Distribution Systems", Jun. 2016.

[146] S. de Jongh, F. Müller, H. Li, B. Georgieva, M. Suriyah, and T. Leibfried, "Machine-learning-based Bayesian state estimation in electrical energy systems", in *CIRED 2020 Berlin Workshop (CIRED 2020)*, vol. 2020, 2020, pp. 341–344. DOI: 10.1049/oap-cired.2021.0053.

[147] C. Aggarwal, *Neural Networks and Deep Learning: A Textbook*. Springer International Publishing, 2018, ISBN: 9783319944630. [Online]. Available: https://books.google.de/books?id=achqDwAAQBAJ.

[148] Y. Hu, A. Kuh, T. Yang, and A. Kavcic, "A Belief Propagation Based Power Distribution System State Estimator", *IEEE Computational Intelligence Magazine*, vol. 6, no. 3, pp. 36–46, 2011. DOI: 10.1109/MCI.2011.941589.

[149] P. Chavali and A. Nehorai, "Distributed Power System State Estimation Using Factor Graphs", *IEEE Transactions on Signal Processing*, vol. 63, no. 11, pp. 2864–2876, 2015. DOI: 10.1109/TSP.2015.2413297.

[150] L. Myers, B. Wang, N. Z. Gong, and D. Qiao, "State Estimation via Inference on a Probabilistic Graphical Model - A Different Perspective", in *2020 IEEE Power and Energy Society Innovative Smart Grid Technologies Conference (ISGT)*, 2020, pp. 1–5. DOI: 10.1109/ISGT45199.2020.9087690.

[151] E. Buchta, M. Duckheim, M. Metzger, P. Stursberg, and S. Niessen, "Calculating Probability of Critical System States by Using Bayesian Distribution System State Estimation", en, Rome, Italy: CIRED 2023, Jun. 2023. [Online]. Available: https://ieeexplore.ieee.org/document/10267222.

[152] E. Buchta, M. Duckheim, and M. Metzger, "Verfahren und Steuereinheit zur Steuerung eines Stromnetzes - Europäisches Patent, EP 4 312 329 A1", Jul. 2023.

[153] E. Buchta, M. Duckheim, M. Metzger, and P. Stursberg, "Verfahren zur Erzeugung von Eingangsdaten für eine Zustandsschätzung eines Stromnetzes, Zustandsschätzung sowie Steuerung eines Stromnetzes - Deutsches Patent, 10 2023 203 985", Apr. 2023.

[154] "Open Energy Information", OpenEI. (2022), [Online]. Available: http://en.openei.org (visited on 04/12/2023).

[155] "Repräsentative elektrische Lastprofile fürWohngebäude in Deutschland auf 1-sekündiger Datenbasis", HTW Berlin (Germany). (2015), [Online]. Available: https://solar.htw-berlin.de/elektrische-lastprofile-fuer-wohngebaeude/ (visited on 04/06/2023).

[156] "Gutachten Digitalisierung der Energiewende Topthema2: Regulierung, Flexibilisierung und Sektorkoplung", BMWK. (2018), [Online]. Available: https://www.bmwk.de/Redaktion/DE/Publikationen/Studien/digitalisierung-der-energiewende-thema-2.pdf (visited on 04/06/2023).

[157] G. Van Rossum and F. L. Drake, *Python 3 Reference Manual*. Scotts Valley, CA: CreateSpace, 2009, ISBN: 1441412697.

[158] A. Hüneburg and V. Breisig. “Intelligent, leistungsstark, flexibel: Stromnetze der Zukunft - Der Weg zum Klimaneutralitätsnetz – Was kommt nach 2030?”, Verband der Elektro- und Digitalindustrie (ZVEI]. (Feb. 2023), [Online]. Available: https://www.zvei.org/fileadmin/user_upload/Presse_und_Medien/Publikationen/2023/Maerz/Stromnetze_der_Zukunft_Studie/2023-02-17_ZVEI_Stromnetze_2030_final_Anpassungen_ZVEI.pdf (visited on 08/20/2023).

[159] “Doppelter Haushaltsstromverbrauch mit Elektroauto”, Verband der Bayerischen Energie und Wasserwirtschaft (vbew). (2021), [Online]. Available: https://www.vbew.de/energie/presseinfos-energie/news/doppelter-haushaltsstromverbrauch-mit-elektroauto (visited on 09/02/2023).

[160] A. Angioni, T. Schlosser, F. Ponci, and A. Monti, “Impact of Pseudo-Measurements From New Power Profiles on State Estimation in Low-Voltage Grids”, en, *IEEE Trans. Instrum. Meas.*, vol. 65, no. 1, pp. 70–77, Jan. 2016, ISSN: 0018-9456, 1557-9662. DOI: 10.1109/TIM.2015.2454673. [Online]. Available: http://ieeexplore.ieee.org/document/7312455/ (visited on 03/22/2021).

[161] E. Manitsas, R. Singh, B. C. Pal, and G. Strbac, “Distribution System State Estimation Using an Artificial Neural Network Approach for Pseudo Measurement Modeling”, *IEEE Transactions on Power Systems*, vol. 27, no. 4, pp. 1888–1896, 2012. DOI: 10.1109/TPWRS.2012.2187804.

[162] R. Singh, B. C. Pal, and R. A. Jabr, “Statistical Representation of Distribution System Loads Using Gaussian Mixture Model”, *IEEE Transactions on Power Systems*, vol. 25, no. 1, pp. 29–37, 2010. DOI: 10.1109/TPWRS.2009.2030271.

[163] A. Ghosh, D. Lubkeman, M. Downey, and R. Jones, “Distribution circuit state estimation using a probabilistic approach”, *IEEE Transactions on Power Systems*, vol. 12, no. 1, pp. 45–51, 1997. DOI: 10.1109/59.574922.

[164] E. Buchta, D. Tomaselli, M. Duckheim, P. Stursberg, and M. Metzger, “Netzzustandsschätzung sowie Steuerung eines Stromnetzes - Deutsches Patent, 10 2023 203 031.4”, Mar. 2023.

[165] N. Demydov, M. Duckheim, M. Metzger, P. Stursberg, and E. Buchta, “Method for operating a power supply network, computer program and electronically readable data carrier - US Patent, US 18/322,124 ”, May 2023.

[166] E. Aumann, E. Buchta, D. Westermann, and S. Niessen, “Novel temperature sensing for switchgear bushings based on the built-in capacitive coupler”, *IEEE Transactions on Power Delivery*, pp. 1–9, 2024. DOI: 10.1109/TPWRD.2024.3386605.

[167] E. Buchta, M. Duckheim, and M. Metzger, “Ermittlung von Messstellenorten innerhalb eines Stromnetzes - Deutsches Patent, 10 2024 204 066.5 ”, Apr. 2024.

A Appendix

A.1 List of Contributions

Following contributions originated during the course of this thesis:

First-author publications

1. E. Buchta, M. Duckheim, M. Metzger, P. Stursberg, and S. Niessen, “Calculating Probability of Critical System States by Using Bayesian Distribution System State Estimation”, en, Rome, Italy: CIRED 2023, Jun. 2023. [Online]. Available: https://ieeexplore.ieee.org/document/10267222

2. E. Buchta, M. Duckheim, M. Metzger, P. Stursberg, and S. Niessen, “Leveraging behavioral correlation in distribution system state estimation for the recognition of critical system states”, *Energies*, vol. 16, no. 20, 2023, ISSN: 1996-1073. DOI: 10.3390/en16207180. [Online]. Available: https://www.mdpi.com/1996-1073/16/20/7180

Other publications and published patent applications

1. E. Buchta, M. Duckheim, and M. Metzger, “Verfahren und Steuereinheit zur Steuerung eines Stromnetzes - Europäisches Patent, EP 4 312 329 A1”, Jul. 2023

2. E. Buchta, M. Duckheim, M. Metzger, and P. Stursberg, “Verfahren zur Erzeugung von Eingangsdaten für eine Zustandsschätzung eines Stromnetzes, Zustandsschätzung sowie Steuerung eines Stromnetzes - Deutsches Patent, 10 2023 203 985”, Apr. 2023

3. N. Demydov, M. Duckheim, M. Metzger, P. Stursberg, and E. Buchta, “Method for operating a power supply network, computer program and electronically readable data carrier - US Patent, US 18/322,124 ”, May 2023

4. E. Buchta, D. Tomaselli, M. Duckheim, P. Stursberg, and M. Metzger, “Netzzustandsschätzung sowie Steuerung eines Stromnetzes - Deutsches Patent, 10 2023 203 031.4”, Mar. 2023

5. E. Aumann, E. Buchta, D. Westermann, and S. Niessen, “Novel temperature sensing for switchgear bushings based on the built-in capacitive coupler”, *IEEE Transactions on Power Delivery*, pp. 1–9, 2024. DOI: 10.1109/TPWRD.2024.3386605

6. E. Buchta, M. Duckheim, and M. Metzger, “Ermittlung von Messstellenorten innerhalb eines Stromnetzes - Deutsches Patent, 10 2024 204 066.5 ”, Apr. 2024

A.2 Appendix for Model Chapter

A.2.1 Linear Affine Transformation for Normal Distribution

One time assuming a normal distribution Φ_x according to equation 3.33 and a linear relation between y and x:

$$y = Ax + b \tag{A.1}$$

Then is the normal distribution for y equal

$$\Phi_y = \mathcal{N}\left(y \mid A\mu_x + b, A\Sigma_x A^{\mathrm{T}}\right) \tag{A.2}$$

Another time assuming a complex valued normal distribution $\Phi_x^{\mathsf{C}} = \mathcal{N}\left(x \mid \mu_x, \Gamma_x, C_x\right)$ and again the linear relation A.1, then the complex valued normal distribution for y is given by

$$\Phi_y^{\mathsf{C}} = \mathcal{N}\left(y \mid A\mu_x + b, A\Gamma_x A^{\mathrm{T}}, AC_x A^{\mathrm{T}}\right) \tag{A.3}$$

A.2.2 Linearized Taylor Series

The linearized Taylor series of function $f(x)$ at linearization point a is given by:

$$f(x;a) \approx f(a) + \nabla f(a)^{\mathrm{T}}(x-a) \tag{A.4}$$

The ∇ operator is a vector whose components are the partial derivative operators $\frac{\partial}{\partial x}$ for vector x.

A.2.3 Jacobi Matrix of Measurement Function

In table A.1 are the possible entries for Jacobi-matrix of measurement function are given. These are partial deviations of $h_{\text{full}}(x)$ with respect to V_{re} and V_{im}. The required physical equations are:

$$I_{\text{bus}} = Y_{\text{bus}}^* V^* \tag{A.5}$$

$$S_{\text{bus}} = diag(V) Y_{\text{bus}}^* V^* \tag{A.6}$$

$$I_{\text{f}} = Y_{\text{f}} V_{\text{f}} = Y_{\text{f,re}} V_{\text{re}} - Y_{\text{f,im}} V_{\text{im}} + j \cdot \left(Y_{\text{f,re}} V_{\text{im}} + Y_{\text{f,im}} V_{\text{re}}\right) \tag{A.7}$$

$$S_{\text{f}} = diag(V_{\text{f}}) Y_{\text{f}}^* V_{\text{f}}^* \tag{A.8}$$

The links to the full equation of partial deviations are given behind every entry. The partial deviations for the ”to” elements are equivalent to ”from” elements by substitute all ”f” indices by ”t”.

Table A.1: Jacobi-matrix H entries for measurement function $h_{\text{full}}(x)$

Partial deviation of	∂V_{re}		∂V_{im}	
P_{bus}	$\frac{\partial P_{\text{bus}}}{\partial V_{\text{re}}} = Re\left(\frac{\partial S_{\text{bus}}}{\partial V_{\text{re}}}\right)$	A.9	$\frac{\partial P_{\text{bus}}}{\partial V_{\text{im}}} = Re\left(\frac{\partial S_{\text{bus}}}{\partial V_{\text{im}}}\right)$	A.10
P_{f}	$\frac{\partial P_{\text{f}}}{\partial V_{\text{re}}} = Re\left(\frac{\partial S_{\text{f}}}{\partial V_{\text{re}}}\right)$	A.11	$\frac{\partial P_{\text{f}}}{\partial V_{\text{im}}} = Re\left(\frac{\partial S_{\text{f}}}{\partial V_{\text{im}}}\right)$	A.12
P_{t}	$\frac{\partial P_{\text{t}}}{\partial V_{\text{re}}} = Re\left(\frac{\partial S_{\text{t}}}{\partial V_{\text{re}}}\right)$		$\frac{\partial P_{\text{t}}}{\partial V_{\text{im}}} = Re\left(\frac{\partial S_{\text{t}}}{\partial V_{\text{im}}}\right)$	
Q_{bus}	$\frac{\partial Q_{\text{bus}}}{\partial V_{\text{re}}} = Im\left(\frac{\partial S_{\text{bus}}}{\partial V_{\text{re}}}\right)$	A.9	$\frac{\partial Q_{\text{bus}}}{\partial V_{\text{im}}} = Im\left(\frac{\partial S_{\text{bus}}}{\partial V_{\text{im}}}\right)$	A.10
Q_{f}	$\frac{\partial Q_{\text{f}}}{\partial V_{\text{re}}} = Im\left(\frac{\partial S_{\text{f}}}{\partial V_{\text{re}}}\right)$	A.11	$\frac{\partial Q_{\text{f}}}{\partial V_{\text{im}}} = Im\left(\frac{\partial S_{\text{f}}}{\partial V_{\text{im}}}\right)$	A.12
Q_{t}	$\frac{\partial Q_{\text{t}}}{\partial V_{\text{re}}} = Im\left(\frac{\partial S_{\text{t}}}{\partial V_{\text{re}}}\right)$		$\frac{\partial Q_{\text{t}}}{\partial V_{\text{im}}} = Im\left(\frac{\partial S_{\text{t}}}{\partial V_{\text{im}}}\right)$	
V_{mag}	$\frac{\partial V_{\text{mag}}}{\partial V_{\text{re}}}$	A.13	$\frac{\partial V_{\text{mag}}}{\partial V_{\text{im}}}$	A.14
V_{ang}	$\frac{\partial V_{\text{ang}}}{\partial V_{\text{re}}}$	A.15	$\frac{\partial V_{\text{ang}}}{\partial V_{\text{im}}}$	A.16
$I_{\text{f,mag}}$	$\frac{\partial I_{\text{f,mag}}}{\partial V_{\text{re}}}$	A.17	$\frac{\partial I_{\text{f,mag}}}{\partial V_{\text{im}}}$	A.18
$I_{\text{t,mag}}$	$\frac{\partial I_{\text{t,mag}}}{\partial V_{\text{re}}}$		$\frac{\partial I_{\text{t,mag}}}{\partial V_{\text{im}}}$	
$I_{\text{f,ang}}$	$\frac{\partial I_{\text{f,ang}}}{\partial V_{\text{re}}}$	A.19	$\frac{\partial I_{\text{f,ang}}}{\partial V_{\text{im}}}$	A.20
$I_{\text{t,ang}}$	$\frac{\partial I_{\text{t,ang}}}{\partial V_{\text{re}}}$		$\frac{\partial I_{\text{t,ang}}}{\partial V_{\text{im}}}$	

$$\frac{\partial S_{\text{bus}}}{\partial V_{\text{re}}} = diag(V)(Y_{\text{bus}})^* + diag(Y_{\text{bus}}V)^* \tag{A.9}$$

$$\text{with } \frac{\partial V}{\partial V_{\text{re}}} = diag(1) \text{ and } \frac{\partial I_{\text{bus}}}{\partial V_{\text{re}}} = Y_{\text{bus}}$$

$$\frac{\partial S_{\text{bus}}}{\partial V_{\text{im}}} = j \cdot (diag(Y_{\text{bus}}V)^* + diag(V)(Y_{\text{bus}})^*) \tag{A.10}$$

$$\text{with } \frac{\partial V}{\partial V_{\text{im}}} = -j \cdot diag(1) \text{ and } \frac{\partial I_{\text{bus}}}{\partial V_{\text{im}}} = j \cdot Y_{\text{bus}}$$

$$\frac{\partial S_{\mathrm{f}}}{\partial V_{\mathrm{re}}} = diag(V_{\mathrm{f}})(Y_{\mathrm{f}})^* + diag(Y_{\mathrm{f}}V)^* C_{\mathrm{f}} \tag{A.11}$$

$$\text{with } \frac{\partial V_{\mathrm{f}}}{\partial V_{\mathrm{re}}} = C_{\mathrm{f}} \text{ and } \frac{\partial I_{\mathrm{f}}}{\partial V_{\mathrm{re}}} = Y_{\mathrm{f}}$$

$$\frac{\partial S_{\mathrm{f}}}{\partial V_{\mathrm{im}}} = j \cdot (diag(Y_{\mathrm{f}}V)^* C_{\mathrm{f}} + diag(V_{\mathrm{f}})(Y_{\mathrm{f}})^*) \tag{A.12}$$

$$\text{with } \frac{\partial V_{\mathrm{f}}}{\partial V_{\mathrm{im}}} = j \cdot C_{\mathrm{f}} \text{ and } \frac{\partial I_{\mathrm{f}}}{\partial V_{\mathrm{im}}} = j \cdot Y_{\mathrm{f}}$$

$$\frac{\partial V_{\mathrm{mag}}}{\partial V_{\mathrm{re}}} = diag(V_{\mathrm{mag}})^{-1} diag(V_{\mathrm{re}}) \tag{A.13}$$

$$\frac{\partial V_{\mathrm{mag}}}{\partial V_{\mathrm{im}}} = diag(V_{\mathrm{mag}})^{-1} diag(V_{\mathrm{im}}) \tag{A.14}$$

$$\frac{\partial V_{\mathrm{ang}}}{\partial V_{\mathrm{re}}} = -diag(V_{\mathrm{ang}}^2)^{-1} diag(V_{\mathrm{im}}) \tag{A.15}$$

$$\frac{\partial V_{\mathrm{ang}}}{\partial V_{\mathrm{im}}} = diag(V_{\mathrm{mag}}^2)^{-1} diag(V_{\mathrm{re}}) \tag{A.16}$$

$$\frac{\partial I_{\mathrm{f,mag}}}{\partial V_{\mathrm{re}}} = diag(I_{\mathrm{f,mag}})^{-1} diag(I_{\mathrm{f,re}}) Y_{\mathrm{f,re}} + diag(I_{\mathrm{f,mag}})^{-1} diag(I_{\mathrm{f,im}}) Y_{\mathrm{f,im}} \tag{A.17}$$

$$\frac{\partial I_{\mathrm{f,mag}}}{\partial V_{\mathrm{im}}} = diag(I_{\mathrm{f,mag}})^{-1} diag(I_{\mathrm{f,re}}) Y_{\mathrm{f,im}} + diag(I_{\mathrm{f,mag}})^{-1} diag(I_{\mathrm{f,im}}) Y_{\mathrm{f,re}} \tag{A.18}$$

$$\frac{\partial I_{\mathrm{f,ang}}}{\partial V_{\mathrm{re}}} = -diag(I_{\mathrm{f,mag}}^2)^{-1} diag(I_{\mathrm{f,im}}) Y_{\mathrm{f,re}} + diag(I_{\mathrm{f,mag}}^2)^{-1} diag(I_{\mathrm{f,re}}) Y_{\mathrm{f,im}} \tag{A.19}$$

$$\frac{\partial I_{\mathrm{f,ang}}}{\partial V_{\mathrm{im}}} = diag(I_{\mathrm{f,mag}}^2)^{-1} diag(I_{\mathrm{f,im}}) Y_{\mathrm{f,im}} + diag(I_{\mathrm{f,mag}}^2)^{-1} diag(I_{\mathrm{f,re}}) Y_{\mathrm{f,re}} \tag{A.20}$$

A.2.4 Inverse of the Sum of Matrices including a Matrix Product

Assuming A,B,C and D are all matrices the following theorem [99] holds:

$$(A + CBD)^{-1} = A^{-1} - A^{-1}C(B^{-1} + DA^{-1}C)DA \tag{A.21}$$

A.2.5 Linearized Transformation of Variance from Rectangular to Polar Form

Assuming a linearized function according to A.1 and the linear affine transformation for normal distribution A.2, then A from equation A.2 is equal $\nabla f(a)^{\mathrm{T}}$. And as $A\Sigma A^{\mathrm{T}}$, then the linearized function for the variance is given by

$$var[f(x;a)] \approx \nabla f(a)^{\mathrm{T}} \Sigma_{xx} \nabla f(a) \tag{A.22}$$

Now the first function is given calculation the magnitude from rectangular form

$$f_1(x) = x_{\text{mag}} = \sqrt{x_{\text{re}}^2 + x_{\text{im}}^2} \tag{A.23}$$

The derivation of $f_1(x)$ for x_{re} and x_{im} result in

$$\nabla f_1(x) = \begin{pmatrix} \frac{\partial f_1(x)}{\partial x_{\text{re}}} \\ \frac{\partial f_1(x)}{\partial x_{\text{im}}} \end{pmatrix} = \begin{pmatrix} \frac{x_{\text{re}}}{x_{\text{mag}}} \\ \frac{x_{\text{im}}}{x_{\text{mag}}} \end{pmatrix} = \frac{1}{x_{\text{mag}}} \begin{pmatrix} x_{\text{re}} \\ x_{\text{im}} \end{pmatrix} \tag{A.24}$$

The second function is calculating the phase from rectangular form

$$f_2(x) = x_{\text{ang}} = \arctan \frac{x_{\text{im}}}{x_{\text{re}}} + const. \tag{A.25}$$

The derivation of arctan is $\frac{1}{1+x^2}$, there the derivation of $f_2(x)$ for x_{re} and x_{im} result in

$$\frac{\partial f_2(x)}{\partial x_{\text{re}}} = \frac{1}{1 + (\frac{x_{\text{im}}}{x_{\text{re}}})^2} \frac{-x_{\text{im}}}{x_{\text{re}}^2} = \frac{-x_{\text{im}}}{-x_{\text{im}}^2 + x_{\text{re}}^2} = \frac{-x_{\text{im}}}{x_{\text{mag}}^2} \tag{A.26}$$

$$\frac{\partial f_2(x)}{\partial x_{\text{im}}} = \frac{1}{1 + (\frac{x_{\text{im}}}{x_{\text{re}}})^2} = \frac{1}{x_{\text{re}}} = \frac{x_{\text{re}}}{x_{\text{mag}}^2} \tag{A.27}$$

$$\nabla f_2(x) = \frac{1}{x_{\text{mag}}^2} \begin{pmatrix} -x_{\text{im}} \\ x_{\text{re}} \end{pmatrix} \tag{A.28}$$

A.3 Appendix for Result Chapter

A.3.1 Connected Customers

Table A.2: Overview of connected grid customers

Customers type connected to MV buses	number of buses connected to the respective customer type	number of consumers
LV rural 1	1	13
LV rural 2	9	99
LV rural 3	6	118
LV semi urban 4	23	41
LV semi urban 5	22	104
LV urban 6	18	111
G0	3	1
G1	4	1
G2	1	1
G3	4	1
G5	1	1
G6	1	1
PV	5	
Wind	3	
Biomass	1	
Hydro power	1	

A.3.2 Computation Time

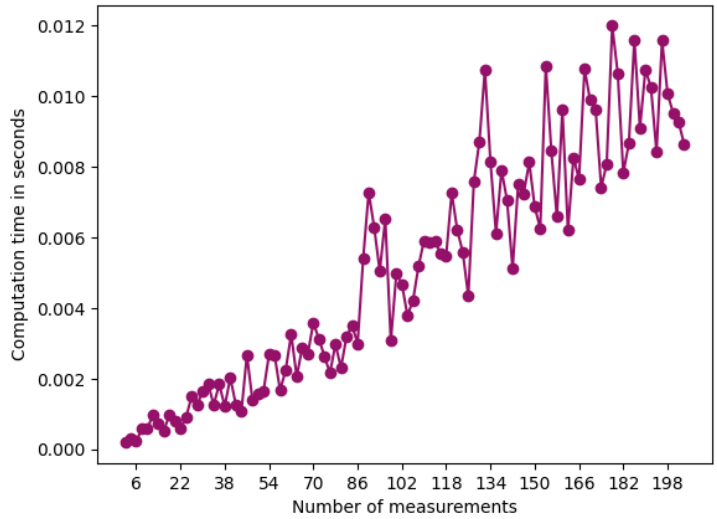

(a) Online state estimation

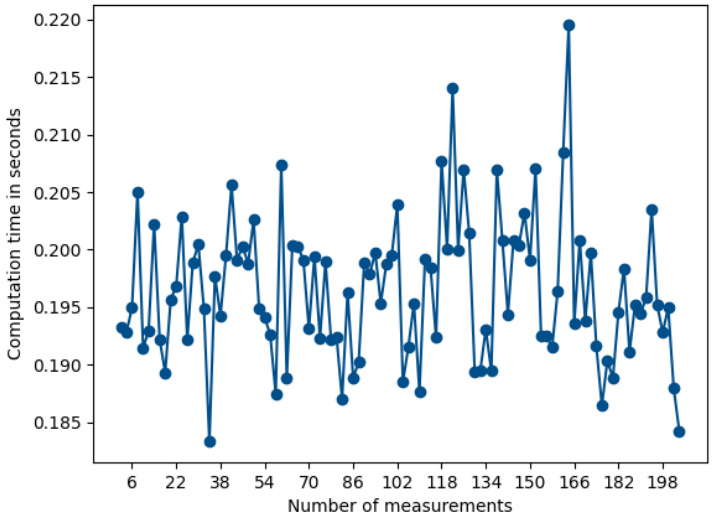

(b) Online state estimation with subsequent calculation of probability of critical system state

Figure A.1: Computation time for (a) only online state estimation (b) with subsequent calculation of probability of critical system state with varying number of measurements obtained using Python on an Intel Core i7-9850H CPU with 16 GB RAM

A.3.3 Results for Higher Measurement Coverage

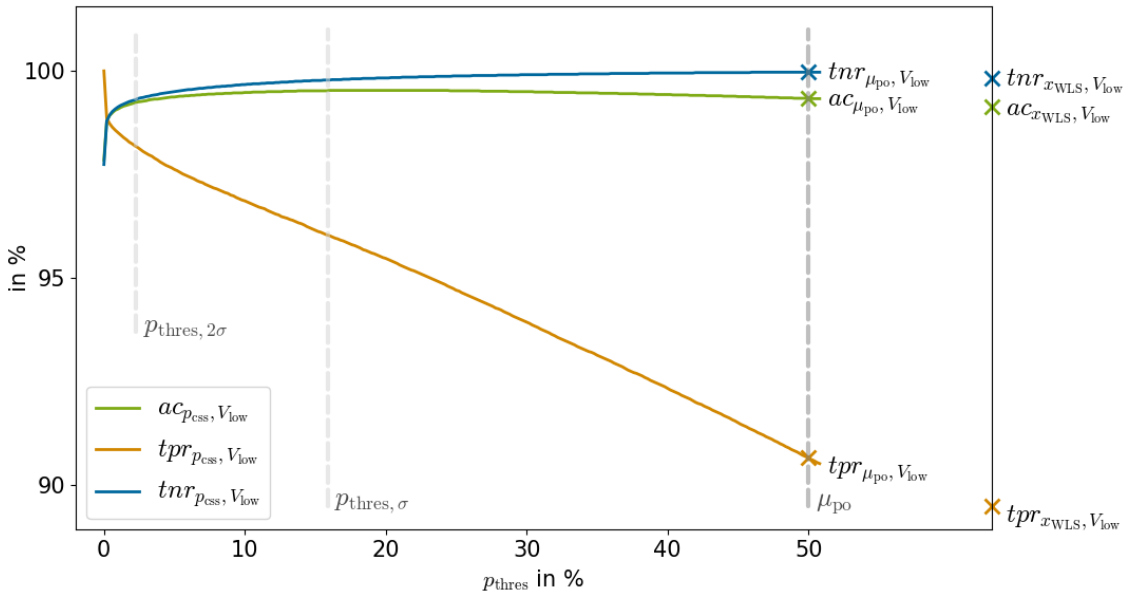

Figure A.2: Aggregated accuracy $ac_{\hat{x},lim}$, true-positive $tpr_{\hat{x},lim}$ and true-negative rate $tnr_{\hat{x},lim}$ for the different state estimation results $\boldsymbol{p}_{\text{css}}$, $\boldsymbol{\mu}_{\text{po}}$, and $\hat{\boldsymbol{x}}_{\text{WLS}}$ for violating V_{low} (-6 %) for higher measurement coverage

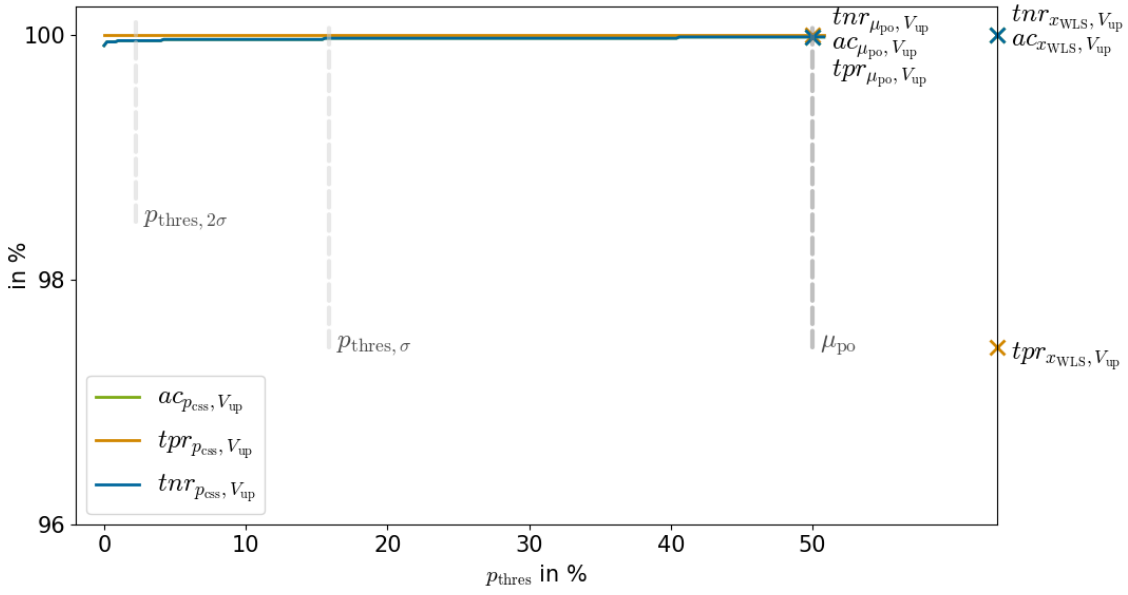

Figure A.3: Aggregated accuracy $ac_{\hat{x},lim}$, true-positive $tpr_{\hat{x},lim}$ and true-negative rate $tnr_{\hat{x},lim}$ for the different state estimation results $\boldsymbol{p}_{\text{css}}$, $\boldsymbol{\mu}_{\text{po}}$, and $\hat{\boldsymbol{x}}_{\text{WLS}}$ for violating V_{up} (+6 %) for higher measurement coverage

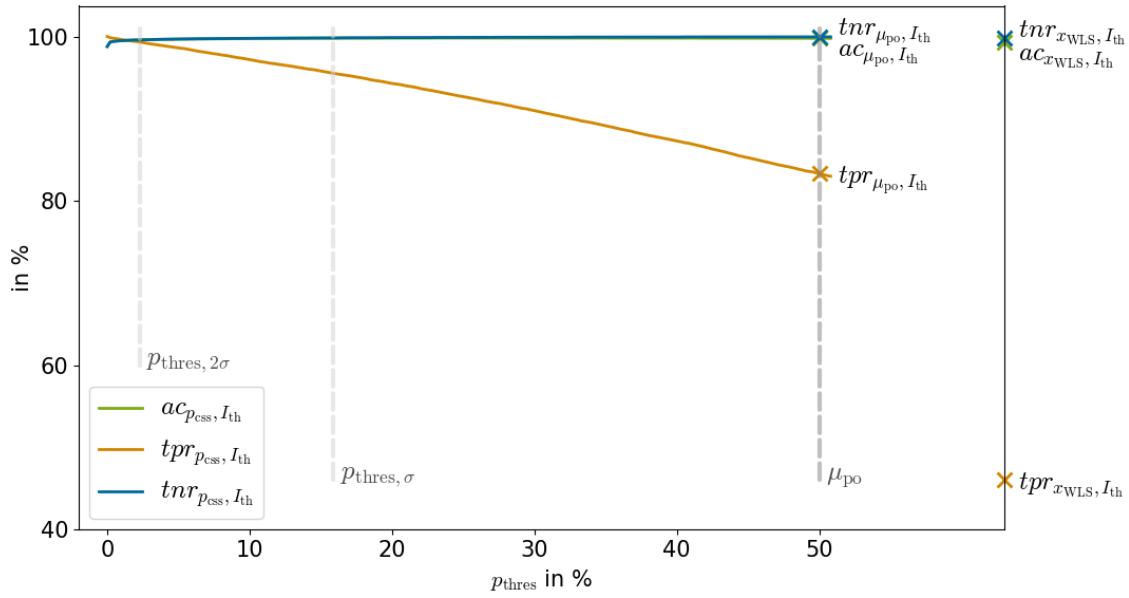

Figure A.4: Aggregated accuracy $ac_{\hat{x},lim}$, true-positive $tpr_{\hat{x},lim}$ and true-negative rate $tnr_{\hat{x},lim}$ for the different state estimation results $\boldsymbol{p}_{\text{css}}$, $\boldsymbol{\mu}_{\text{po}}$, and $\hat{\boldsymbol{x}}_{\text{WLS}}$ for violating I_{th} for higher measurement coverage